# RESEARCH ACTIVITIES IN OPTOELECTRONICS AND ELECTRONICS MANUFACTURING 2003





PUBLISHER

VTT Electronics, Kaitoväylä 1, P.O.Box 1100, FI-90571 OULU, FINLAND
Tel. +358 8 551 2111, Fax +358 8 551 2320
Electronic mail: ele.info@vtt.fi

VTT ELECTRONICS, OULU 2004

# PREFACE

VTT Electronics is one of the six operative units in VTT, the Technical Research Centre of Finland, an independent, multi-field contract research organisation. The main task of VTT Electronics is to work as a strategic R&D partner for electronics industry, thus for its part ensuring the prospected growth in this sector. At VTT Electronics, 70 of its 300 staff members are experts in optics and optoelectronics.

The main goal of Optoelectronics research area is to assist companies in utilizing advanced optical, photonic and optoelectronic technologies in their products. Our core competenceis are in the advanced technologies and integration methods of optoelectronic modules and instruments. This focus includes challenging research and development aims in modelling, simulation and design, new advanced materials, cost-effective fabrication, manufacturing and packaging applied for multi-technological solutions in optics, optical communication, optical measurements as well as sensors and instrumentation. A new 'BioOulu'activity was started on 'biomicrosystems' in co-operation with University of Oulu and VTT Biotechnology focusing to R&D and commercial exploitation of multidisciplinary disposable biosensor systems for point-of-care diagnostics, environmental sensing and food safety.

In this report you will find extended abstracts concerning some of the published research work carried out in 2003. The abstracts of the examination theses completed by our personnel and a list of publications are also included.

Oulu, February 16, 2004

Further information: www.vtt.fi/ele

Jouni Tornberg
Head of Optoelectronics research
***Jouni.Tornberg@vtt.fi***

Harri Kopola
Research professor
***Harri.Kopola@vtt.fi***

# TABLE OF CONTENTS

# Simulation Tool for Evaluation and Optimisation of an Imaging System

### *INTRODUCTION*

There are various factors that have to be taken into account when designing imaging systems: imaging quality, mass manufacturability, materials, detector, cost, imaging conditions, etc. It is not possible to optimise all of them individually in many designs, so there is a need to find the optimal balance between them. The imaging system of a cellular phone is an example of a design with conflicting requirements: there is a need for a lens design with good imaging quality, wide-angle and small F-number, but the design also has to be low cost, simple and mass manufacturable. In addition, due to the cost and power consumption, the imaging quality of the image sensor and the image processing capability are compromised. It is a challenging task to balance all the above-mentioned factors and it became apparent that there is a need to simulate the entire imaging system in the specification and designing phase. A simulation tool for fast image quality evaluation was developed. The tool enables numerical and visual evaluation and optimisation of the lens design.

### *SIMULATION ENVIRONMENT*

Simulators that simulate some part of an imaging system, e.g. image sensor or the lens system, are available and have been published [1]. There are also a few published imaging system simulation methods or tools [2], [3].

We have developed a simulation tool that comprises two software modules: one for the evaluation of the lens design and one for the evaluation of the image sensor [4]. The tool enables 1) quick visual image quality evaluation, 2) visual and numerical evaluation of the image sensor showing the effects of image sensor noise in the image with given imaging conditions, 3) lens optimisation using quality metrics called the Subjective Quality Factor (SQF), 4) simulation of the effect of ambient temperature, 5) estimation of total noise, and 6) computation of the signal-to-noise (SNR) ratio. Figure 1 shows the overall organisation of the simulation tool.

### *IMAGE QUALITY EVALUATION AND LENS DESIGN OPTIMISATION*

The lens system is modelled in the Zemax® environment with a customized simulation tool. The model provides realistic imaging from a planar object surface to a planar detector surface for a rotationally symmetric imaging optical system. The model predicts not only the image blurring due to the optical aberrations but also the possible geometric distortion of the image.

The previous methods used to simulate the realistic image quality of an optical imaging system include 1) direct ray tracing, and 2) convolution methods using Modulation Transfer Function (MTF) or Point Spread Function (PSF). Our simulation method is close to the convo-

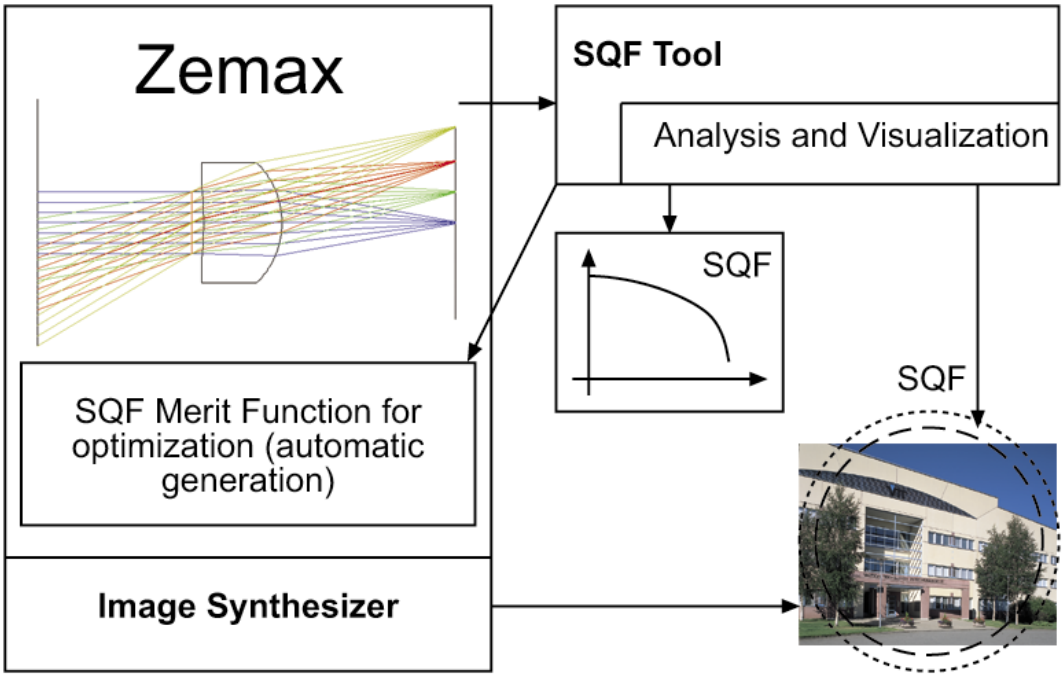


***Figure 1: Overall organization of the simulation tool.***

***Figure 2: Example of imaging simulation. Left: Original image. Middle: Imaging with a distorting lens. Right: Imaging with a blurring lens.***

lution methods. We use terms such as 'pointwise convolution' or 'circular convolution' to describe where each point in the image is replaced with the PSF produced by the lens to simulate the imaging, but the PSF varies with the field points. The method is useful for rotationally symmetric optics, since only the radial field-dependence of the PSF has to be calculated by ray tracing, whereas the azimuthal dependence can be calculated by rotating the PSF. The use of rotational symmetry decreases the number of rays to be traced in order to simulate the performance of the lens.

The Image Processing Simulation Environment (IPSE) is faster than direct ray-tracing methods and more versatile than convolution methods. The quality of the final image depends on the lens design. The most pronounced feature, often seen in the simulated image, is the slight circular variation in the intensity. Simulated example images are shown in Figure 2.

When designing imperfect imaging systems, it is important to judge the image quality in the same way as a human observer would perceive it, i.e. to estimate the 'subjective image quality' of the imaging system. Reviews of these quality measures are given in [5] and in [6]. We have used a modified version of the Subjective Quality Factor (SQF) [7] introduced by Granger and Cupery [8] in our simulations. We use the normalized contrast sensitivity of the Human Visual System (HVS) as a weighting factor for the MTF of the imaging system instead of integrating over a defined range of frequencies. SQF replaces the time-consuming visual image quality evaluations by humans.

Usually, objective measures, such as a spot size or an MTF, are used as an optimisation criteria for a lens design. Our simulation tool enables the optimisation from the subjective quality point of view. The SQF estimation is relatively slow, so the lens is first optimised using the objective criteria and the final optimisation is done using the SQF criterion. It is clear that the SQF optimisation improves the design in the SQF sense, although the improvement is not always noticeable or consistent over the field points. The obtained image quality was also verified visually using our image synthesizer module. The SQF optimised designs were rated better than the non-SQF optimized designs, especially in the corners of the images.

### *IMAGE SENSOR MODELLING*

The sensor modelling tool simulates how a CMOS image sensor creates a digital image when a fictitious input scene is incident on the sensor, e.g. through an imaging optics. Generally, device modelling is a complex task as different models may be needed for different pixel structures and different sensor functionality. However, by confining it to typical characteristics of common photodiode-based Active-Pixel Sensors (APS) we were

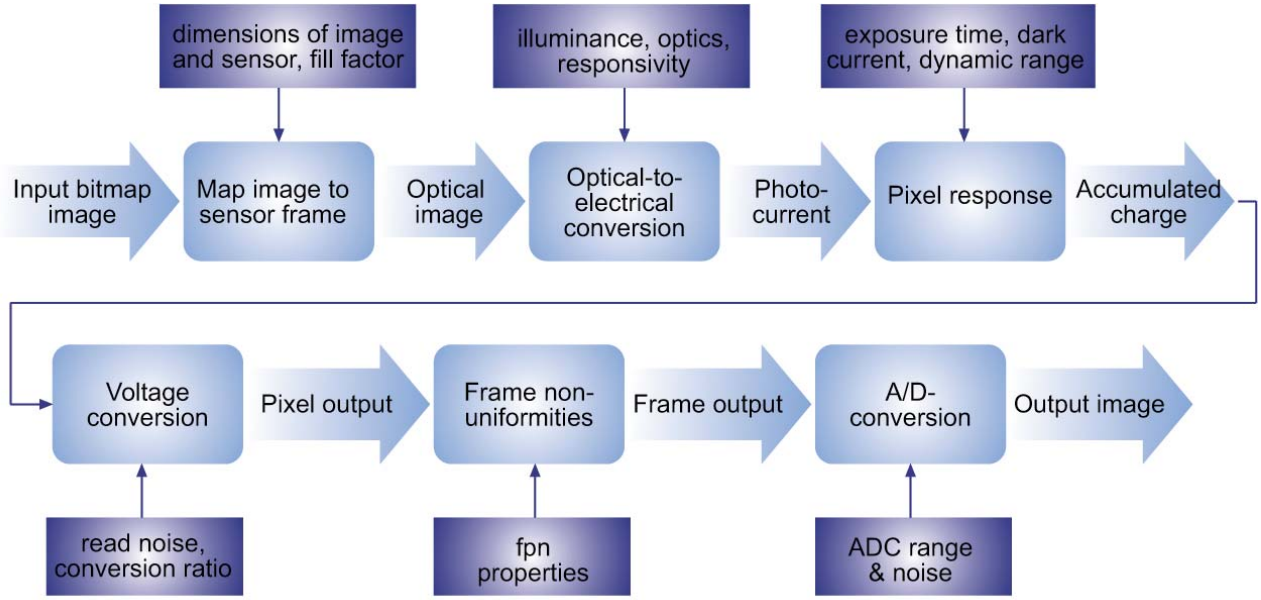


***Figure 3: Simplified flow chart of the image sensor modelling procedure.***

able to build a modular procedure that models the operational blocks and noise sources, and is thus able to demonstrate the estimated visual quality of the sensor's output image.

Our modelling tool is a stand-alone application that has been developed in the Matlab environment. The input scene is provided to the simulator as an RGB or monochrome bitmap image file. In addition, the simulator takes several input parameters that define the input image (illuminance and 'physical' dimensions), imaging conditions, and features and specifications of the sensor, as well as simulation control. The simplified modelling procedure is presented in Figure 3.

## CONCLUSIONS

We have presented a new tool for visualizing, designing and optimising the image quality of an imaging system. The visualization shows the imaging performance of the designed lens system. The image sensor is modelled using a separate module and enables visual evaluation of the effects of various noise sources on the quality of the image. Any signal processing blocks (such as compression) may be easily added to the simulation system. The designed simulator has proven to be useful when designing lenses for imaging systems used in cellular phones.

## REFERENCES

1. R. C. Short, D. Williams, A. E. Jones, ***Image capture simulation using an accurate and realistic lens model***, Proc. of SPIE, Vol. 3650, pp. 138-148, 1999.
2. J.L. Olivès, B. Lamiscarre, M. Gazalet, ***Optimization of Electro-Optical Imaging System with an Image Quality Measure***, In EI'97, Electronic Imaging: Science and Technology, IS&T/ SPIE's Symposium, San Jose, USA, 9-14 February 1997.
3. J.L. Olivès, ***Optimisation globale de systemè imageur à l'aide de criterères de qualité visuelle,*** Doctoral Thesis, 1998.
4. T. T. Kolehmainen, J. Aikio, M. Karppinen, A.-J. Mattila, J.-T. Mäkinen, K. Kataja, K. Tukkiniemi, P. Karioja, ***Simulation of imaging system's performance***, Optical Science and Technology, San Diego, USA, 3 - 8 Aug. 2003, Optical modeling and performance predictions, Proceedings of SPIE, Vol. 5178, pp. 204-212, 2003.
5. P. G. J. Barten, ***Contrast sensitivity of the human eye and its effects on image quality***, SPIE Optical Engineering Press, Bellingham, Washington USA, 1999.
6. T. L. Williams, ***The optical transfer function of imaging systems***, Institute of Physics Publishing, Bristol and Philadelphia, 1999.
7. J.L. Olivès, T. T. Kolehmainen, J. Aikio, K. J. Kataja, P. Karioja, T. Vuori, T. Mustonen, ***Imaging lens design using subjective quality metrics***, Optical Sys-

tems Design SPIE's International Symposium, St. Etienne, France, 30 September - 3 October 2003. Proc. of SPIE, Vol. 5249.

8. E. M. Cranger and K. N. Cupery, An optical merit function (SQF), which correlates with subjective image judgements, Phot. Sci. Eng. 16, pp. 221-230, 1972.

Janne Aikio
***Janne.Aikio@vtt.fi***

Mikko Karppinen
***Mikko.Karppinen@vtt.fi***

Kari Kataja
***Kari.J.Kataja@vtt.fi***

Antti-Jussi Mattila
***Antti-Jussi.Mattila@vtt.fi***

Pentti Karioja
***Pentti.Karioja@vtt.fi***

Jukka-Tapani Mäkinen
***Jukka-Tapani.Makinen@vtt.fi***

Timo T. Kolehmainen
***Nokia Mobile Phones, Elektroniikkatie 3, P.O BOX 50, FIN-90571 OULU, Finland***

Kari Tukkiniemi
***VTT Information Technology, P.O BOX 1200, FIN-02044 VTT, Finland***

# 3D FDTD Simulations of Super Resolution

### 1. INTRODUCTION

We have used 3D finite difference time domain (FDTD) modelling to study the writing and reading performance of super resolution (SR) structures[1-4] that have a bulk light scattering center (LSC) or donut-shaped aperture scatter in their active layers. Figure 1a shows a donut-shaped aperture system that is compromised of a void surrounded by an Ag donut centered at the optical axis of the laser beam. Figure 1b shows a bulk Ag cylinder located at the optical axis of the laser beam in an $AgO_x$ active layer. In both cases the super resolution layer active is sandwiched between two dielectric ($ZnS\text{-}SiO_2$) films and this three-layer stack is deposited directly onto the phase change (PC) data layer of the disk, where amorphous phase marks are located within the crystal phase background material. In addition, the systems include another insulating layer between the data layer and the Al reflector layer.

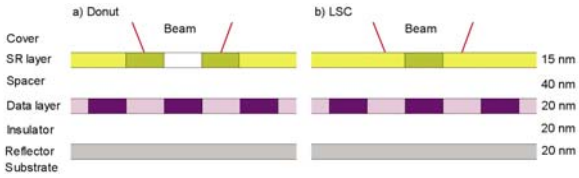


***Figure 1. Schematic drawings of (a) a bulk donut and (b) LSC SR geometries.***

### 2. MODEL

Here we report the results using a 3D FDTD model to compute the optical fields that occur within the PC layer of an optical data storage medium that incorporates a SR structure that has an $AgO_x$ active layer. We have not used any land-groove structure in the model; the different layers are just planar thin films. The writing performance of the system was estimated by studying the absorption profile inside the PC data layer. The written mark size in the data layer is assumed to be the same as the full-width-half-maximum of the absorption profile inside the PC data layer. The readout performance was modelled by calculating the modulation of the optical power reflected from a track of periodic amorphous data marks of varying length in the PC data layer, which initially has a crystalline phase.

### 3. NUMERICAL RESULTS

Figure 2 shows some examples of calculated readout signal modulation as the function of mark size when the focused playback spot has wavelength $\lambda$ = 650 nm and numerical aperture NA = 0.6. The label 'DVD' indicates the reference curve, which is obtained from a DVD –type rewritable disk with no super resolution layer. The resolution limit ($\lambda$/4NA = 270 nm) of the conventional optical system is marked with a vertical dotted line and the modulation of the reference system at this point with a horizontal dotted line. The diameter (the central void in the ring structure) of the two SR aperture types is 200 nm. Improved readout performance over the conventional disk at high storage densities (recorded mark size < 350 nm) is clearly shown with both types of apertures. However, the null point at the 462 nm mark size in the modulation curve with the LSC-type aperture are problems if the mark size is varied at the disk in such a way that this null point is crossed. The nulls arise from the fact that the reflectance from the disk from the on-mark and off-mark situations changes at this point.

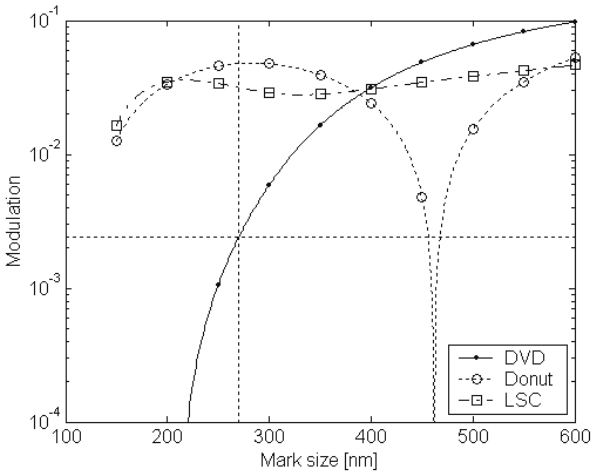


***Figure 2. Readout modulation curves from donut and LSC-type SR aperture geometries. DVD is the reference modulation curve calculated without the SR layer structure (DVD-RW type of media).***

In Figure 3 we show cross-sections of the absorption density in the data layer obtained with different diameter donut apertures and (as a reference) the Gaussian-shaped focused spot profile that scans the data layer in a DVD-RW type of system. It is clearly seen that when the diameter of the SR aperture is 200 nm, the full-width-half-maximum (FWHM) (185 nm) of the absorption profile is significantly smaller than the FWHM of the reference curve (545 nm). On the other hand, when the SR aperture diameter is 100 nm, the absorption profile exhibits 3 peaks and its total FWHM (720 nm) is effectively increased. In addition, we can see that the FWHM (265 nm) obtained with the 300 nm diameter SR aperture is larger than with the 200 nm SR aperture, which indicates that some kind of minimum would occur when the SR aperture diameter is near 200 nm with these disk structures.

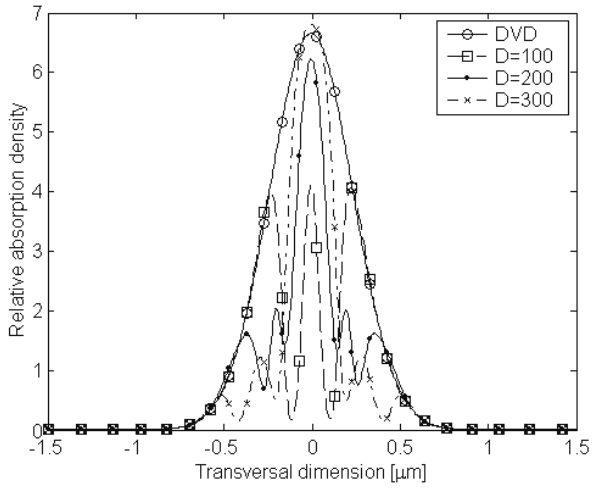


***Figure 3. Absorption cross-section curves with different diameter ring-type apertures. RW is the reference curve in DVD-type media.***

### *4. DISCUSSION AND CONCLUSION*

The recent experiments have shown that the $AgO_x$ layer is decomposed to the small Ag particles and oxygen when it is heated with a focused laser beam. In addition, the whole SR, spacer and data layer structure is permanently damaged, and only works as a write-once media[5]. A similar effect was also shown for the $PtO_x$ material[6]. However, in our model the aperture only exists in the region that is heated by the readout laser beam - that is, the aperture is considered to work as a dynamical window. If you consider the case where there is always an aperture in the same location where there is a mark (write-once media), the readout process modelled in this paper no longer holds. Nevertheless, we have shown that both LSC and donut-shaped SR structures exhibit improved performance over the conventional phase-change disk, and because both of these types of structure have been observed in experiments[7] we believe that these structures (especially the donut-shaped SR aperture) are close to the real behaviour of the metallic SR structures. Here we note that in a recent work, Lin et al.[8] showed a donut-shaped aperture when the Ag particle system is illuminated with a readout laser spot. Therefore, we suggest that the donut-shape aperture model can be used in numerical simulations to study the performance of the SR disks. Finally, the reason for the change in the signal power levels at the detector from the on-mark and off-mark situations, and, therefore, the null point in the modulation curve, need to be studied in more detail, but this is left for the future.

The readout characteristics of two bulk-type Ag SR structures were studied using the 3D FDTD method. The proposed oxygen aperture system using a bulk Ag donut is currently closest to the experimental data, which can explain the improved readout performance from the SR disk. However, in reality, the $AgO_x$ layer decomposed to small particles rather than a bulk sheet of Ag and the readout characteristics of such a particle aperture might perform differently. Finally, the reversed signal levels are shown as a null in the modulation curve.

### *REFERENCES*

1. J. Tominaga, T. Nakano, and N. Atoda: Appl. Phys. Lett. 73, 2078 (1998).
2. H. Fuji, J. Tominaga, L. Men, T. Nakano, H. Katayama and N. Atado: Jpn. J. Appl. Phys. 39 (2000) 980.
3. C. Peng: Appl. Opt. 40 (2001) 3922.
4. T. Nakano, Y Yamakawa, J. Tominaga and N. Atado: Jpn. J. Appl. Phys. 40 (2001) 1531.
5. T. Kikukawa, A. Tachibana H. Fuji and J. Tominaga: Jpn. J. Appl. Phys. 42 (2003) 1038.
6. T. Kikukawa, T. Nakano, T. Shima, and J. Tominaga: Appl. Phys. Lett. 81 (2002) 4697.
7. F.H. Ho, H.H. Chang, Y.-H. Lin and D.P. Tsai: Jpn. J. Appl. Phys. 42 (2003) 1000.
8. B.S. Lin, D.P. Tsai and W.C. Lin: Tech. Dig. ISOM03 (2003) Th-H-02.

Kari Kataja
***Kari.J.Kataja@vtt.fi***

Juuso Olkkonen
***Juuso.Olkkonen@vtt.fi***

Janne Aikio
***Janne.Aikio@vtt.fi***

Dennis Howe
***Optical Sciences Center, University of Arizona, Tucson AZ 85721-0094***

# On Surface Plasmon Enhanced Near-Field Transducers

### *INTRODUCTION*

Modern optical technologies such as near-field scanning optical microscopy (NSOM), optical data storage (ODS), and heat assisted magnetic recording (HAMR) demand efficient near-field light sources that provide light confinement well beyond the fundamental diffraction limit. Accordingly surface plasmon enhanced near-field transducers, which are devices that confine the incident illumination to a sub-wavelength near-field spot, have attracted great interest. Usually, light that appears in the near field of a sub-wavelength sized radiating transducer either decays rapidly with distance from the transducer (i.e., the light filed is evanescent), or the light diverges rapidly with distance from the transducer. Therefore the target surface to be illuminated has to be in the near-field of the transducer. In theory, extremely small light spots can be achieved if photons are forced through a metallic aperture that is close enough to the target surface. In practice, the viability of such systems is problematic since the transmission efficiency of nano-apertures decays roughly as $\boldsymbol{d}^{-4}$[1], where ***d*** is the aperture size. However, it has been recently proposed and even demonstrated [2-5] that the transmission efficiency of nano-apertures can be greatly enhanced with the aid of surface plasmon polaritons (SPPs) and localized surface plasmons (LSPs). The primary goal of our work is to determine how SPPs enhance the light transmission of sub-wavelength sized near-field transducers.

### *SURFACE PLASMON POLARITONS*

A dielectric/metal-interface can support collective oscillations of induced surface charge density that are excited by an incident light field, if the metal exhibits negative dielectric permittivity at the light frequency. A surface plasmon polaritons (SPP) is the composite electromagnetic disturbance that occurs when an incident light field couples resonantly with such an oscillating surface charge density distribution. Since induced surface charge density is proportional to the discontinuity of the electric field component normal to the interface, only transverse magnetic (TM) light can excite SPPs. A semi-infinite dielectric/metal-interface (in which both the metal and dielectric mediums are very thick) can support only a bound SPP mode whose field amplitude decays exponentially with distance on the both sides of the interface. Since at any frequency, SPPs have larger momentum than light at all incident angles, directly incident light cannot excite any SPP modes. Usually SPPs are excited by propagating evanescent optical fields produced either by total internal reflection from a prism located in the vicinity of the metal film, or by a grating deposited on the surface of the metal film.

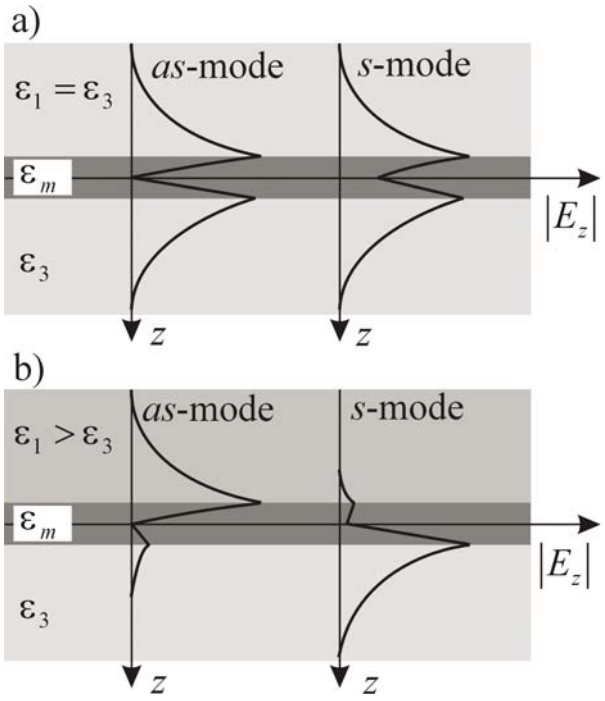


***Figure 1: a) Amplitude of electric field component normal to the metal film in the antisymmetric (as) and symmetric (s) SPP modes when the thin metal film ($\varepsilon_m$) is in the symmetric environment ($\varepsilon_1 = \varepsilon_3$). b) The same as a) but now the metal film is in the antisymmetric environment ($\varepsilon_1 > \varepsilon_3$).***

In optically thin metal films, there is a coupling between the SPPs associated with each dielectric/metal-interface. Four thickness dependent SPP modes result: symmetric (***s***) and antisymmetric (***as***) modes which each branch into a pair of modes - one bound and the other leaky. The nature of these modes depends strongly on the thickness of the metal film as well as the refractive indices of the adjacent media. In the antisymmetric mode, the amplitude of the electric field component normal to the metal film exhibits a zero inside the film (cf. Fig. 1), while the symmetric mode maintains its phase across the film. In the bound mode, the SPP field amplitude decays exponentially with distance on both sides of the thin film, while the leaky mode radiates some power into an adjacent dielectric medium. A thin film having the same dielectric materials on both sides (symmetric structure) can support only bound SPP modes [6].

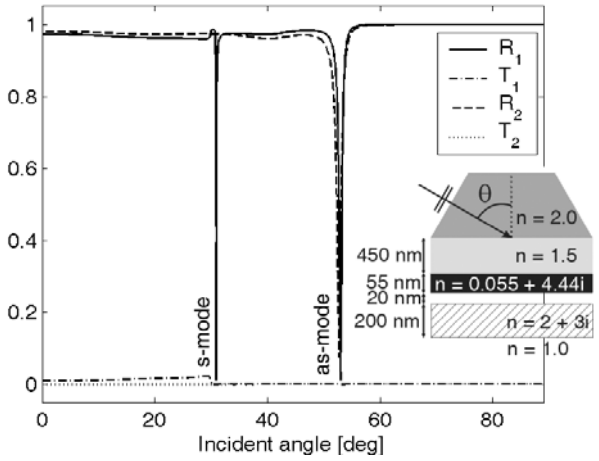


***Figure 2: Light transmission (T) and reflection (R) from a multilayer structure (shown in the insert) that supports SPPs. In the case ($R_1$,$T_1$), the recording medium (n = 2 + 3i) is not present.***

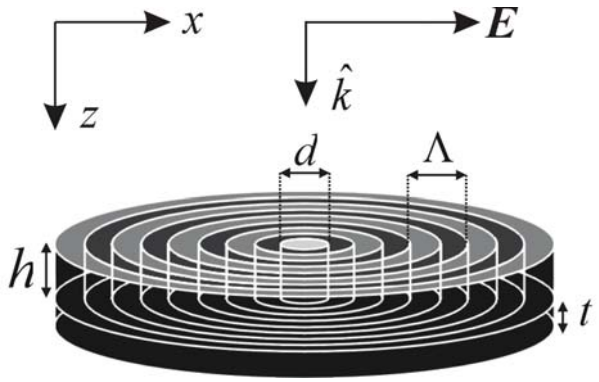


***Figure 3: Schematic illustration of the modeled structure.***

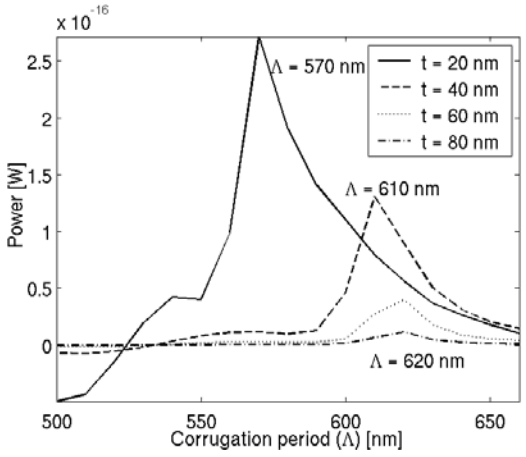


***Figure 4: Integrated power 20 nm below the corrugated aperture structure as a function of the corrugation period for several thickness of the base layer (t).***

Let us consider a three-layer structure, where the thin metal film ($\varepsilon_m$) is sandwiched between the semi-infinite dielectric layers ($\varepsilon_1$, $\varepsilon_3$) as illustrated Fig. 1. We assume that the illumination is incident on the $\varepsilon_1$ side. When $\varepsilon_1 = \varepsilon_3$ (see Fig. 1a)), the electric field component normal to the metal film, which is the strongest field component, decays exponentially on both sides of the film. When, for example, an optical recording medium is inserted 20 nm below the metal film, the SPP field will be strongly disturbed and the SPPs will no longer propagate along the metal film. On the other hand, when $\varepsilon_1 > \varepsilon_3$ (see Fig. 1b)), the electric field of the antisymmetric mode is highly localized in the $\varepsilon_1$ medium; consequently structures below the metal film will only slightly disturb the ***as***-mode. To further illustrate this, we show light transmission and reflection from a multi-layer stack that supports propagating SPPs in Fig. 2. $R_1$ and $T_1$ curves show the transmission and reflection curves, respectively, in the absence of the recording medium (***n*** = 2 + 3i), while $R_2$ and $T_2$ show the corresponding curves in the presence of the recording medium. Interestingly, this multi-layer stack supports the ***s***- and ***as***-modes without the recording medium, while only the ***as***-mode remains when the recording medium is inserted below the metal film. Our conclusion is that only SPPs that propagate on the incident surface of a near-field transducer can enhance light transmission through the transducer in the presence of a recording medium.

### *LIGHT TRANSMISSION THROUGH A HOLE IN A CORRUGATED METAL FILM*

We have developed a parallelized Body-of-Revolution Finite Difference Time Domain (BOR-FDTD) tool, which allows examination of light interaction with cylindrically symmetric structures in a time efficient manner. This tool was used to study the transmission of a normally incident plane wave through a cylindrical hole in a cylindrically corrugated metal film.

The modeled structure is schematically shown in Fig. 3. A normally incident plane wave having wavelength of 650 nm impinges on a silver metal film that has surface corrugations with period Λ and depth ***h***. The thickness of the base layer, i.e., the residual metal beneath the grooves is denoted by ***t***. A cylindrical hole with diameter ***d*** is centered on the axis of the corrugations**.** In our study, ***h*** and ***d*** are fixed parameters having values ***h*** = 90 nm and ***d*** = 100 nm.

Figure 4 shows the transmitted power as a function of the corrugation period for several thickness of the base layer. The transmitted power was computed by integrat-

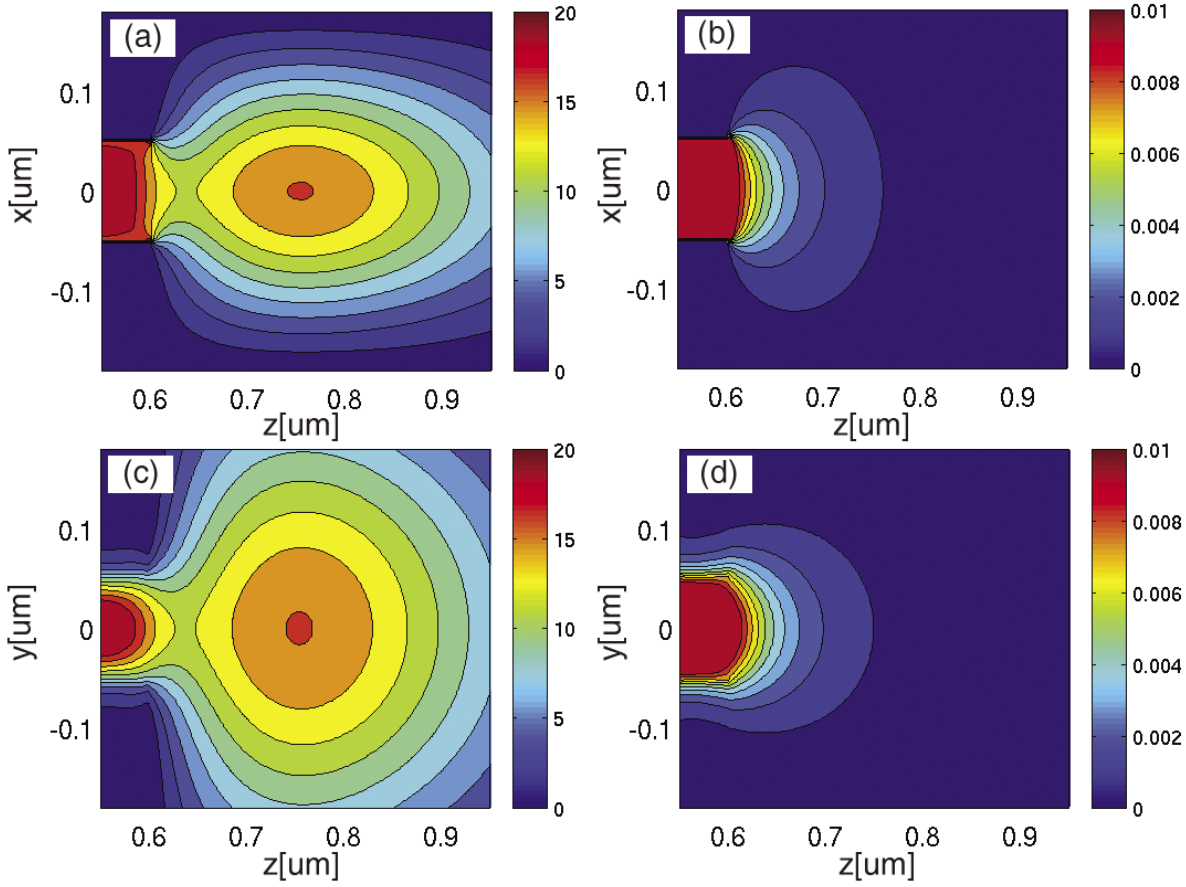


***Figure 5: Longitudinal component of the time-averaged Poynting vector on the exit side of the aperture in the xz- and yz-planes with (a), (c) and without (b), (d) the surface corrugations. The incident plane wave is $E_x$-polarized.***

ing the ***z***-component of the time-averaged Poynting vector over a circular disk centered below the aperture and having radius of 300 nm. Results clearly show that the corrugation period providing the highest transmission depends strongly on the thickness of the base layer. Assuming that surface corrugations only slightly disturb the SPPs propagating in the base layer, the SPPs will be excited when the grating period equals the SPP wavelength. For example, the wavelengths of anti-symmetric bound SPPs (that can be excited by 650 nm light) versus Ag film thickness (assuming planar thin Ag films) are: $\lambda_{SPP}$(20nm) = 567 nm, $\lambda_{SPP}$(40nm) = 618 nm, $\lambda_{SPP}$(60nm) = 628 nm, which are in rather good agreement with the peaks shown in Fig. 4.

We shall now illustrate how surface corrugations enhance the light transmission trough the central hole. Figure 5 shows the longitudinal component of the time-averaged Poynting vector on the exit side of the aperture with and without the surface corrugations, when the thickness of the base layer is 20 nm. From Fig. 5 we observe that the illumination "hot spots" directly behind the central holes in the uncorrugated and corrugated structures are elliptical, i.e., the near-field light exhibits more confinement in the ***x***-direction. In addition, the hot spot of the uncorrugated aperture is immediately behind the aperture, while the hot spot of the corrugated aperture gains its tightest focus at a distance of 100-200 nm beyond the exit surface of the aperture. We also note that the surface corrugations enhance the near-field light transmission by three orders of magnitude.

### *DISCUSSION AND CONCLUSION*

Surface plasmon polaritons posses interesting properties that may be utilized to achieve efficient light confinement beyond the fundamental diffraction limit. Our numerical analysis showed that cylindrical corrugations around a single aperture in a metal film significantly enhance the light transmission through the aperture and that the excitation of bound anti-symmetric SPP modes produces this transmission enhancement. It was also shown that antisymmetric SPP mode can reside in a planar metal film even when a thin film recording medium is inserted below the metal film and close to it.

***REFERENCES***

[1] H. A. Bethe, “Theory of Diffraction by Small Holes,” Physical Review, Vol. 66 (1944).

[2] T. Thio, K. M. Pellerin, R.A. Linke, H. J. Lezec, and T. W. Ebbesen, “Enhanced light transmission trough a single subwavelength aperture,” Optics Letters, Vol. 26, No. 24 (2001).

[3] Wei-Chih Liu, and Ding Ping Tsai, “Optical tunneling effect of surface plasmon polaritons and localized surface plasmons,” Physical Review B, Vol. 65, 155423 (2002).

[4] J. A. Porto, F. J. Garcia-Vidal, and J. B. Pendry, “Transmission resonances on metallic gratings with very narrow slits,” Physical Review Letters, Vol. 83, No. 14 (1999).

[5] I. Avrutsky, Y. Zhao, and V. Kochergin, “Surface-plasmon-assisted resonant tunneling of light through a periodically corrugated thin metal film,” Optics Letters, Vol. 25, No. 9 (2000).

[6] J. J. Burke, G. I. Stegeman, and T. Tamir, “Surface-polariton-like waves guided by thin, lossy metal films,” Physical Review B, Vol. 33, No. 8 (1986).

Juuso Olkkonen
***Juuso.Olkkonen@vtt.fi***

Janne Aikio
***Janne.Aikio@vtt.fi***

Dennis Howe
***Optical Sciences Center, University of Arizona, Tucson AZ 85721-0094***

Kari Kataja
***Kari.J.Kataja@vtt.fi***

# Coupled-field Modelling of Interferometric Hydrophone with Self-supported Mandrel

***SUMMARY***

A novel design of an interferometric hydrophone transducer is presented. It consists of a coil of fibre embedded in a layer of epoxy. Finite Element modelling of such transducer is difficult due to anisotropic mechanical properties of its structure. An approach based on laminate modelling techniques was adopted. Static and modal Finite Element analysis was conducted, as was a coupled-field acousto-mechanical analysis.

## *1. INTRODUCTION*

One of the most sensitive optical fibre hydrophone types are interferometric hydrophones. Typically, they work in Michelson interferometer configuration, shown in Figure 1, in which both sensing and reference arms are placed under water in close proximity in order to compensate the temperature influence on the operating point of the sensor.

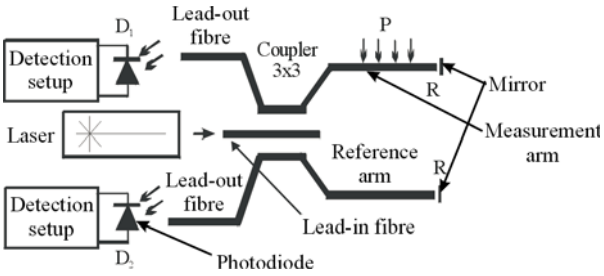


***Fig.1 Optical fibre hydrophone using a Michelson interferometer configuration with 3x3 coupler.***

An important part of these sensors is the transducer, which responds to incident acoustic wave by changing optical path length of the sensing arm fibre. Often an air-backed mandrel transducer is used [1]. This transducer, whose cross-section is shown in Figure 2a, consists of an aluminium cylinder on which several turns of optical fibre were wound. This cylinder is supported by a stiff metal structure in such a way that a waterproof assembly is created. The space under the aluminium cylinder is filled with air, allowing the cylinder to deform in response to incident acoustic wave. This deformation is measured by the sensing fibre wound on the cylinder.

In transducer from Figure 2a differential hydrostatic pressure acting on the aluminium cylinder can be high, as the pressure inside the structure is close to atmospheric pressure while the outside pressure may reach several MPa. As a result the cylinder must have a sufficient strength to withstand it. Increasing strength leads to increased stiffness, which limits sensitivity of the transducer.

If hydrostatic pressure on both sides of the cylinder can be made equal, it does not have to withstand high pressures. Therefore, its stiffness can be greatly reduced, making it more sensitive to the acoustic wave. This is an important advantage, although any pressure equalization method seems difficult to implement for transducers operating below few hundred meters.

If a high stiffness is not required then the sensing structure can be implemented as a ‘laminate-like’ coil of optical fibre embedded in a layer of epoxy, as shown in Figure 2b. A principal advantage of such structure is that no energy of acoustic wave is wasted in the cylinder, which can lead to a higher sensitivity of the self-supported transducer.

## *2. MODELLING OF TRANSDUCER*

Finite Element modelling of self-supported mandrel transducers having several layers of many fibre turns each represents a challenge as it is impossible to approximate mechanical properties of such transducer by properties of the cylinder on which the fibre is wound. A direct model, in which fibre and epoxy in which it is embedded are represented by different sets of finite elements, is difficult to analyse for 2-D and is intractable for 3-D analysis, due to excessive number of elements. Assuming that

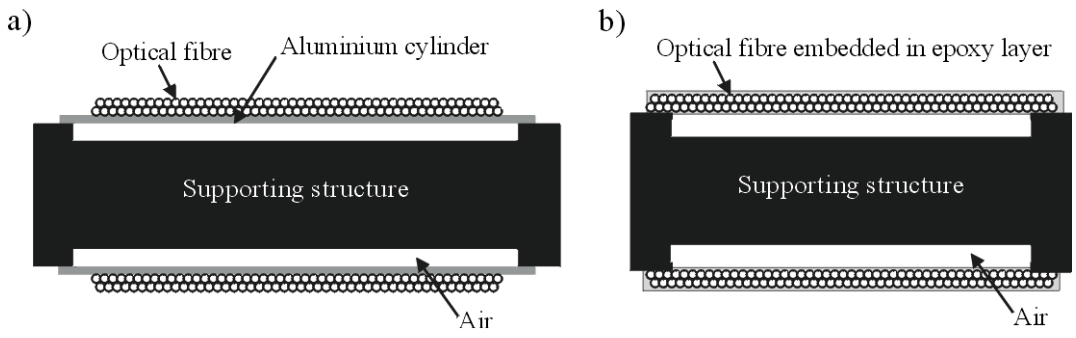


***Fig.2 Cross-section of an air-backed mandrel transducer. a) standard design, b) self-supported design.***

a mandrel having 4 layers of 100 fibre turns each has to be modelled in 2-D using 200 elements per one fibre turn (i.e. 100 elements for the fibre and 100 elements for epoxy around that fibre), resulting number of elements is 80 000. In 3-D, if the mandrel has radius of 20 mm and good shape of elements has to be preserved, the number of elements reaches $5\ 10^8$.

Therefore, another approach was adopted, based on a method developed during research on composite structures and having a proven track record. Central to that method is the assumption that regularly distributed fibre aligned in one direction (as shown in Figure 3) embedded in epoxy can be treated as a homogeneous, orthotropic material (i.e. a material which has the same mechanical properites for all directions perpendicular to the direction of the fibre, but different properties in the direction of the fibres). Elastic properties (i.e. Young moduli E, shear moduli G and Poisson's ratios ν) of such material are functions of those of fibre and epoxy, as well as of volume fractions (i.e. ratios of the volume of particular materials to the volume of the whole structure) of fibre and epoxy in the structure.

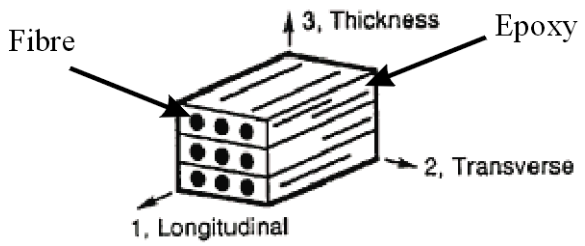


***Fig.3 Optical fibre embedded in epoxy.***

Modelling steps in this method are summarised in Figure 4. The whole process is performed as follows. Based on fibre and epoxy elastic parameters, as well as on fibre diameter, elastic properties of corresponding orthotropic material are calculated using formulae known from mechanics of materials. Subsequently, a Finite Element model is created using elastic parameters of this material and its analysis is performed. From this analysis values of stress and strain in the orthotropic materials are obtained in in the post-processing stage. Values of strain and stress in fibre and epoxy are calculated based on these data using another set of mechanics-of-materials. Knowing stress or strain in the fibre as well as elasto-optical coefficients of the fibre`s material, a change of optical path length can be calculated.

Several important assumptions are made during this process, which may have an impact on the accuracy of analysis. Firstly, the epoxy, which is assumed to be an isotropic material, may in fact have be an orthotropic material. Secondly, stress and strain across the fibre`s cross-section are assumed to be constant, which may not be the case. Finally, in orthotropic material acoustic wave propagates as a plane wave, whereas in the real structure sound velocities in fibre and in epoxy differ, affecting the way in which an acoustic wave is propagated.

### *2.1. Static analysis*

In order to calculate the sensitivity a two-dimensional axisymmetrical model of the mandrel transducer was created, using elastic properties of an equivalent orthotropic material. The model allowed for easy choice of mandrel dimensions, number of fibre layers, and turns per layer, as well as diameter of the fibre. Here, as well as in all following modelling the ends of the mandrel were fully constraied (i.e. no movement was possible).

Several configurations of transducers were modelled. Example results for transducers having 200 turns of silica glass fibre per layer and using a 125 μm singlemode fibre are shown in Table 1.

Obtained results confirmed theoretical predictions stating that the induced phase change should increase with

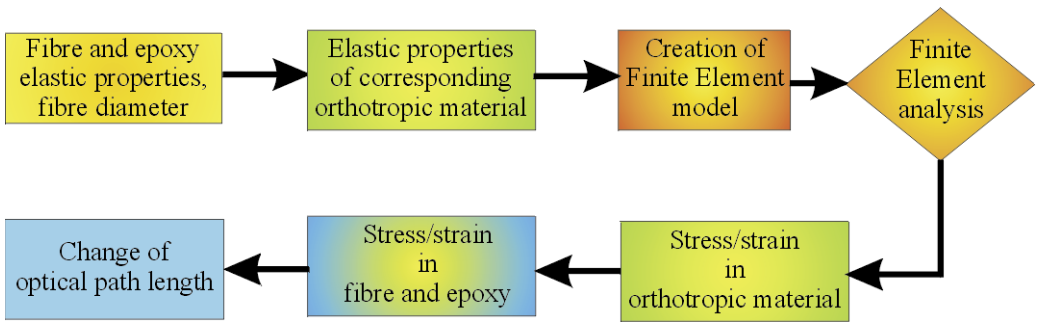


***Fig.4 Finite Element modelling procedure for self-supported air-backed mandrel transducer.***

***Table 1. Phase change induced by pressure of 200 Pa acting on transducer as a function of the number of fibre layers and diameter.***

| radius [mm] | Number of layers | | |
|---|---|---|---|
| | 2 | 4 | 8 |
| 15 | -61.1 | -60.5 | -59.2 |
| 20 | -108.5 | -107.7 | -106.1 |
| 25 | -169.4 | -168.5 | -166.5 |

increasing mandrel radius. An important feature of this transducer is a relative independence of the phase change from the number of fibre layers. This stems from the fact that increasing the number of fibre layers increases the length of fibre subjected to strain, but at the same time increases the stiffness of the mandrel, thereby lowering strain acting on a unit length of fibre. This phenomenon can be taken advantage of for achieving optimum frequency response, i.e. response free form mechanical resonances in the operating frequency band of sensor.

### *2.2. Modal analysis*

An important characteristics of a mandrel transducer is its lowest resonanse frequency. As a rule a transducer should be operated below its first resonanse frequency to assure constant sensitivity and flat phase characteristics.

In order to investigate properties of different mandrel designs modal analysis was used to calculate the frequency of the lowest resonanse mode. In modal anaysis it is not possible to take advantage of the symmetry, as certain resonance modes may not be identified if a simplified model (e.g. 2-D axisymmetrical) is used.

Therefore, a model made from 3-D shell elements was used. The lowest resonance frequency was ranging from 1.5 kHz to 4.5 kHz, depending on the number of fibre layers and number of turns per layer. In all instances the lowest resonance mode was ‘quasi-bending’ mode, shown in Figure 5.

It should be noted, however, that the analysis presented above was conducted for a transducer suspended in air, rather than for one immersed in water. Therefore, calculated resonance frequencies should be treated with caution.

### *2.3. Coupled-field acousto-mechanical modelling*

A Finite-Element coupled field acousto-mechanical analysis of mandrel hydrophones is difficult, especialy if the range of frequencies is broader than a decade. On one hand domain in which the model is located cannot be

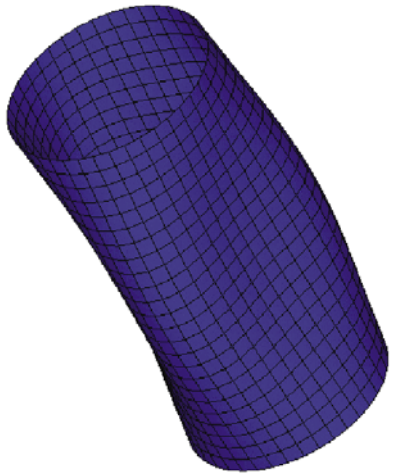

***Fig.5 Lowest resonance mode of an air-backed self-supported mandrel transducer.***

smaller than 1/10 of the ***longest*** wavelength used in analysis (1.5 m for 100 Hz in water) to allow for effective suppression, by special attenuating elements, of acoustic wave reflected from the boundary of the domain. On the other hand, maximum size of an element cannot be bigger than 1/10 of the ***shortest*** wavelength used in analysis (7.5 mm for 20 kHz in water) in order to avoid excessive distorsion of high frequency waves propagating in the domain. Finally, in order to preserve a good shape of finite elements in the thin walls of the mandrel, element size in that part of the model has to be kept below 1 mm. This creates a significant difficulty in interfacing the mandrel to the rest of the model.

Taking into account limitations of available software, a two-dimensional model was built and tested, instead of a full 3-D model. Modelled mandrel had radius R=25 mm, 8 layers of of 125 µm glass fibre, 100 turns per layer. Plane strain state was assumed in the mandrel. Source of the sound was modelled as a stiff plate with harmonic displacement boundary conditions applied to it. Resulting Finite Element model is shown in Figure 6.

After preliminary tests, the response of the transducer was calculated for frequency range 100 Hz – 15 kHz. Young modulus of coating/epoxy was 4 GPa. As it can be seen in Figure 4.4, a mechanical resonance is present in the transducer at around 4 kHz, limiting the useful frequency range to approximately 2 kHz. Subsequently, Young modulus of coating/epoxy was increased to 8 GPa and analysis was repeated. As seen in Figure 7, magnitude of the induced phase shift is lower, but the resonance frequency shifted to around 6-8 kHz, increasing the useful frequency range to approximately 3.5 kHz.

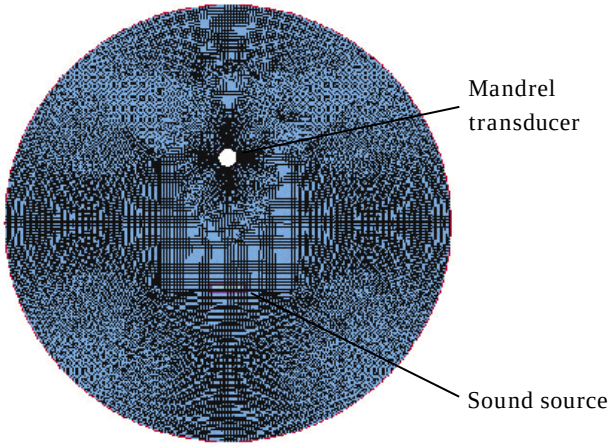


*Fig.6 Finite element model of air-backed self-supported mandrel transducer immersed in water.*

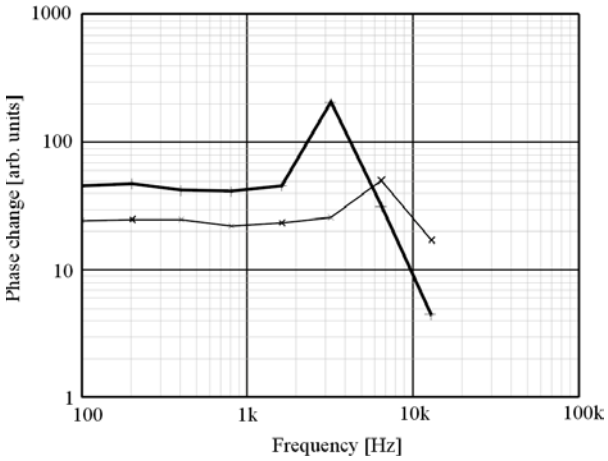


*Fig.7 Frequency response of an air-backed self-supported mandrel transducer. -+- – $E_{coat}$=4 GPa, -×- – $E_{coat}$=8 GPa.*

From the data presented above it can be seen that sensitivity can be traded for increased bandwidth. However, it seems extremely unlikely that a transducer having sufficient sensitivity and a useful frequency range over 10 kHz can be built using this design. Moreover, as stated in the previous Section, by using a two-dimensional model certain resonances may not detected.

### 3. CONCLUSIONS

A novel design of an interferometric hydrophone transducer is presented and principles of its modelling are described. Modelling results indicate that this transducer can be used in low to medium frequency applications. Its sensitivity can be traded off for operating bandwidth, with operation up to 10 kHz seeming possible. Moreover, its sensitivity can be further improved by using a low diameter (e.g. 80μm) optical fibre.

### 4. ACKNOWLEDGEMENTS

Authors would like to thank Hannu Lahtinen from University of Oulu for fruitful discussions and encouragement. Moreover, a scholarship of the Finnish Academy for Pawel Wierzba is acknowledged.

### REFERENCES:

1. S. Knudsen, A. B. Tveten, A. Dandridge ja K. Blotekjaer: Low frequency transduction mechanisms of fiber-optic air-backed mandrel hydrophones. Proceedings of 11th International Conference on Optical Fiber Sensors (OFS'11), Japan Society of Applied Physics, 1996, pp. 208-211

Pentti Karioja
***Pentti.Karioja@vtt.fi***

Paweł Wierzba
***Gdansk University of Technology, Dept. of Optoelectronics, Narutowicza 11, PL-80952 Gdansk, Poland.***

# Increased Conductivity in $H_2$ Annealed of $In_2O_3$-$SnO_2$ Thin Films


***ABSTRACT***

Single-layered $In_2O_3$-$SnO_2$ coatings, with an Sn/(Sn+In) ratio of 25-50 at.-%, were fabricated by a spin-coating method using coating solutions prepared from tin and indium 2-isopropoxyethoxides. The electrical conductivity of the air- and $H_2$-annealed samples was analyzed. The maximum conductivity for the air-annealed samples was obtained with the smallest investigated Sn content, being 24 S/cm. However, $H_2$ annealing induces a massive irreversible increase in the conductivity of the films with the specific Sn content of 30-40 at.-%. The highest reproducible relative conductivity increase was 7600 % (1 S/cm → 76 S/cm). The effect of the $H_2$ annealing on the chemical composition and the crystal structure of the fabricated films was investigated.


## *1. INTRODUCTION*

Impurity-doped indium oxide (ITO, where Sn/(Sn+In) ~ 9 at.-%) is conventionally used in transparent conducting films in optoelectronic devices. However, research and development of alternative materials with enhanced physical properties and reduced cost due to the lower amount of expensive indium is rapidly expanding as well. Some ternary oxides have shown promising results, such as $GaInO_3$, $Zn_2In_2O_5$, $In_4Sn_3O_{12}$, $ZnSnO_3$, and $Zn_2SnO_4$ [1,2].

Sol-gel processing of ternary oxides has only been reported for $In_6WO_{12}$ thin films [3]. The reason for this may be in the relatively low conductivities achieved for the sol-gel-derived single-layer impurity-doped binary oxides (Sb:$SnO_2$ [4] and ITO). However, the conductivities of sol-gel films can be enhanced via suitable post-treatment techniques, either by creating oxygen vacancies in the material [5] and/or by removal of the oxygen depletion layer at the grain boundaries [6]. This can be achieved via plasma treatments or annealing of the samples under reducing atmosphere [2,7,8].

We have investigated the sol-gel fabrication on ternary $In_4Sn_3O_{12}$ single-layered coatings. Even though, the expected ternary $In_4Sn_3O_{12}$ oxide phase [9,10] was not detected in X-ray powder diffraction (XRD) measurements; the $H_2$ annealing was found to strongly affect the conductivity of some formed binary-binary $SnO_2$-$In_2O_3$ films. In this paper, we report on the effects of the precursor composition and annealing on the electrical and optical properties of the $In_2O_3$-$SnO_2$ films fabricated via the single layer sol-gel process.

## *2. EXPERIMENTAL*

Alkoxide solutions used were prepared using commercial Indium(III)isopropoxide ($In(OPr^i)$) and tin(IV)isopropoxide ($Sn(OPr^i)$) as precursors. The Sn/(Sn+In) ratios in coating solutions ranged from 25 to 50 at-%. Sample films were prepared from solutions via spin coating. The deposited films were then dried at 140°C for 30 minutes, after which they were further annealed in a belt furnace under air atmosphere in order to crystallize the materials. In addition to this, some samples were further annealed in $H_2/N_2$ atmosphere using the same furnace and temperature program.

Electrical and optical measurements were recorded of the air- and (air+$H_2$)-annealed slab films deposited on borosilicate glass substrates. Film thicknesses were also mea-

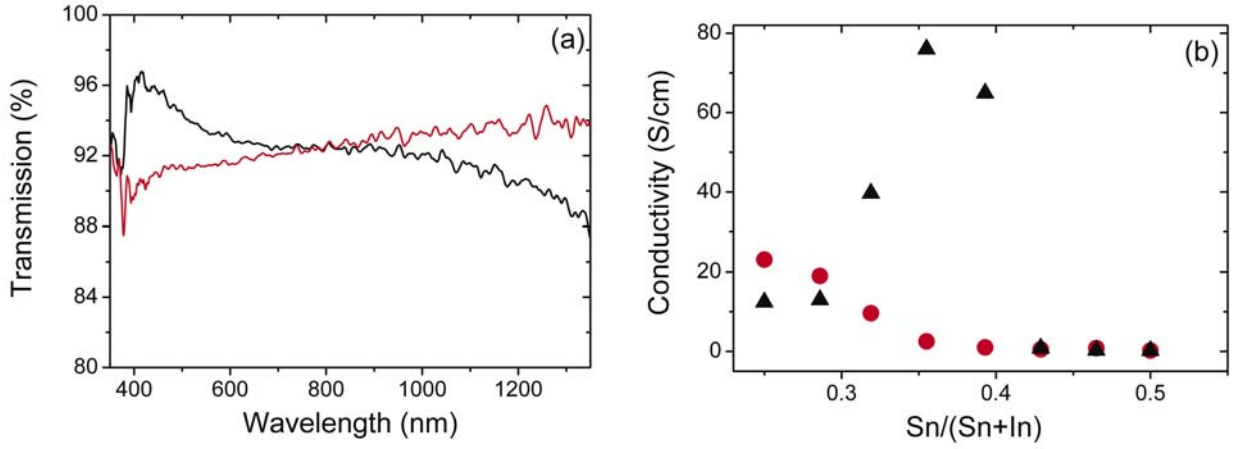


***Figure 1. a) Optical transmissions of (—) air-annealed and (—) air-annealed + $H_2$-annealed samples. Film thicknesses were 70 nm and an Sn/(Sn+In) ratio of 35.5 at.-% for both samples. b) Electrical conductivity as a function of increasing Sn at.-% of air-annealed samples (●) and Air- and $H_2$-annealed samples (▲).***

sured. Sheet resistances ($R_s$) were measured using a linear four-point method. The composition of films deposited on Si-substrates was investigated using XPS. X-ray powder diffraction was applied to the crystal structure studies of films deposited on Si-substrates.

### 3. RESULTS AND DISCUSSION

#### 3.1 Electrical and optical properties

The air- and $H_2$-annealed coatings had transmission values higher than 85 % at visible wavelengths. The main difference between the spectra of investigated air- and $H_2$-annealed highly conducting samples is the decreased transmission at near-infrared region, probably due to the increased carrier concentration [11]. In Figure 1a, transmission spectra of air- and $H_2$-annealed samples with an Sn/(Sn+In) ratio of 35.5 at.-% are shown as an example.

The electrical conductivities of the air-annealed films (60-70 nm) increased with decreasing Sn levels as shown in Figure 1b. The maximum conductivity value for air-annealed samples was 24 S/cm, which corresponds to a sheet resistance value of 6200 Ω/□.

In the case of (air+$H_2$)-annealed samples, the conductivities were not monotonically related with the decreasing Sn levels. For the films with high Sn contents, hydrogen annealing did not provoke changes in conductivities. (Air+$H_2$)-annealed films with low Sn contents yielded conductivities below those measured for the samples annealed in air only. However, at around Sn/(Sn+In) ratios of 35 at.-% the $H_2$ annealing had increased the films' conductivities markedly. The maximum conductivity measured, 76 S/cm at 35.5 at-%, corresponds to a sheet resistance of 1950 Ω/□.

#### 3.2 Chemical composition and crystal structure

According to the high-resolution XPS surface measurements, all the tin detected on the surface of the air-annealed films had only a chemical state ($Sn^{4+}$), while the (air+$H_2$)-annealed film also had a minor component indicative of reduced Sn. The partial reduction of Sn may also account for the somewhat lower O/(Sn+In) ratios of the hydrogen-annealed samples.

The Sn/(Sn+In) ratios in the air-annealed samples were higher than the nominal ones for all the samples. For the (air+$H_2$)-annealed sample, the Sn/(Sn+In) ratio was below the nominal value and the sputter profiles for both indium and tin were more even throughout the bulk of film. According to the XRD measurements, all the measured samples were polycrystalline and with patterns corresponding to $In_2O_3$. However, the background intensities for the (air+$H_2$)-annealed samples were somewhat lower, which seems to indicate a decrease in amorphous material (in the film or at the films-substrate interface). Furthermore, the relative intensity of the reflection at 33° was much reduced after the hydrogen annealing, see Figure 2. The reason for that lowering is not fully understood at this point, but it clearly indicates some phase changes due to the $H_2$ annealing.

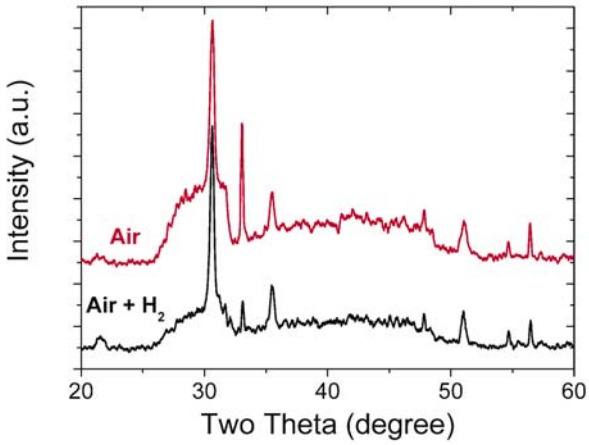


***Figure 2. XRD diffractograms of (—) air-annealed and (—) air-annealed + $H_2$-annealed samples with Sn/(Sn+In) ratios of 35.5 at-%.***

### 4. CONCLUSIONS

We have studied the effects of the reductive annealing and mixing ratios on the properties of thin films with an Sn/(Sn+In) ratio of 25-50 at.-%, fabricated by spin coating. $H_2$ annealing was found to induce a clear, irreversible increase in the film conductivity at Sn/(Sn+In) ratios around 35 at-%. In all the films studied, hydrogen annealing was also found to enhance partial reduction of the tin and a decrease in oxygen content on the surface; the latter might contribute to higher conductivity via oxygen vacancies. However, we also found that the hydrogen annealing caused a reduction in amorphous material and the formation of a diffusion layer at the films-substrate interface. XRD measurements did not show any sign of the expected formation of ternary $In_4Sn_3O_{12}$. XPS and XRD analysis gave us some hints about the processes affecting the drastic increase of the conductivities at the certain Sn content region. However, much more intensive work is required in order to fully understand the phenomena.

***REFERENCES***


1. T. Minami, J. Vac. Sci. Technol. A 17, 1765 (1999).
2. A.J. Freeman, K.R. Poeppelmeier, T.O. Mason, R.P.H. Chang, and T.J. Marks, MRS Bull. 25, 45 (2000).
3. W.S. Dabney, N.E. B.S. Luisi, A.P. Richard, and D.D. Edwards, Thin Solid Films 411, 192 (2002).
4. G. Gasparro, J. Pütz, D. Gantz, and M.A. Aegerter, Solar Energy Materials & Solar Cells 54, 287 (1998).
5. D. Kohl, Sensors and Actuators 18, 71 (1989).
6. S.–S. Park, and J.D. Mackenzie, Thin Solid Films 274, 154 (1996).
7. T. Kololuoma, and J.T. Rantala, Electr. Lett. 26, 172 (2000).
8. T.D. Senguttuvan, and L.K. Malhotra, Thin Solid Films 289, 22 (1996).
9. T. Minami, Y. Takeda, S. Takata, and T. Kakumu, Thin Solid Films 308-309, 13 (1997).
10. N. Nadaud, N. Lequeux, M. Nanot, J. Jove, and T. Roisnel, J. Solid State Chem. 135, 140 (1998), and references therein.
11. J.R. Bellingham, W.A. Phillips, and C.J. Adkins, J. .Mat. Sci. Lett. 11, 263 (1992).



Terho Kololuoma
***Terho.Kololuoma@vtt.fi***



Arto Maaninen
***Arto.Maaninen@vtt.fi***

Leena-Sisko Johansson
Joseph M. Campbell
***Helsinki U. of Technology, Centre for Chemical Analysis, P.O.Box 6100, FIN-02015 TKK, Finland***

Juha T. Rantala
***Silecs Oy, Tietotie 3, FIN-02150 Espoo, Finland***

# Low-cost Differential Refractometer Using Sol-gel Integrated Waveguides

### *1. INTRODUCTION*

Optical sensors using integrated optics implementations of common-path differential interferometer have been the subject of research for over a decade[1]. A planar or a rib single-mode waveguide, which is used as a sensing element, changes its birefringence as a result of refractive index changes of the medium in which it is immersed. As a result, a phase difference is introduced between polarisation modes propagating in the sensing waveguide. The combination of a long sensing waveguide (up to 30 mm) and high-resolution ($10^{-4}$ rad) detection setups using micro-interferometric techniques yields a very high resolution of the measurement. Apart from refractive index measurement, differential interferometer sensors can be used to measure relative humidity [1] or as a biosensor to detect the binding of analyte-molecules to a specific capture layer on the waveguide surface [2]. The influence of temperature can be eliminated by suitable sensor design and by two-wavelength or two-waveguide operation[2].

However, this sensor can exhibit problems typical to fibre optic chemical sensors, such as hysteresis or performance deterioration in a hostile environment. Moreover, for certain applications a low-cost disposable sensor is preferred, as the development of fully reversible reactions is not economically viable.

The authors decided to address these shortcomings by employing recent advances in sol-gel technology, which enables low-cost batch manufacturing of single mode waveguide structures. These structures, which can be protected by a layer of low refractive index chemically inert materials, can form a platform for a (bio-) chemical sensor or can be used for refractive index measurement. Manufacturing issues of sol-gel waveguides are presented in this paper and the modelling of waveguides is discussed. The potential applications of the sensors are discussed as well.

### *2. SOL-GEL MATERIALS AND POLYMER PLANAR WAVEGUIDES*

In contrast to techniques such as conventional inorganic sol-gel technology, sputtering, thermal oxidation, chemical vapour deposition (CVD), plasma enhanced CVD, flame hydrolytic deposition, low temperature sol-gel technology avoids using high temperature treatments (over 1000°C) or multi-step etching processes. Due to the good workability of materials and low cost of processing, the sol-gel process has become an appealing technique for manufacturing optical integrated devices in a single process.

Photopatternable ORMOSILs (organically modified silanes) have been investigated in recent years due to the simplification of processing and temperature compatiblity with on-silicon processes. The inorganic network within the ORMOSIL's improves thermal stability, scratch resistance and hardness of material, whereas an organic network ensures good flexibility, toughness and compatibility with various polymer substrates [3,4,5]. Figure 1 shows a typical example of ORMOSIL's structure employed in sol-gel processing.

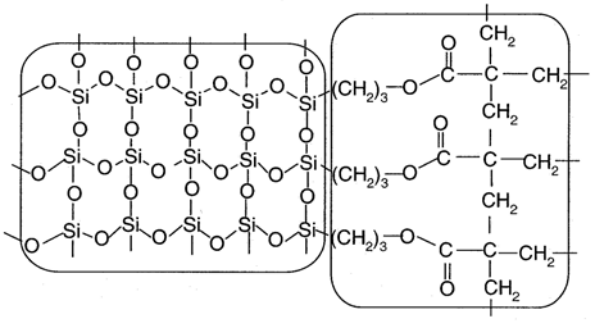

***Figure 1: Picture of organically modified silane used in sol-gel processing.***

Sol-gel processed thin films have tunable refractive indices that can vary in range from 1.3 to 1.6 and their optical birefringence is easy to obtain. Optical attenuation values start from 0.1 dB/cm and thickness is in the range of 0.5-100 μm.

Waveguides made of sol-gel, organically modified materials can be made using various, relatively simple, low-cost techniques such as embossing, UV-irradiation through the binary mask and direct laser writing.

Various materials can be used in each of these techniques. Possible substrates are glass, quartz, semiconductor material wafer, metals and plastics. The most appealing approach is roll-to-roll embossing of the waveguide structures on polymer films coated with sol-gel waveguide material. This method would significantly lower production costs , and make integrated optics components more feasible. Figure 2 shows a 1x4 splitter made of organical-

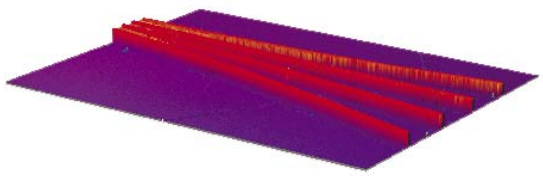

***Figure 2: Interferometer, 3D image of a sol-gel splitter processed on a PET plastic substrate.***

ly modified, sol-gel material, which was processed using UV-irradiation through the patterned binary mask. The 1x4 splitter was processed on polyethyleneterephthalate (PET) polymer foil.

### 3. PRINCIPLE OF SENSING AND SENSING STRUCTURES

Optical sensors using integrated optics implementations of common-path differential interferometer have been the subject of research for over a decade [1]. A planar or a rib single-mode waveguide, which is used as a sensing element, changes its birefringence as a result of refractive index changes of the medium in which it is immersed.

Polarised light is launched into a rib waveguide in such way that the two lowest waveguide modes, i.e. TE and TM are excited with equal amplitudes (Figure3).

Propagation constants of the two modes, $\beta_{TE}$ and $\beta_{TM}$, depend on refractive indices $n_w$ and $n_s$, as well as on the refractive index $n_m$ of the medium surrounding the waveguide. Phase difference $\Delta\phi$ between TE and TM modes existing in the waveguide can be expressed as:

$$\Delta\phi = (\beta_{TE} - \beta_{TM})l$$

where ***l*** is the length of the waveguide, and is a function of the refractive index $n_m$. If ***l*** = 10 mm, measurement resolution of $n_m$ can be as good as $10^{-6}$.

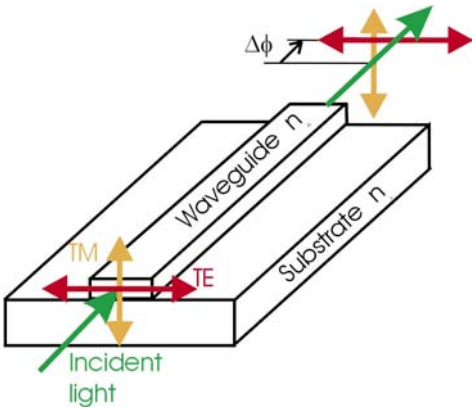


***Figure 3: Principle of sensing.***

Figure 4 shows examples of sensing structures in the case of biosensing. Shape and thickness of the protective coating can be used to modify propagation characteristcs of the waveguide and mode field distribution. The desired antigen, in the case of the biosensor type, can be attached to the waveguide surface by the surface modification of the waveguide itself, or by special modifications of the waveguide materials in the synthesis steps.

### 4.MEASUREMENT OF PHASE DIFFERENCE AND SENSOR SET-UPS

The most accurate method of phase difference between TE and TM modes is based on Multi-Channel Polarimetry with a resolution up to 2π/2000 rad and Wollaston or Nomarski Prisms with a resolution up to 2π/1000 rad.

The measurements are performed as follows. TE and TM modes are collimated by lens CL (Figure 5). Nomarski (or Wollaston) prism NP changes propagation directions of TE and TM modes, so that they make angle α. Polariser A brings the modes into interference, creating a fringe pattern on the CCD detector. The position of the fringe pattern depends on the phase difference $\Delta\phi$, which is to be measured.

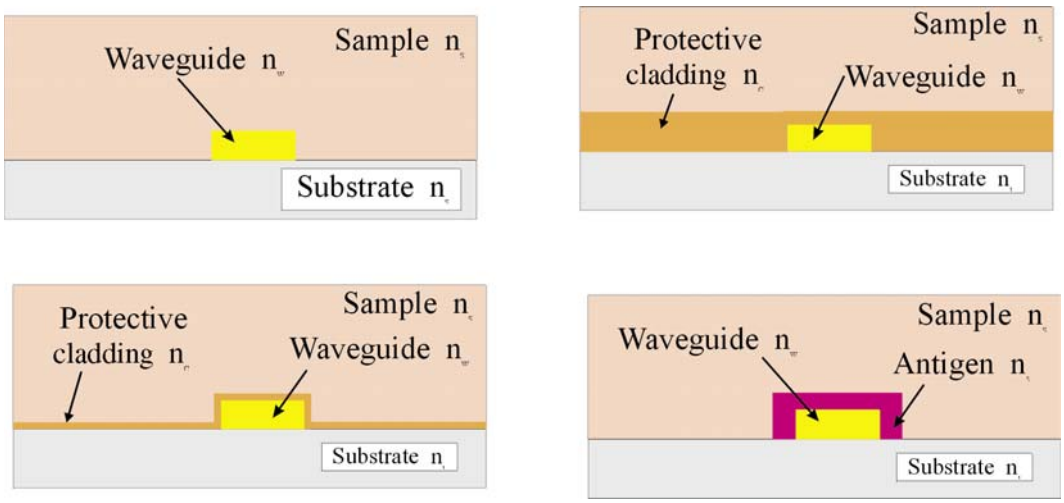


***Figure 4: Examples of the bio-sensing, integrated optics structures.***

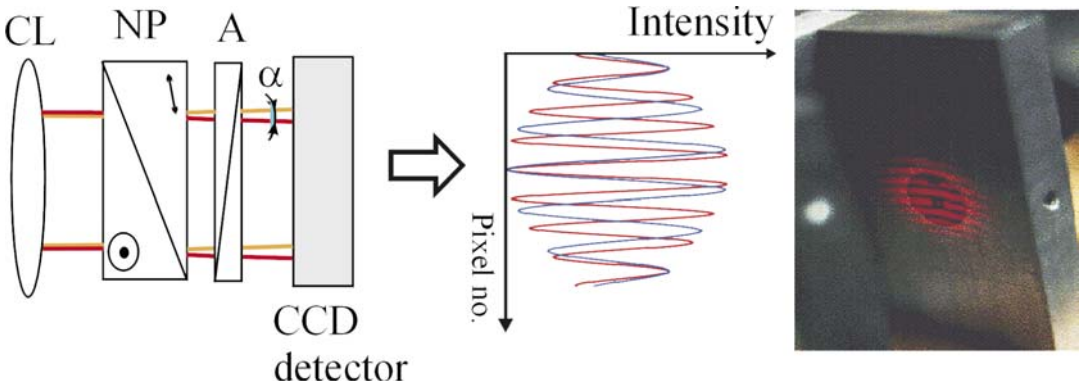


***Figure 5: Phase difference measurement set-up.***

Figure 6 shows examples of the sensors set-up in which sol-gel waveguides can be employed. The substrate used in these cases can be made in the future from cheap, plastic materials and the waveguide component can be processed using low-cost, mass production techniques, such as embossing.

Two methods for the modelling of the sensor can be employed, and they are Finite Element Method (FEM) and Beam Propagation Method (BPM). The primary objectives of the modelling are the investigation of mode field distribution in a broad range of structures, optimisation of light interaction with the sample (or anti-gen layer), and optimisation of coupling between the light source and sensing structure. Also, measurement should be made temperature independent.

Repeatable coupling of light into the sensing structure is an existing problem. Tolerances better than 1 μm and long term alignment are required. If a disposable sensing part is used, the active alignment is necessary. (Figure 7)

To eliminate the influence of the temperature problem the measurement of phase difference must be carried out for two wavelengths or a sensing part design with temperature compensation must be developed.

The cost of the optical part of the sensor can also be a problem. Due to alignment needs and the use of polarising components the cost is relatively high (around 1000USD).

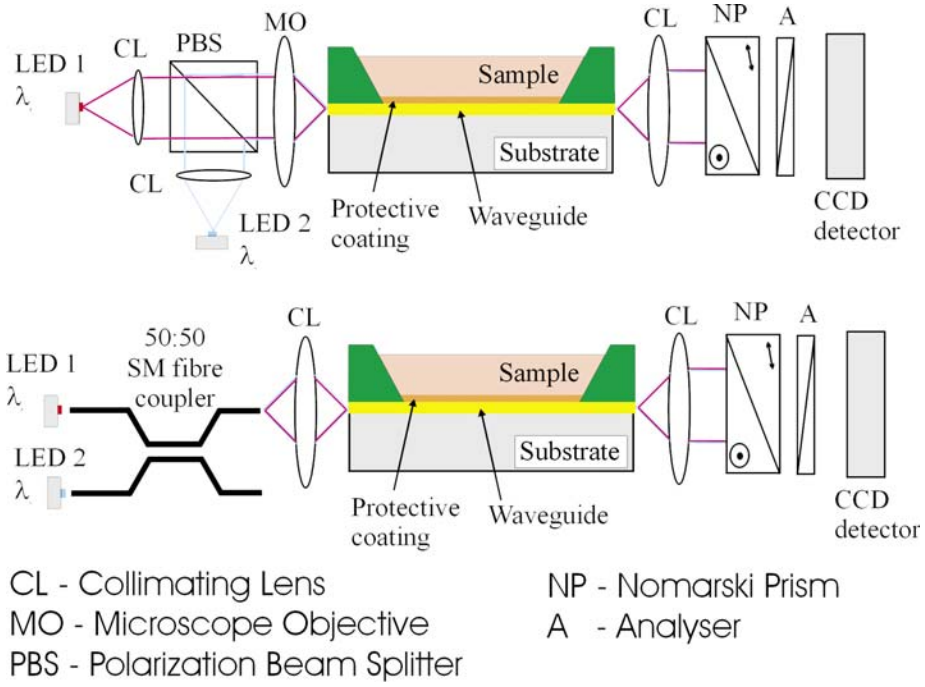


***Figure 6: Integrated optics sensors set-ups.***

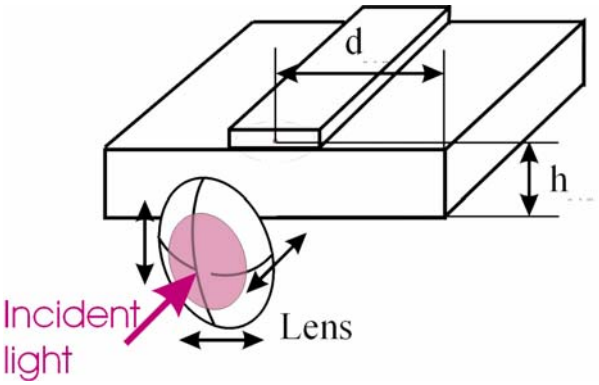


***Figure 7: Coupling of the light.***

### *5. CONCLUSIONS*

Differential refractometers using sol-gel integrated waveguides are a promising group of sensors with a broad range of potential applications. They allow a complex refractive index to be measured with a high resolution, based on which detection of several chemical compounds can be implemented. Designs with disposable sensing part are possible. As a result, chemical reactions that are not reversible can be used, which significantly broadens the scope of use of such a sensor.

Further modelling and experimental research is needed in order to assess the properties of these sensors. Currently, the most important obstacle to the widespread application of the presented sensors is the repeatability of launching light into the sensing structure.

### *6. REFERENCES*

1. W. Lukosz, Ch. Stamm, "Integrated Optical Interferometer as Relative Humidity Sensor and Differential Refractometer", ***Sensors and Actuators A***, 25-27, 185-189 (1991).
2. Ch. Stamm, R. Dangel, W. Lukosz, "Biosensing with the integrated-optical difference interferometer: dual-wavelength operation", ***Optics Communications*** ,153 347–359 (1998).
3. A. H. Kärkkäinen, J. T. Rantala, A. Maaninen, G. E. Jabbour, and M. R. Descour, "Siloxane based hybrid glass materials for binary and grayscale mask photoimaging", ***Adv.Mat***. 14 (7), 535-540 (2002).
4. W. Que, Y. Zhou, Y. L. Lam, Y. C. Chan and C. H. Kam, "Optical and microstructural properties of sol-gel derived titania/organically modified silane thin films", ***Thin Solid Films*** 358, 16-21 (2000).
5. S. I. Najafi, T. Touam, R. Sara, M. P. Andrews amd M. A. Fardad, "Sol-gel glass waveguide and grating on silicon", ***J.Lightw.Techn.***16(9), 1640-1646 (1998).

Maja Kusevic
***Maja.Kusevic@vtt.fi***

Pentti Karioja
***Pentti.Karioja@vtt.fi***

Pawel Wierzba
Marcin Gnyba
***Gdansk University of Technology, Department of Optoelectronics, ul.Narutowicza 11, PL-80-952 Gdansk, Poland***

# Mechanical and Electrical Properties of HeraLock ® HL2000 Zero Shrink Low Temperature Co-fire Ceramics

### *I. INTRODUCTION*

The increasing need for low cost and electrically functional materials has reinforced the place of low temperature co-fired ceramic (LTCC) technology as a key foundation of high frequency modules and components. Conventional free shrinkage LTCC has many benefits, but there are some key drawbacks. Typical x,y- shrinkage is 13% ±0.2% leading to several problems. Internal metallization patterns should be in a favorable way to avoid warpage. Due to the high dimensional tolerances, accurate solder paste printing on a large panel is problematic. The shrinkage also causes an unrecoverable loss in available surface area for circuit layout, especially in the case of large panels with multiple numbers of circuits.

There are several methods for the co-firing of LTCC laminates, where the x,y- shrinkage can be reduced practically to zero, thus enabling very small dimensional tolerances. In these methods, the laminate is constrained during firing to prevent the x,y- shrinkage. In practice, the shrinkage is transferred to the z plane. The constraining mechanism enables very small dimensional tolerances and can, if well designed, re-balance the forces that lead to lack of flatness. Therefore, 100% solid ground planes are possible for shielding. Another benefit of constrained sintering compared to the free sintering method is that the number of circuits from the same laminate area is increased typically 20...40%.

The constraining is typically accomplished by using constraining tape layers which are laminated on both sides of the LTCC stack. Also, pressure can be applied during sintering to constrain the x,y- shrinkage. After firing, the constraining layers need to be mechanically removed, which is an extra process step. The constraining tape can also reduce the freedom of choice of co-fired top layer materials due to risk of unwanted interactions.

The latest innovation in zero shrink LTCC processing is a self-constraining tape system, developed by Heraeus. In the new HeraLock ® technology, the HL2000 LTCC tape consists of two separate layers. Another layer contains particles of glass, ceramic and organic binder and another, self-constraining layer, consists of refractory ceramic and wetting agent.

The processing of the HeraLock system (HL2000 tape) is similar to the processing of free sintered LTCC substrates. In practice, the x,y- shrinkage can be reduced to close to zero. Typically, z shrinkage is 29%. The HeraLock system potentially offers the same benefits as the conventional constrained sintering methods - improved accuracy and increased number of parts/panel, but without any additional process steps. This will give a clear cost benefit. Cost efficiency is further increased if low cost green cutting is used for the part singulation. For the other zero shrink LTCC processes, a costly dicing process must be used. Also, co-fired surface conductors can be used for the HeraLock system.

This paper presents some results of the mechanical and electrical performance of the HeraLock system.

### *2. PROCESSING*

A 5” x 5” test circuit consisting of 8 tape layers was manufactured for the characterization of high-frequency properties of HL2000. The test circuit contained, e.g., microstrip lines and resonators. The vias were filled using stencil printing. Conductor lines were screen-printed with 325-mesh screen except in the case of surface conductors, where 400-mesh screen was used. The main difference in the processing was a lower lamination pressure, compared to other LTCC systems. This was required to allow the organic binders to evaporate properly from the LTCC substrate during the co-firing process. In these experiments, the lamination pressure was as low as 1000 psi, whereas 3000 psi is typically used in the free sintering LTCC process.

### *3. RESULTS*

The x,y- shrinkage of HeraLock substrates was as low as 0.2% with the tolerance of ±0.04%. A photograph of an 11” x 7” part cut on the diagonal whilst unfired is shown in Fig. 1. One half was fired and then re-matched to the other half, which is still unfired. The lack of shrinkage is clearly visible.

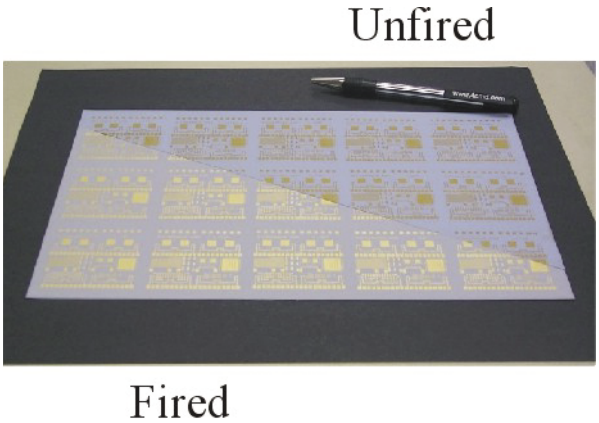


***Figure 1. Photograph of a single part divided to show lack of shrinkage during firing.***

The repeatability of printed and fired line width was excellent. The variation of the surface line width was ±3 µm. Fig. 2 shows a photograph of a round spiral inductor with a line width of 90 µm.

***Figure 2. Spiral inductor with line width of 90 µm.***

The S-parameter measurements were made by a network analyzer at the frequency range 4-40 GHz. Table 1 shows the normalized mean attenuation values for 110 and 220 µm wide microstrip lines, and Table 2 presents the normalized attenuation values of microstrip ring resonators calculated from the measurements.

***Table 1. Average attenuation values [dB/cm] of 110 and 220 µm wide microstrip lines.***

| Frequency [GHz] | 4 | 20 | 40 |
|---|---|---|---|
| 110 µm line width | 0.17 | 0.71 | 1.12 |
| 220 µm line width | 0.12 | 0.56 | 0.94 |

***Table 2. Normalized attenuation values [dB/cm] of microstrip ring resonators at peak frequencies.***

| Frequency [GHz] | 5.7 | 11.2 | 16.7 |
|---|---|---|---|
| Attenuation [dB/cm] | 0.145 | 0.305 | 0.375 |

Straightforward comparison between different technologies is difficult due to different geometries and material parameters. However, some estimation can be made. It can be found out that HeraLock values are comparable with the conventional Heraeus LTCC system CT2000 and better than the DuPont 951 tape or most of the PWB systems.

### *4. CONCLUSIONS*

Mechanical and electrical properties of HeraLock ® HL2000 were studied. It offers very small shrinkage of 0.2% with the tolerance of ±0.04%. It was shown that the attenuation of this LTCC tape system is competitive with other, more traditional LTCC tapes, even at millimeter waves. The good high-frequency performance together with dimensional accuracy open many application fields for this novel tape system.

Markku Lahti
***Markku.Lahti@vtt.fi***

Kari Kautio
***Kari.Kautio@vtt.fi***

# Fabrication and Characterization of Optical Polymer Waveguides Embedded on Printed Wiring Boards

***ABSTRACT***

In this study the low-cost planar multimode (MM) polymer waveguides have been fabricated into printed wiring boards (PWB). For this purpose, the commercially available optical poly(methylmetacrylate), polyolefin, epoxy and polyimide were evaluated and used for the fabrication of waveguides with the lithographic rib-cladding and groove-filling fabrication processes. The key optical properties such as the refractive index, intrinsic absorption and birefringence of the tested materials were characterized. In-plane ($n_{TE}$) and out-of-plane ($n_{TM}$) refractive indices (RI) of the slab waveguides were measured by using the prism coupling method at the wavelengths of 633...1550 nm. The calculated birefringence values $\Delta n$ ($n_{TE}$ - $n_{TM}$) showed that the PMMA, the polyolefin and the epoxy exhibited very low birefringence, which is a required property of the polarization independent passive components. The RI maps were used in the cladding/core design, after which the waveguides were fabricated by employing the polymers having 3-5% difference in the refractive index. The absorption losses measurements with the prism coupling showed 0.1...0.5 dB/cm intrinsic absorption. With the selected materials, passive optical waveguide test structures (straight and bent waveguides, splitters, and crossings) with rectangular cross sectional shapes were also fabricated. The optical loss of the resulting waveguides was measured using the waveguide cut-back method.

***1. INTRODUCTION***

In fast evolving communication world the combination of optical and electrical technologies enables large quantities of data to be generated and transported at very high rates and with minor losses over long distances. The short-range on-board high-speed (~10Gb/s/ch) optical interconnections are currently under intensive investigation in many laboratories worldwide. Majority of the optical interconnection realizations are based either on free space connects with diffractive elements or on guided wave connections [1-3]. Although optical fibers can provide high information carrying capacity in point-to-point connections, they are not feasible in high-density circuitry mainly due to that viable solutions for volume production are not available and because of difficult optical passive component fabrication. Therefore, the most promising guided wave technologies for chip-to-chip routings are based on integrated optics, which permit production of photonic circuits on planar means. Although polymers have higher intrinsic losses, inferior thermal stability and mechanical properties compared with currently used silica-based glasses or semiconductor materials, they are particularly attractive because of the ability to be processed easily at low temperatures on several low-cost substrates.

In recent years, intensive research activities have been carried out of to develop low-loss optical polymers and some are currently commercially available [4]. Typical polymer classed used in optical applications include acrylates, polyimides, polycarbonates, olefins and epoxies. In addition to limited availability of high performance optical polymers, major technical challenges are related to the cost-efficient waveguide fabrication, package integration, efficient light coupling and beam turning, and robust automatic optical component assembly. Furthermore, as an immature technology, photonics suffers from lack of standardized package designs, several fabrication problems and insufficient or unknown reliability of materials and packages.

To address some of the aforementioned challenges, the feasibility of selected commercial polymer systems as optical on-board interconnections will be studied in this paper. The key optical properties of the selected polymers are characterized. Two lithographic-based waveguide fabrication processes will be demonstrated. The reliability of the waveguides is characterized by interfacial adhesion test and by studying the stability of the optical properties under changing temperature and when exposured to air pollutants.

***2. MATERIALS AND METHODS***

In order to implement the optics into printed circuit boards, the compatibility of the optical polymers with the board materials and processes was set as the primary criterion in materials' screening. Several low-loss optical polymers conventionally used in plastic fibers such as polycarbonates, styrene plastics and polyolefins, are available only in foils or granules, and therefore they can not be utilized by liquid deposition methods, like spin deposition or roller coating. On the other hand, majority of the high performance polymer systems, like fluorinated polyimides, halogenated acrylates or polysiloxanes are designed for silicon based integrated optics and usually not thick film process scalable. This in turn is a problem, when tolerance relaxed large-cored waveguide devices are fabricated on-board level.

The other qualitative screening parameters for the optical waveguide materials were:

- High optical transparency
- Refractive index match

- Low birefringence
- Excellent adhesion to polymer substrates
- Easy application and processing
- Scalability to thick film processing
- Good long-term stability under various environmental conditions
- High heat resistance
- High moisture resistance
- CTE matching to PWB substrate

From the commercially available polymers, poly(methylmethacrylate) (950KPMMA, MicroChem), highly crosslinked multi-functional acrylate-based photopolymer (Truemode, Teraherz Photonics), epoxy-based glycidyl ether derivative of bisphenol-A novolac (SU-8, MicroChem), cyclo-olefin copolymer (Topas, Ticona), and polyimide (PI2525, DuPont), were selected for waveguide evaluation. Additionally, a mercaptoester optical adhesive (NOA, Norland Adhesives) was selected for index matching purposes. Selected properties of the materials are given in Table 1.

The polymer waveguides were optically characterized for their in-plane ($\boldsymbol{n}_{TE}$) and out-of-plane ($\boldsymbol{n}_{TM}$) refractive indices, intrinsic absorption and birefringence. Measurements were carried out by using the Metricon prism coupling method. The adhesion of the cladding/core polymers was measured with pneumatic stud-pull method. The stability of the optical properties of the selected waveguide polymers was tested under temperature cycling (IEC 68-2-14N) and flowing multi-gas (IEC-68-2-60) tests. Structural characterization was carried out by optical and scanning electron microscopy (SEM).

### *3. WAVEGUIDE FABRICATION PROCESS*

The large cored 50-150 x 50-100 μm (width x thickness) step index waveguides with the refractive index profile Δn of 0.03...0.05 were fabricated on the IS410 (ISOLA AG) 0.7 mm thick and 10x10 cm sized FR-4 substrates. Because the available refractive index (RI) tunable polymers mostly failed in other selection criteria, step index structures were fabricated by combining the existing optical-grade polymers. Large index profile and core dimensions were designed to increase the coupling efficiency and allow greater tolerance in optoeletronic component assembly.

The two lithography-based, groove-filling and rib-cladding processes were used in waveguide formation (Figure 1). In the rib-cladding process, the waveguides cores are photopatterned on top of under-cladding and sealed with upper-cladding polymer coating. The waveguide cores are formed of higher index polymer cladded with the lower index material to result total internal reflection (TIR) waveguiding structure. In the groove-filling waveguide fabrication process, the optical core/cladding layers are formed into photodefined groove structures by one- or two-step filling process. In the two-step filling process, additionally the under cladding is deposited into the grooves. Waveguide processing was carried in the 100-class cleanroom environment. Grooves were filled with similar squeegee blading process that is used in SMD paste printing. Photopatterning by UV lithography or direct laser writing enables well-defined structure formation on large area substrates and smooth sidewalls as compared with the replicative fabrication methods for example embossing.

***Table 1: Some properties of the selected optical polymers.***

| | Tradename | | | | | |
|---|---|---|---|---|---|---|
| | 950KPMMA | Truemode | SU-8-50,2000 | Topas 5013 | Pyralin PI2525 | NOA 81 |
| Material | PMMA | Acrylate | Epoxy | Polyolefin (COC) | Polyimide | Mercapto-ester adhesive |
| Manufacturer | MicroChem | Teraherz Photonics | MicroChem | Ticona | DuPont | Norland |
| Patterning Technique | Lithographic | Lithographic | Lithographic | Inj. mold, embossing, extrusion | RIE | Dispense |
| Thickness (um) | 1-5 | 1-200 | 1-2000 | 1-100 | 1-20 | 1-100 |
| CTE (ppm) | 54-72 | 60 | 47-57 | 60-70 | 40-50 | 210 |
| Tg (C) | 95-105 | 180 | 200 | 135-140 | 320 | 30 |
| Water Absorption (%) | 0,3-0,4 | -- | 0,08-0,15 | <0.01 | 0,3 | 0,16 |

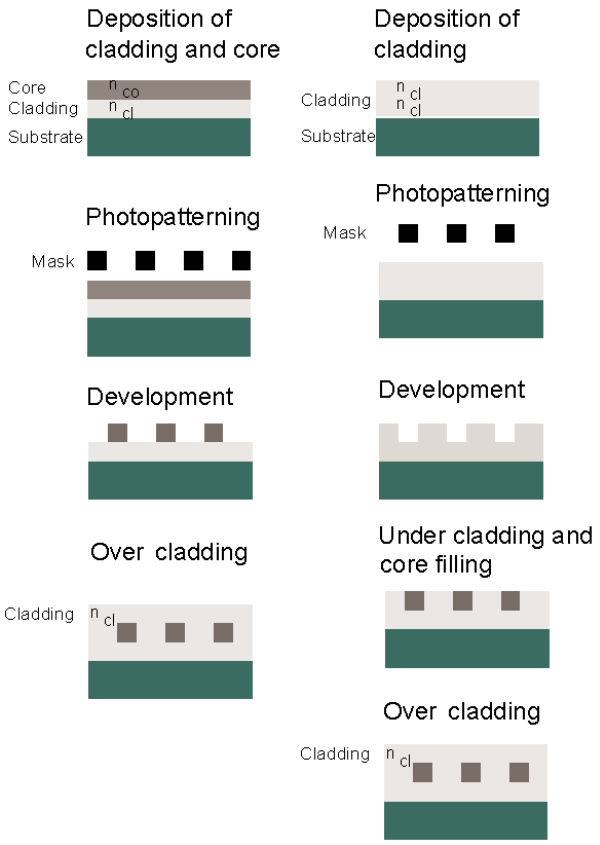


***Figure 1: Lithographic rib cladding and groove filling waveguide fabrication processes.***

The 5-inch lithographic mask with dark and light field test geometries was designed. The optical test geometries contained straight waveguides of 5-10 cm in length and 25-200 µm in width. Line/space designs resulted 250-µm pitch to be coupled to a standard arrayed optoelectronic component. Other passive test structures were 45/60/75/90-degree x-junctions, 1x4 couplers and bendings with differing radius angles.

### *4. RESULTS AND DISCUSSION*

The refractive indexes ($\boldsymbol{n}_{TE}$, $\boldsymbol{n}_{TM}$) of the tested polymers were measured with the Metricon prism coupling method at the wavelengths of 633/830/1300/1550 nm. The measurements were carried out of the slab waveguides fabricated quartz glass substrate, the $n_{TE}$ values are presented in Figure 2. As the optical properties depend on the process parameters and application (such as laminate characteristics, degree of cure, molecular orientation in spin deposition, thermally induced internal stresses) the data given by vendor can be used only as referential. The lowest absorption losses (< 0.1 dB/cm) at all wavelengths were obtained with the acrylate-based 950KPMMA and True-mode polymer (the latter measured from the preformed sample). Other tested polymers resulted 0.3 - 0.5 dB/cm absorption at 830 nm.

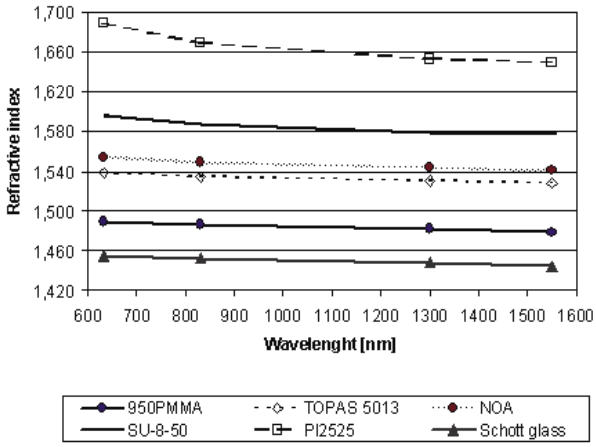


***Figure 2: In-plane refractive indices ($n_{TE}$) of the tested materials measured using prism coupling method.***

The modeling results of the effects of process induced waveguide imperfections such as micro-cracks and side-wall rouhgness showed that signal attenuation as a result of scattering can easily cause total functional failure of the light transmission even at relatively short transmission lengths. Therefore, even though the optical structures are geometrically similar to those formed in electronic circuits, the optics require well-defined structures and highly smooth surfaces. From the selected materials, epoxy-based negative acting SU-8 polymer had shown very low roughness measured with Atomic Force Microscopy (AFM) [5], excellent surface planarization, and patterning characteristics and was therefore used as structural layer in groove filling waveguide fabrication process. The modeling results are presented in [6].

The refractive index maps were used in cladding/core material design. Examples of the optical waveguide fabricated by two lithography-based processes are presented in Figures 3 and 4.

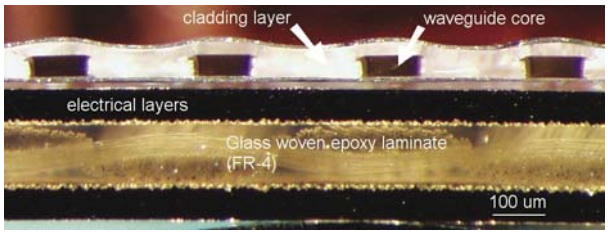


***Figure 3: Cross section sample of the epoxy cored COC/SU-8/COC waveguides on FR-4 substrate.***

***Figure 4: PMMA/SU-8/PMMA waveguides on FR-4 substrate fabricated with two-step groove filling process. After photolithographic waveguide groove structure patterning, 950PMMA is deposited by spinning as undercladding. SU-8 waveguide cores are then squeegee printed and top-cladded with PMMA cladding layer.***

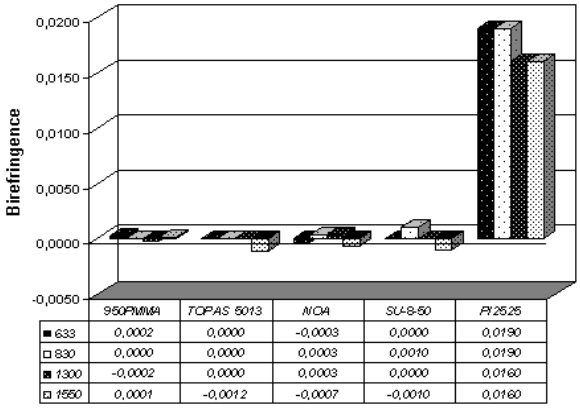


| | 950PMMA | TOPAS 5013 | NOA | SU-8-50 | PI2525 |
|---|---|---|---|---|---|
| ■ 633 | 0,0002 | 0,0000 | -0,0003 | 0,0000 | 0,0190 |
| □ 830 | 0,0000 | 0,0000 | 0,0003 | 0,0010 | 0,0190 |
| ■ 1300 | -0,0002 | 0,0000 | 0,0003 | 0,0000 | 0,0160 |
| □ 1550 | 0,0001 | -0,0012 | -0,0007 | -0,0010 | 0,0160 |

***Figure 5: Birefringence (Δn) of the tested polymers processed as slab waveguides on quarz glass substrate.***

The calculated birefringence values Δn ($\boldsymbol{n}_{TE}$ - $\boldsymbol{n}_{TM}$) showed that in addition to acrylate-based polymers (950KPMMA and Truemode), the cyclo-olefin copolymer (Topas) had very low birefringence. A nonzero n value indicates that the material is anisotropic and therefore birefringent. This has an effect to the polarization dependent loss, which is not allowed in waveguide applications. The polymers that have three-dimensionally cross-linked structure have intrinsically very low birefringence values, because they do not suffer orientation during polymerization. However, the birefringence of the cured layer do not depend only on the polymer composition and film thickness, but also the substrate where it is processed. Low coefficient of thermal expansion (CTE) especially in inorganic substrates like quarz or silicon result that the substrate is much more firm than waveguide polymer film applied on top of it. When the substrate-waveguide system is cooled, the optical film tends to shrink more than substrate and stress-induced birefringence is caused. When optical polymer waveguide layers are deposited on an organic substrate, significant reduction of the birefringence and thus polarization independency is achieved.

As the waveguides were fabricated by using two different polymers in cladding/core layers, intrinsically good wetting characteristics of the materials was required. Even though chemical surface treatments like plasma or RIE would promote the adhesion, these cannot be used in cladding/core interface because the treatments roughens the surface to improve the adhesion and this in turn lowers the cladding/core surface smoothness causing signal attenuation as a result of scattering. The cladding/core interfacial adhesion was characterized by using the pneumatic pull-stub adhesion test. It was found that of the tested core/cladding systems PI/epoxy, epoxy/PMMA and epoxy/COC, polyimide's adhesion to epoxy was 83% higher when compared to that with PMMA and over 250% when compared with epoxy/COC. To study the effects of the environmental stresses on the above mentioned waveguide systems, the specimens were further subjected to changing temperature, humidity and exposure to air pollutants. These test results are presented in Ref. [7].

The stability of the waveguide materials' optical and mechanical properties was studied by exposing the slab waveguides for thermal shock (IEC 68-2-14N +125°C/-45°C, dwell 15min/15min) and air pollutants in flowing multi-gas (IEC-68-2-60, $NO_2$ 200±20ppb, $SO_2$ 200±20ppb, $H_2S$ 100±20ppb at the 75±5% RH/30±2°C) reliability tests. After 170 h in thermal shock and 500 h at the flowing multi-gas testing period, negligible change of refractive index or absorption was observed in the prism coupling measurements. Additionally, no delamination or peeling off from the substrate was observed. As a conclusion, the selected polymers showed acceptable optical characteristics and environmental stability under the reliability tests conducted. Yet, to characterize the long-term reliability of the polymers, longer tests should be conducted.

### *5. SUMMARY AND CONCLUSIONS*

In this study, optical polymer waveguides were fabricated on printed circuit boards. The optical properties of the se-

lected commercially available poly(methylmetacrylate), polyolefin, epoxy and polyimide were measured by using prism coupling and cut-back methods. The processability and compatibility to selected substrates were evaluated. The polymers with the absorption losses of 0.1-0.5 dB/cm in the datacom wavelength region were screened for further tests. The stability of the waveguide materials' optical and mechanical properties was studied under environmental temperature cycling and flowing multigas reliability tests.

The results showed that lithography process can be used to fabricate low-loss polymer optical waveguides on FR4-based substrates. Yet, the lack of available photo-patternable high performance polymers limits the wide implementation of the optical technology. Additionally, since the photonics employ variety of designs comprising of dissimilar materials, many new reliability and fabrication challenges are met. In addition, several issues relating to packaging and integration are to be solved before optics can be implemented efficiently and cost-wise into printed wired boards.

### *6. ACKNOWLEDGEMENTS*

The authors wish to thank M.Sc. Riia Lankinen for her contribution with experimental part of the research and Teemu Alajoki and Jarkko Tuominen for their contribution with the optical measurements. The research was part of ELMO technology program and was financially supported by the Finnish electronics industry and the Finnish National Technology Agency.

### *7. REFERENCES*

[1] Chen, R.T., Lei L., Choi C., Liu, Y.J., Bihari, B., Wu, L., Tang, S., Wickman, R., Picor, B., Hibb-Brenner, M.K., Bristow, J., Liu, Y.S. "Fully embedded board-level guided-wave optoelectronic interconnects" Proc. of the IEEE, Vol. 88 Is. 6, 2000. pp. 780–793.

[2] Schröder H., Bauer J., Ebling F., Scheel W. "Polymer Optical Interconnects for PCB" IEEE Proc. Polytronic 2001. pp. 337–343.

[3] Plant, Kirk "Optical Interconnects at the Chip and Board Level: Challenges and Solutions", Proc. of IEEE, Vol. 88, No. 6, 2000. pp. 806–818.

[4] Eldata L., Shacklette L. "Advanced in Polymer Integrated Optics" IEEE J. Sel. Topics in Quantum Electronics. Vol. 6, No. 1, 2000. pp. 54–68.

[5] J. Ge and J.K. Kivilahti "Effects of surface treatments on the adhesion between a multifunctional photoresist and Cu and Cr/Cu metallizations" J. of Applied Physics, 92, p. 3007, 2002.

[7] Turunen M., Immonen M., Kivilahti J.K. "Evaluation of the Environmental Reliability of Polymer Wave Guides Fabricated on Printed Wiring Board", IEEE Proc. of Polytronic 2003, Montreux, Switzerland, 21–23 Oct. 2003, p. 91-95.

Mikko Karppinen
***Mikko.Karppinen@vtt.fi***

Marika Immonen
Jorma Kivilahti
***Laboratory of Electronics Production Technology,***
***Helsinki University of Technology,***
***P.O.Box 3000, FIN-02150 Espoo, Finland***

# Packaging and Component Technologies of Future Electronics

## 1. INTRODUCTION

This report includes surveys of future trends in electronics packaging and component technologies from both international and national standpoints. The emphasis of the report is in the miniatyrisation of electronics and in its consequencies on technologies in the long term. The report is mainly based on existing international roadmaps such as ITRS2002 and the Japanese Jisso Technology Road Map JEITA2001. National views and trend expectations have been studied by a questionnaire list sent to R&D people in the Oulu area electronics industry and research laboratories.

The report reviews the most important technologies in electronics manufacturing, their expectations and needs as well as their relationship to the increasing effectiveness of electronics circuits, increasing memory and data storage capacity, signal integrity and reliability of circuits.

Besides the trends of decreasing dimensions and increasing tolerance demands in electronics, the most important targets of development are increasing modularity of devices, combining of electronics, photonics and mechanical components into the same devices, development of new 3 dimensional design and testing tools and introducing new electronics materials.

## 2. MINIATURIZATION

The investigation shows that miniaturization continues on all levels of electronics realization during the time period of 10 years: increasing wiring density on the silicon chip, increasing wiring density on the substrate, increasing number of wiring layers, increasing contact density of components and stacking of silicon components into 3D-structures. As shown in Figure 2, there are clear growth expectations for MEMS components, optical components, active polymer based components and nanotechnical components.

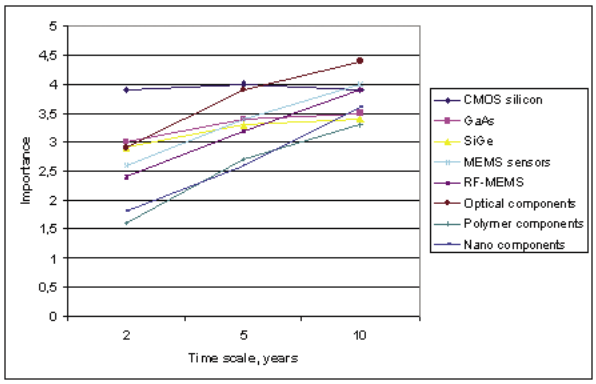


***Figure 2. Trends in component technologies for the time scale 2 – 10 years. Scale 1...5 for importance.***

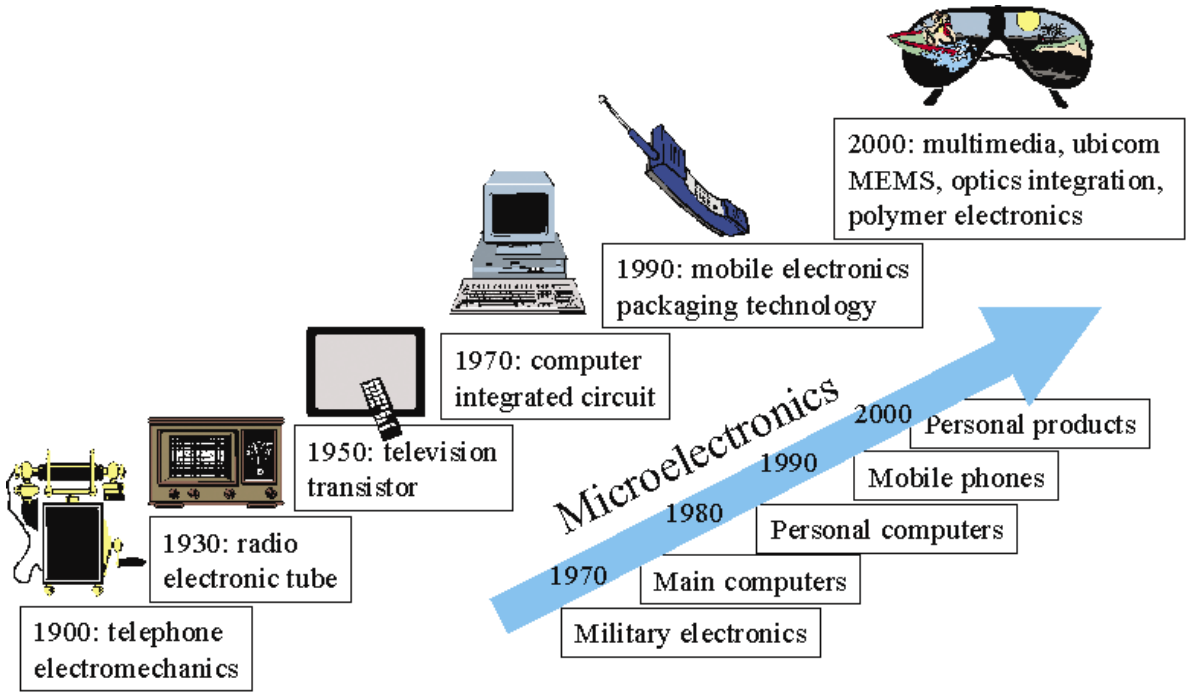


***Figure 1. Applications as well as related innovations and technologies in the area of telecommunication.***

### *3. TRENDS*

The next 10 years in electronics is going to be a very interesting time period because the decreasing dimensions of components will come nearer to atomic dimensions. The new processing technologies for component manufacturing will require enormous investments and development work. In interconnection and packaging technologies the challenges are in more and more complicated systems, where the design and testing will become very difficult.

Implementation of photonics and new polymeric materials, as well as new bioelectronic applications, requires new types of skills compared with those offered by traditional education of electronics engineers. Finland should provide conditions for new fields in electronics application and participate in development of new technology solutions. This requires investment in research, development and education.

Miniaturization is not an end in itself in electronics. Instead, the driving force comes from the applications, e.g. in mobile telecommunication. Nowadays the actual electronics have only a share of 10 per cent of the size of a mobile phone. The user interface, display, mechanics, antenna and battery take the major part of the volume. The development in miniaturization however makes it possible to add new functions and improve its performance, e.g. increasing its capacity in data and image transfer.

Miniaturization and new cost effective packaging concepts are needed in applications related to ambient intelligence where small size intelligent sensors are utilized. New manufacturing technologies based on polymer electronics make possible the implementation of electronics and optoelectronics in completely new application areas such as in consumer packages and printed matter.

The complete report in Finnish is obtainable from the following address: www.vtt.fi/inf/pdf/tiedotteet/2003/T2213.pdf

Jaakko Lenkkeri
***Jaakko.Lenkkeri@vtt.fi***

Tuomo Jaakola
***Tuomo.Jaakola@vtt.fi***

Terho Kololuoma
***Terho.Kololuoma@vtt.fi***

Mikko Karppinen
***Mikko.Karppinen@vtt.fi***

Tero Majamaa
***Tero.Majamaa@faf.mil.fi***

# Reliability of Solder Joints of LTCC Modules

### 1. INTRODUCTION

Low temperature co-fired ceramic (LTCC) technology is a multilayer electronic packaging technology, which has arisen much interest because of its capability to provide high-density packaging solutions with good performance at high frequencies. Applications of LTCC technology often require joining of LTCC modules on a printed circuit board. Solder lands on an LTCC module are usually made from a silver-based metallization, which reacts upon soldering with the solder alloy, causing some concern of the reliability of the module [1-3]. The joint structure resembles that of a ceramic BGA (CBGA) on a printed circuit board with a distinction in the solder land metallization on the module side, however. The reliability estimations of CBGA on FR-4 are thus not valid in the case of LTCC modules on FR-4.

The present investigation is aimed at determining the fatigue life, the failure modes and the reasons for failure in LTCC module / FR-4 joints during thermal cycling. Special attention was given to the metallurgical reactions between Sn and Ag-Pd and Sn and Ag-Pt metallizations [4-6].

### 2. EXPERIMENTAL

The LTCC modules were manufactured using the DuPont 951 tape material. The three different test structures for the attachment of solder balls (10Sn90Pb) onto LTCC are depicted in Figure 1. In the standard structure the balls were attached onto AgPd pad with 62Sn36Pb2Ag solder, in the cavity (depth 0.13 mm) structure the pad was placed one tape layer inside the LTCC, and in the third structure the metallization was of AgPt and a solder resist partly covering the pads was also used. The size of the balls was 0.89 mm, the pitch was 1.5 mm and the balls were placed in matrix form (9x9....20x20). The LTCC modules were reflow soldered onto an FR-4 PCB using the same solder as used for ball attachment onto LTCC. A daisy chain type of connection as shown in Figure 2 was used.

The reliability assessment of the LTCC assemblies was accomplished by exposing them to thermal cycling in temperature ranges of 0 - 80°C, 0 - 100°C and -40 - 125°C. A minimum of 5 minutes' dwell time at the temperature extremes was applied to allow creep/stress relaxation. The ramp rate was limited to less than 5°C/minute in such a way that the cycle times were 1 h (0 – 100°C) and 2.4 h (-40 – 125°C). The solder joint integrity of the high-DNP joints was monitored by measuring resistance changes in the daisy chain networks.

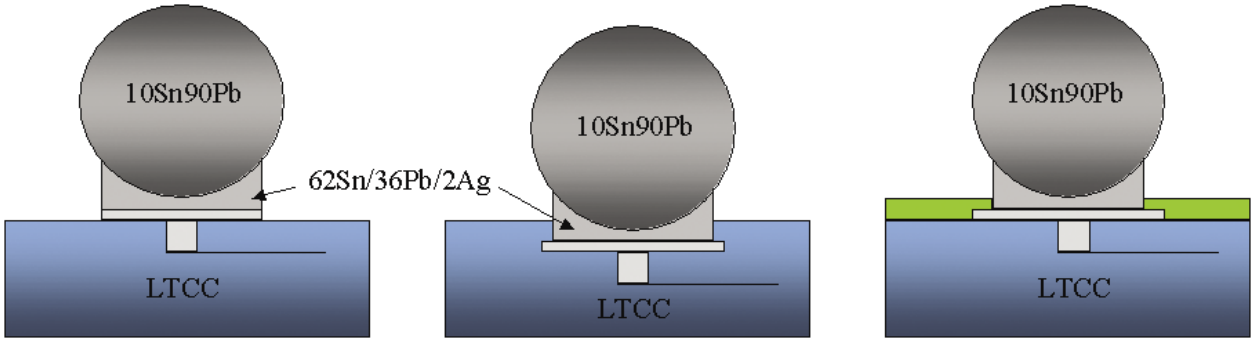


***Figure 1. Solder ball attachment structures: standard (left), cavity (middle) and standard with AgPt metallization and solder resist (right).***

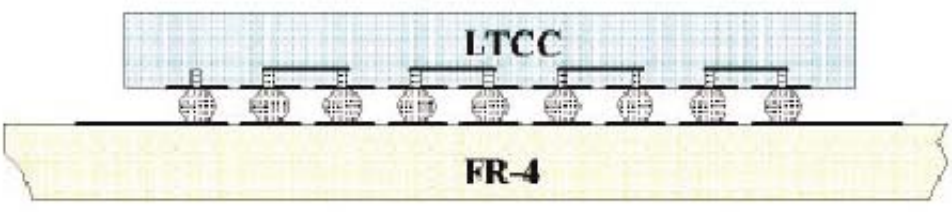


***Figure 2. The LTCC modules were connected using a daisy chain pattern.***

Modules were examined during the thermal cycling test using a Sonoscan D-9000 C-mode scanning acoustic microscope to investigate the initiation and propagation of thermal fatigue cracks in solder joints. The microstructures of the solder joints and fatigue cracks were characterized using a Jeol MS 6400 scanning electron microscope. The element composition in particular areas of the solder joints was evaluated by energy dispersive spectroscopy (EDS).

### *3. RESULTS*

The measured mean and characteristic lifetimes and the Weibull β – parameter for the different configurations studied are shown in Table 1. One can see that the cavity structure is considerably better than the standard structure, and that the AgPt-metallization with solder resist still further improved the results, especially the β -form factor. The considerable improvement in lifetime was shown when using an HIT/PCB with somewhat lower TCE of 12 ppm/°C instead of FR-4 with TCE of 16 ppm/°C.

***Table 1. -Mean and characteristic lifetimes and the Weibull − parameter for the different LTCC/PCB configurations in tests -40 -125°C and 0 - 100°C.***

| Testi | LTCC/ FR-4 Standard | LTCC/ FR-4 Cavity | LTCC/ FR-4 AgPt/ Resist | LTCC/HIT Standard |
|---|---|---|---|---|
| -40 - 125°C | | | | |
| $N_{mean}$ | 334 | 720 | 919 | 588 |
| $N_{char}$ | 362 | 868 | 1013 | 662 |
| | 5.0 | 2.9 | 11.3 | 3.1 |
| 0 - 100°C | | | | |
| $N_{mean}$ | 3254 | | | 4440 |
| $N_{char}$ | 3575 | | | 4890 |
| | 3.9 | | | 3.8 |

The failure mechanisms in the structures were quite different. Figure 3a shows the propagation route of a crack found in the standard structure. The cracking initiated from the interface between LTCC/conductor (right) and propagated into the ceramic. In the final stage the root of the via cracked. Cycling 5000 cycles in the temperature range 20...80°C produced a very different kind of fatigue crack in solder near LTCC side. The propagation route of cracking in the cavity structure is shown in Figure 3c. The crack propagated through the cavity/ solder interphase, and finally the silver filled via was broken.

The measured failure rate of the modules as a function of cycles for the AgPt/resist -structure is shown in Figure 4a, and the route of propagation of the crack is shown in Figure 4b. In this case, the crack propagated in solder near the solder/conductor interface.

From metallographic studies of the joint structures, it was found that the AgPd metallization dissolves during soldering almost completely, and a thick (30μm) intermetallic layer is formed between the via and the solder containing $Ag_3Sn$ and $PdSn_4$ particles in solder matrix. In the case of AgPt conductor, very little dissolving of conductor into solder is evident, only a thin (1...2μm) layer of $Ag_3Sn$ is formed.

### *4. CONCLUSIONS*

The lifetime of standard AgPd/solder joints was found to be relatively short. The reason for this was the quick reaction with tin and the high tensile stresses during thermal cycling. Longer lifetimes were observed when using PCB with TCE more closely matching that of LTCC. The durability of the joints in cycling temperature range of 20...80°C was found to be higher than expected, this was due to low tensile stresses during the cycling, which inhibits the propagation of the crack into the ceramic. Considerable increase in the lifetimes of the joints was achieved by using the cavity structure. This is caused by the lowering of the tensile stresses during thermal cycling due to the support effect of the cavity walls. Still better lifetimes were achieved with the AgPt pads with solder resist on the sides of the pad. The basic reason for this was considered to be due to the very low reaction between the conductor and solder. In addition, the solder resist supports the metallization and thus inhibits the initiation of cracks between the LTCC/metallization interface.

### *REFERENCES*

[1] Cho, Y.S., Needes, C.R., Souders, K.E., Hang, K.W., Donohue, P.C., Niblett, A.R., Amey,D.A:. “LTCC Ceramic Components on Printed Wiring Boards - The Issues and Potential Solutions”, 2000 International Symposium on Microelectronics proceedings, 20. - 22. Sept. 2000, Boston, USA, IMAPS, 2000, pp. 665-668.

[2] Fu, C-Y., Huang, R-F.: “BGA Reliability of Multilayer Ceramic Integrated Circuit (MCIC) Devices”, The Int. journal of Microcircuits and Electronic Packaging, Vol. 23 (4), 2000, pp 393-399.

[3] Pradhu, A., Schafer, W.J., Patil, S.: High Reliability LTCC BGA for Telecom Applications”, 2000 IEEE/

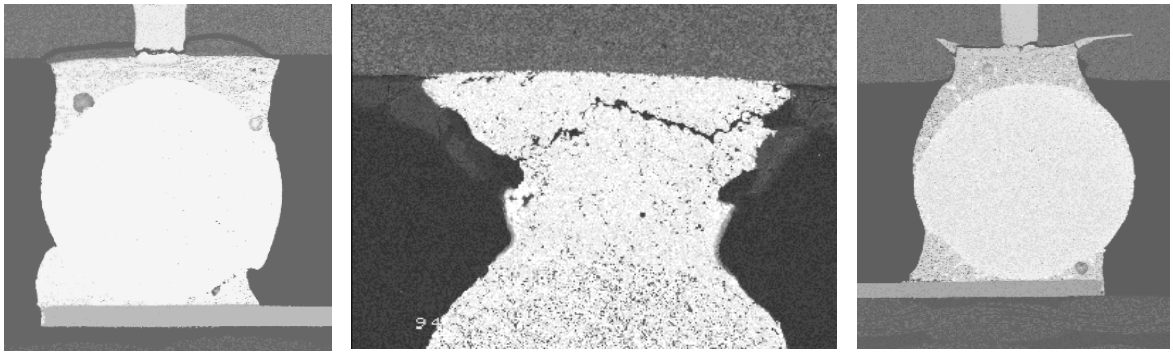

a) -40 - 125°C/standard b) 20 - 80°C/standard c) -40 - 125°C/cavity

***Figure 3. Microstructures of joints with cracking after thermal cycling.***

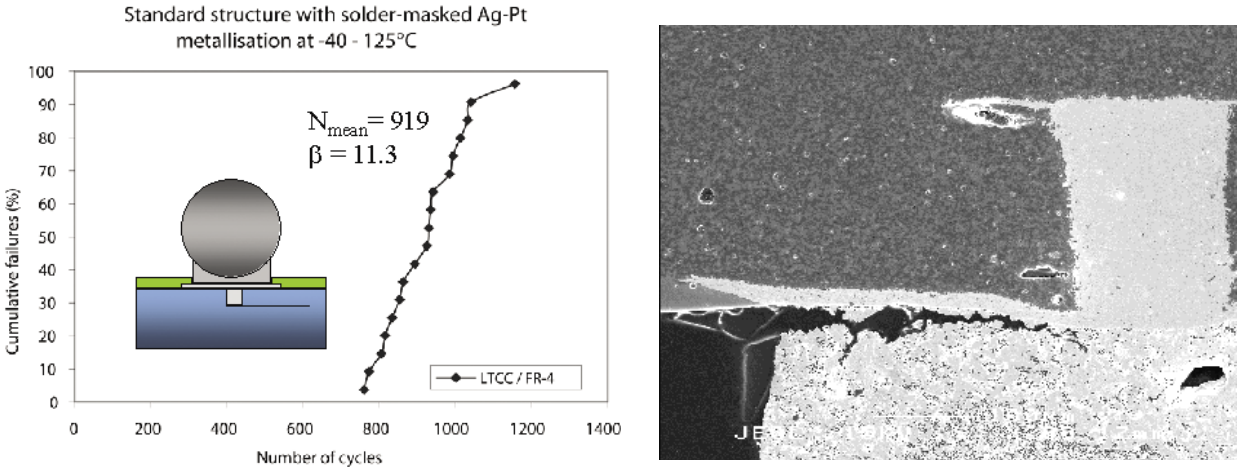


***Figure 4. Cumulative failure as a function of thermal cycles in the temperature range –40...+120°C (left), and a microstructure of the joint after thermal cycling.***

CPMT Int'l Electronics Manufacturing Symposium, pp. 311-323.

[4] Rautioaho, R., Nousiainen, O., Saven, T., Leppävuori, S., Lenkkeri, J.: "Thermal fatigue and metallurgical reactions in solder joints of LTCC modules", Microelectronics Reliablity, Vol. 40, 2000, pp. 1527-1532.

[5] Rautioaho, R., Nousiainen, O., Leppävuori, S., Lenkkeri, J. , Jaakola, T.: "Thermal fatigue in solder joints of Ag-Pd and Ag-Pt metallized LTCC modules", Microelectronics reliability, Vol. 41, 2001, pp. 1643-1648.

[6] Rautioaho, R., Nousiainen, O., Leppävuori, S. and Vähäkangas, J.:"Reliability of solder joints in LTCC / PCB assemblies", European Microelectronics Packaging & Interconnection Symposium, 16. - 18. June 2002, Cracow, Poland, IMAPS, 2002, pp. 153 - 158.

Jaakko Lenkkeri
***Jaakko.Lenkkeri@vtt.fi***

Kari Kautio
***Kari.Kautio@vtt.fi***

Risto Rautioaho
Olli Nousiainen
Jussi Jääskeläinen
***University of Oulu, Materiaalitekniikan laboratorio***

# 20 GHz Wilkinson Power Dividers in LTCC Technology

This article presents some of the results from a collaboration program between VTT and CRC. The program focuses on the application and fabrication of LTCC technology for mm-wave frequency communications. The Wílkinson power dividers presented in this paper have been designed by CRC for the Ferro A6S LTCC system utilising embedded resistors. The test tiles were manufactured by VTT Electronics.

### *CRC BRIEFLY*

The Communications Research Centre (CRC) is the Government of Canada's primary laboratory for research and development in advanced communications technologies. Its R&D addresses rural and remote broadband access, spectrum issues, wireless and satellite communications systems, radio fundamentals, broadcast and multimedia technologies, broadband networks and photonics. CRC (http://www.crc.ca/) is located in the western end of Ottawa, Ontario, and has a technical staff of 220.

### *LTCC PROCESSING*

VTT Electronics has the experience of processing many of the commercially available LTCC material systems (for example, DuPont 951 and 943, Ferro A6S, Heraeus CT 2000 and Heralock). Line width and spacing less than 100 um can be processed with the conductor printing technique, and with UV-sensitive conductor pastes less than 50 um can be realised. The development work for the better quality fine-line conductors is going on practically continuously, using UV-patterning and etching techniques. Some special LTCC materials, like zero-shrink, high- and mixed-K laminates and ferrites, have also been evaluated, as well as the integration of many kinds of passive components and structures.

A very low-loss tape system is desired for millimetre wave applications, and Ferro A6S is one of those systems that is commercially available, and it is one of the most used LTCC systems in VTT Electronics as well.

### *POWER DIVIDERS*

Wilkinson power dividers are important passive components for many communications applications and are widely used in phased array antennae. Development of Wilkinson dividers in LTCC technology will facilitate the integration of phased array signal distribution networks, with the driving electronics and the radiating elements significantly reducing the fabrication difficulties encountered in phased array technology.

A Wilkinson divider allows an input signal to be split equally, and in phase, between the two outputs, and a corporate arrangement of several dividers allows in-phase and equal amplitude signals to be delivered to a multitude of radiating antenna elements. Wilkinson dividers also have high isolation properties due to the use of a 100Ω resistor between the two output arms, which absorbs any reflections coming back to the output ports.

The Ferro A6S LTCC system allows the microwave circuit designer to use resistors ranging from 10 Ω/ to 10 kΩ/. Two types of Wilkinson divider were investigated using 100 Ω/ - a microstrip version and a stripline version.

In its simplest form, a microstrip divider can be positioned on the top surface of an LTCC substrate. However, since the most attractive feature of LTCC technology is the ability to use multiple ceramic layers along with multiple metal layers, the divider will very often be buried within an LTCC system as a stripline component with metallic ground planes above and below the divider. Fig. 1 shows the layout of a stripline Wilkinson divider with one ceramic layer above and below the structure.

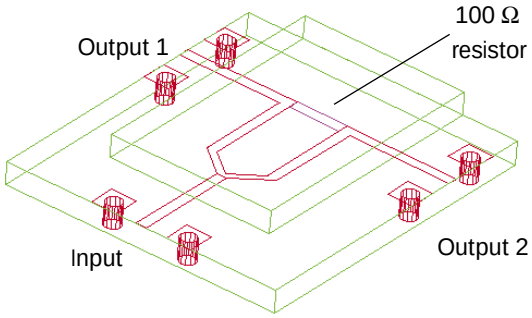


***Figure 1. Wire drawing of a stripline Wilkinson divider.***

Transmission line widths in LTCC depend on the number of layers of ceramic between them and the associated ground planes. While selection of the number of ceramic layers depends on the number and type of circuit functions being integrated together, the positioning of transmission lines in too few or too many layers may make it difficult to realize the desired impedances.

The microstrip and stripline situations not only require different transmission line dimensions but also place different constraints on the fabrication of the resistors. In the case of stripline the resistor is buried within the LTCC material, but in microstrip it can be printed on the top surface of the LTCC. Therefore, the microstrip situation offers an opportunity for resistor trimming if the fabrica-

tion tolerances are too great for the required performance. Multilayer stacking of resistors is an alternative means of reducing the impact of resistor variation, although the interlayer vias used to connect the resistors add reactive impedances to the structure and must be accounted for in the design. An example of a microstrip divider that is being explored using two layers of resistor is shown as a wire drawing in Fig. 2.

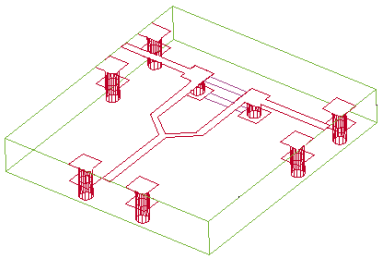

***Figure 2. A microstrip Wilkinson divider with two levels of resistor.***

### POWER DIVIDER TESTING

In order to study the signal distribution performance of LTCC Wilkinson dividers, a series combination of two dividers was designed for operation at 20 GHz. Two microstrip dividers were arranged as shown in Fig. 3 to allow the characteristics of a two-way split to be studied along with those of a four-way split. An input signal at Port 1 will provide a -3 dB split to Port 2 and a –6 dB split to the other two output ports.

The measured results (Fig.4) show that the divider ports are well matched at the design frequency, while the insertion losses are 3.42 dB (Ports 1 to 2), 6.32 dB (Ports 1 to 3) and 6.58 dB (Ports 1 to 4). The excess losses beyond the ideal 3 dB and 6 dB are mostly due to the resistance of the metallization, although there may also be a small amount of signal loss through internal reflection between the dividers and through radiation. The phase balance between Ports 3 and 4 was within 3°.

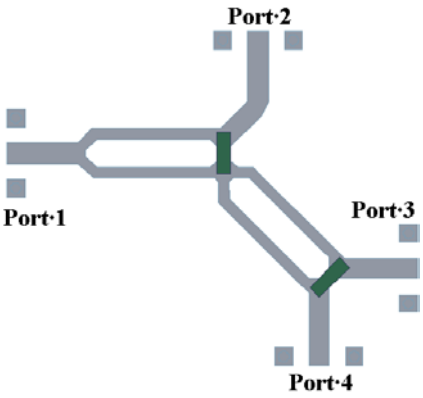


***Figure 3. Layout of two Wilkinson dividers in cascade.***

### CONCLUSION

The Wilkinson power dividers for 20 GHz have successfully been designed and realised in the Ferro A6S LTCC substrate utilising embedded resistors. The achieved performance parameters were good, despite some deteriorative effect on the performance caused by the tolerances of the LTCC resistor.

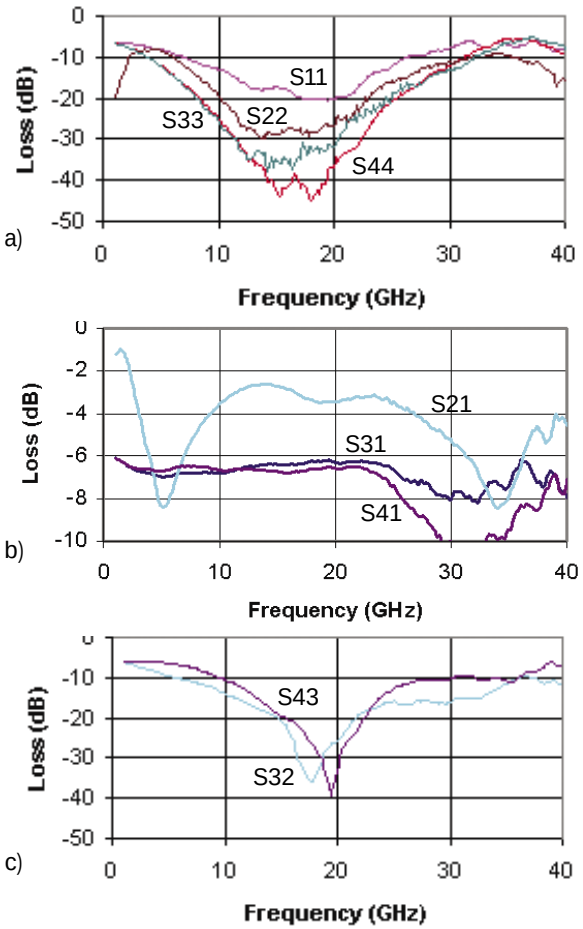


***Figure 4. Performance of cascaded Wilkinson dividers (a) return loss, (b) insertion loss, (c) isolation.***

Alex Panther, Malcolm Stubbs ***CRC***

Kari Kautio
***Kari.Kautio@vtt.fi***

Antti Vimpari
***Antti.Vimpari@vtt.fi***

# Edge-coupled Band-pass Filters in LTCC Modules

### 1. INTRODUCTION

Band-pass filter structures at millimeter waves require typically narrow and accurate conductor lines and spaces. This can be a limiting factor in high-volume production where screen-printing is the most commonly used method. Therefore, the etching technique was used as an alternative when a traditional edge-coupled microstrip filter was studied. This paper presents the realization and measurement results of microstrip filter types.

### 2. MICROSTRIP EDGE-COUPLED BAND-PASS FILTERS

A band-pass microstrip edge-coupled filter was designed and simulated by using Ansoft Ensemble 8.0 simulator. The conductor layer was on the surface of the substrate and the ground layer was 200 µm below it. The size required on the surface was 8 x 4 $mm^2$ and the layout of the designed surface structure is shown in Fig. 1. The designed line widths of W1 and W2 were 200 and 130 µm and the gaps G1, G2 and G3 were 75, 130 and 200 µm, respectively. The length of each resonator was 820 µm.

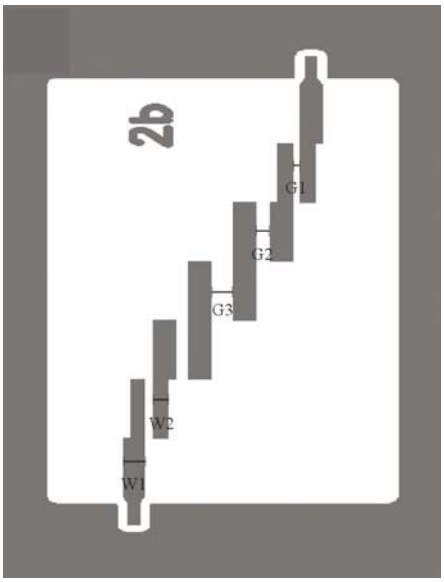


***Figure 1. Layout of the designed microstrip band-pass filter.***

The screen-printed filters were realized on Ferro A6-S tape system using CN33-398 Ag conductor and CN33-343 Ag via fill paste. The surface layer was printed using 400-mesh screen. In the etching technique, 2622D Ag paste was double-printed on top of the fired substrate. Firing was made after both printing steps.

The average line and gap widths and their tolerances were measured, and the results are presented in Table 1. The variation in the mean line widths throughout the filter was quite large in the case of the screen-printed conductors. Also, the tolerances were larger for the printed conductors. A photograph in Fig. 2 shows a typical difference between the printed and etched conductors.

***Table 1. Measured mean dimensions and tolerances of the lines and gaps in the filter structures.***

| | Printed conductors | | Etched conductors | |
|---|---|---|---|---|
| | Mean line width [µm] | Tol. [±µm] | Mean line width [µm] | Tol. [±µm] |
| W1 | 198-218 | 4-5 | 193-196 | 2-4 |
| W2 | 122-136 | 5-6 | 118-125 | 3-4 |
| G1 | 66-77 | 6-9 | 84-84 | 1-5 |
| G2 | 112-129 | 4 | 135-135 | 2-4 |
| G3 | 191 | 7 | 204 | 2 |

***Figure 2. Printed (left) and etched (right) conductors and gap. Designed line and gap widths are 130 and 75 µm, respectively.***

The results of the performance from both filter types are shown in Table 2. Although the accuracy of the conductor lines was worse in the printed conductors, the attenuations and center frequencies of the printed and etched conductors were quite similar. In all structures, the attenuation was less than 1.5 dB at millimeter waves. The main difference was the narrower band-pass in the case of the etched filters as seen in Fig. 3.

***Table 2. Summary of transmission parameter measurements.***

| Filter type | Minimum attenuation [dB] | Center frequency [GHz] | 3-dB relative bandwidth [GHz] |
|---|---|---|---|
| Printed | 1.40 | 42.65 | 7.78 |
| Printed | 1.44 | 42.38 | 7.68 |
| Etched | 1.43 | 42.98 | 6.68 |
| Etched | 1.40 | 42.98 | 6.88 |

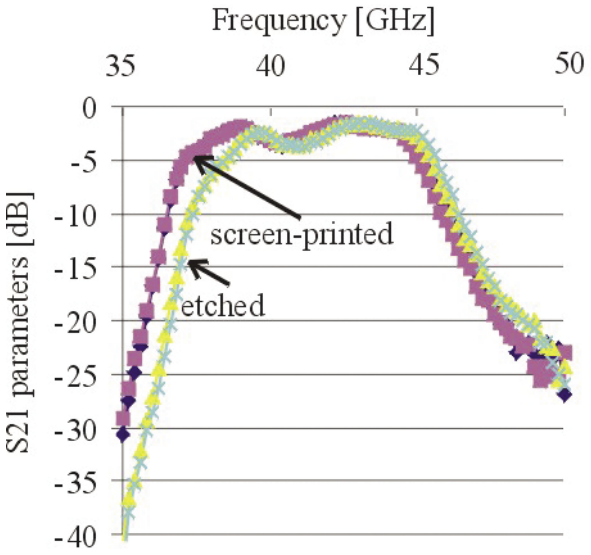


***Figure 3. Transmission parameters of edge-coupled microstrip filters.***

The most obvious and meaningful difference between the printed and etched versions was in the width of the narrowest gap (G1 in Fig. 1). Therefore, the effects of these dimensions were studied more by simulating. The simulations showed that the decrease of the gap width caused a more even band-pass response. Fig. 4 presents a comparison between 2 simulated curves (40 and 80 µm gap width) and the measured etched filter. Removing of a ripple in the band-pass requires the use of a correct manufacturing method. Instead of screen-printing, photoimaging or etching techniques should be used to realize narrow gaps.

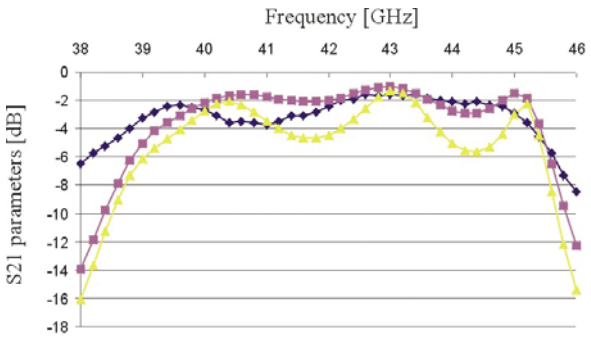


***Figure 4. Simulated (40 (□) and 80 (△) µm gap width) and measured response (◇) of microstrip edge-coupled band-pass filter.***

### *3. CONCLUSIONS*

Two different band-pass filter types were designed, realized and measured at millimeter waves. Dual-mode patch filters resulted in insertion losses less than 3 dB. The repeatability of the performance of the filters was good. The design of the filter package proved to be important. In microstrip edge-coupled filters, the screen-printed and etched filters resulted in quite similar responses in band-pass. The main difference was a steeper edge of the band-pass in the case of the etched filters. The minimum attenuation was less than 1.5 dB.

Markku Lahti
***Markku.Lahti@vtt.fi***

# Millimeter Wave Antennas on LTCC

LTCC (Low Temperature Co-fired Ceramic) -Technology has the capabilities for the integration of the millimeter wave functions in the substrate. In the on-going project, there was a need to design a gain-type antenna integrated in the multi-chip module package. The most interesting solution was a slot-coupled patch antenna array formed by four patch antennas, because then it was possible to place the components on the one side of the substrate and the patch antenna array can radiate out of the other side. The used electromagnetic simulation software calculated the radiation gain of the antenna array to be 8.5 dBi at 42 GHz and the impedance matching in the terms of reflection attenuation to be better than -15 dB over the wanted 40.5 - 43.5 GHz bandwidth.

### *INTRODUCTION*

LTCC-Technology enables the integration of passive electrical functions into the substrate of the electronic device. LTCC itself is a good technology for mm-wave telecommunication applications due to the low-loss and high-performance nature of the utilized ceramic materials and silver conductor metallization. Integrated antennas are commonly of high interest in the mass production telecommunication industry for the cost reduction. Integrated antenna structures are the only reasonable way to realize the high-gain antenna arrays needed in the mm-wave telecommunication to achieve the needed reproducibility of the realized antenna systems.

### *PATCH ANTENNAS ON MM-WAVE BAND*

On the millimeter waves, the patch antenna is the commonly-used antenna type due to the feasible dimensions of the antenna elements. The design dimensions of the mm-wave structures lead to the need of utilizing very accurate conductor patterning techniques. In the case of the current project, the use of the integrated antennas was aimed in the module that has attached mm-wave components on the top of the substrate, and the antenna radiates out of the bottom surface.

The planned concept of the millimeter wave module was directed to design a slot-coupled patch antenna, in which there is a coupling slot in a solid grounded metal layer. The slot must be in the transverse position compared to the feeding microstrip line. That way the use of a via can be avoided. In general, vias are very problematic on the mm-wave frequencies causing very bad reflection to the traveling mm-wave signal if not designed very carefully. The impedance matched optimization of vias results in relatively narrow functional bandwidth. Furthermore, slot-coupled transitions have proved to be very good in the sense of insertion loss, so there is not any real advance of using a via.

Figure 1 presents the construction of the slot-coupled patch antenna. The antenna has, in this case, actually two patches one upon the other. That means one parasitic patch element has been included in the antenna design. The functional bandwidth of the antenna can be increased by using a number of parasitic elements [1]. The specified center frequency is 42 GHz in this case.

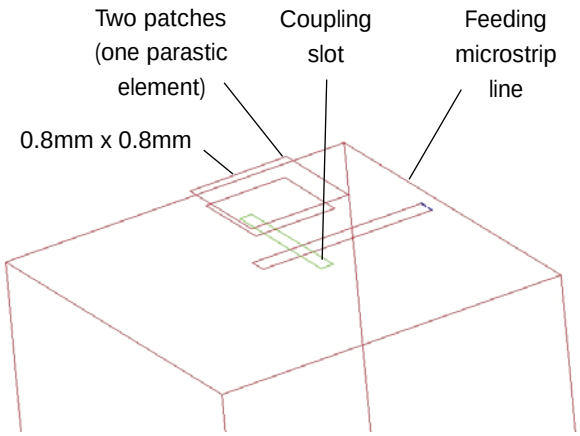


***Fig. 1. The slot-coupled patch antenna.***

All the dimensions of the antenna structure must be designed specifically for each LTCC tape system and substrate stack configuration. In fact, the gain and bandwidth specifications of the antenna may limit the possible useable configurations of the substrate stack. The design of the antenna is ultimately the trade-off between the wanted radiation gain in the main direction and functional frequency bandwidth.

### *PATCH ANTENNA ARRAY DESIGN*

Very often the needed radiation gain cannot be achieved with a single patch antenna. In such a case, several patches can be arranged to form an antenna array. Ideally, doubling the number of the antennas in the array will give 3 dB more radiation gain and will narrow the radiation beam, of course. Figure 2 presents a patch antenna array constituting of four patch antennas.

The best way to design complex antenna systems for the mm-wave band is using some advanced electromagnetic simulation software. As the number of the elements in the antenna array is increased, the solution time in the EM-simulation will be ultimately prolonged unreasonably. To avoid this, a large antenna array can be built from sufficiently small blocks that will be connected

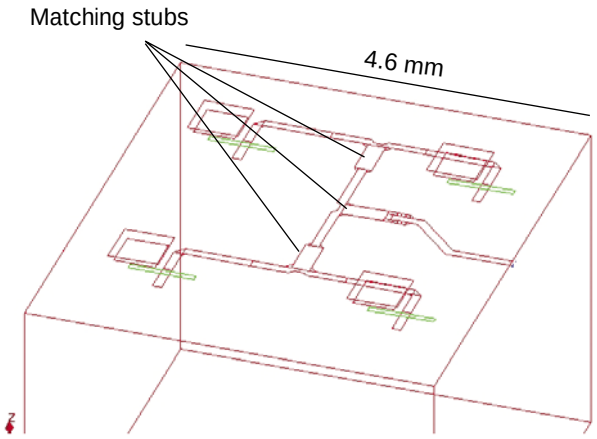


*Fig. 2. The antenna array constituting of the four patch antennas.*

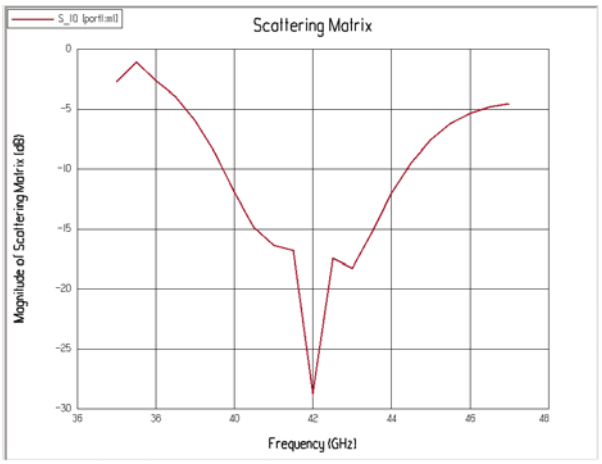


*Fig. 3. The simulated reflection attenuation of the antenna array constituting of the four patch antennas.*

with proper combiners in the ultimate antenna system. In this case, the array constituting of the four patch antennas was reasonable to be optimized by running Ansoft Ensemble v. 8.0 planar EM-simulation software. The larger arrays can be built by combining the needed number of the building blocks together. Figures 3 and 4 present the simulated performance of the antenna array constituting of the four patch antennas designed for DuPont 943 low-loss LTCC tape system. The simulation predicts the matching to be fairly good on the desired band 40.5 - 43.5 GHz and the gain to be 8.5 dBi at 42 GHz, which is pretty good, as well.

In an antenna array, separate antennas must usually be fed quite accurately in the same phase not to distort the radiation pattern. The antennas must be placed sufficiently far away from each other to avoid the antennas being interactive and deteriorating the performance of the array.

The simulations of the antenna structures showed that the deviation in the dimensions of the silver conductor patterns in the LTCC substrate must be very small to ensure proper antenna functionality. Especially, the coupling slot between the feeding microstrip line and the patch stack is very important for the antenna impedance matching.

Figure 5 presents the measured reflection attenuation of the array constituting of the four patch antennas. The best matching occurred between 45 - 48 GHz and was very good. Indeed, the realized and measured patch antenna array seems very promising in the matching point of view.

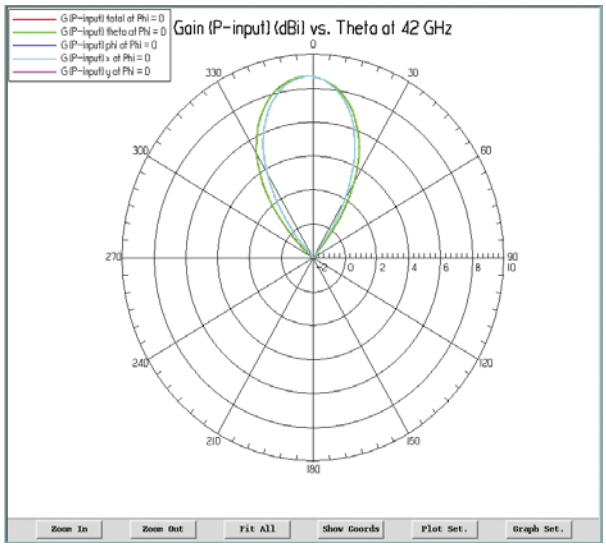


*Fig. 4. The simulated radiation beam of the antenna array constituting of the four patch antennas.*

The difference between the wanted and realized functional frequency span is easily caused by the manufacturing tolerances of the silver conductor patterns, and redesign would likely correct this error. That can be considered as a tuning action, which is usual in the high frequency design.

## CONCLUSION

Antenna arrays with four slot-coupled patch antennas were designed and realized. The antenna array was satisfactorily functional in the measurements, but this kind of antenna structure pointed to be quite sensitive to the physical manufacturing tolerances. That was seen as an

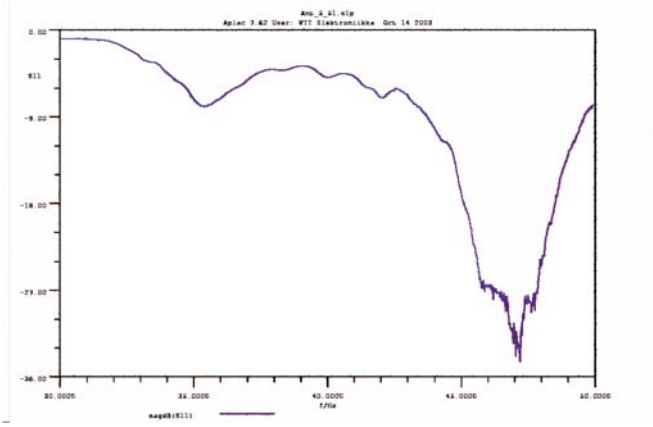

***Fig. 5. Measured reflection attenuation of the antenna array constituting of the four patch antennas.***

error in the functional frequency span of the antenna structure. However, slot-coupled patch antennas may be feasible antenna structures up to at least 45 GHz if designed carefully enough to handle the effects of the manufacturing tolerances.

### *REFERENCES*

[1] Lehto A. & Räisänen A (1994) RF- ja Mikroaaltotekniikka (pp. 101 - 105). Otatieto, Espoo.

Antti Vimpari
***Antti.Vimpari@vtt.fi***

# MEMS Packaging Using Precision Machined LTCC Substrates

## 1 INTRODUCTION

Reliable, reproducible and high-yield packaging technologies are essential for meeting the cost and performance objectives set for modules using MEMS devices. Photonic modules consist of optical, electrical and mechanical parts with different packaging levels including glass elements, passive and active chips, submounts and packaged components. Typically, device alignment and attachment is critical. Therefore, for cost-effective packaging, the alignment should be done passively using precision machined parts.

We employed low-temperature co-fired ceramic (LTCC) technology to process multilayer substrates for MEMS packaging [1]. LTCC technology has several benefits, such as, stability, low dielectric loss, possibility to machine cavities into the substrate and compatibility with hermetic sealing. In addition, the fair match of the thermal expansion coefficient ($\alpha_{LTCC} \approx 6 \cdot 10^{-6}$ 1/K) to silicon ($\alpha_{Si} \approx 2.5 \cdot 10^{-6}$ 1/K) reduces packaging-induced thermomechanical stresses.

Here we present the use of LTCC substrate as a wiring board for a silicon surface micromachined Fabry-Perot interferometer (FPI) device [2]. FPI is an electrically controlled optical bandpass filter that is widely used in spectroscopy. We applied the FPI device to demonstrate a wavelength tunable diode laser in an external cavity configuration [3].

## 2 PRECISION SUBSTRATE

The MEMS module consists of the FPI chip, a glass lens mounted on a metal sleeve and a LTCC substrate as shown in Fig. 1. The FPI contains a movable and a stationary mirror both having a reflectance of 97 %. The chip area is 2.8 · 2.8 $mm^2$, diameter of the clear aperture 1 mm and thickness 500 µm. FPI chips were fabricated at VTT Microelectronics Centre in Espoo, Finland.

We used Du Pont 951 material to process the LTCC substrates that served as the mounting platform and wiring board for the electrical connections. The substrates consisted of eight tape layers each having an unfired thickness of 130 µm. A mechanical tool was used to punch holes into the LTCC sheets in order to open cavities for the FPI chip and the silicone inserts were placed into the openings to prevent their dimensional distortions during the lamination process.

The cavities served as reference marks during the assembly and they also enabled the passive alignment of

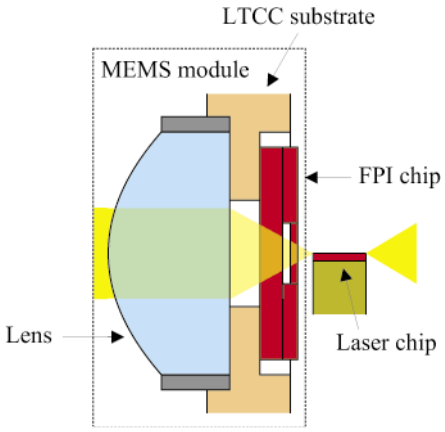


***Figure 1. Side view of the FPI module.***

the FPI chip and the lens. Typically, cavity dimensions possess horizontal and vertical tolerances of ± 20 µm and ± 10 µm, respectively.

## 3 FPI AND LASER ASSEMBLY

Because FPI devices are sensitive to stress-induced degradation, low stress die attach techniques are necessary. We attached the FPI chip to the center of the LTCC cavity with two drops of high viscosity UV curing adhesive as shown in Fig. 2. This material is easy to use, has excellent adhesion to the LTCC surfaces and remains flexible after curing. The FPI was bonded to the substrate via 25-µm Au wires.

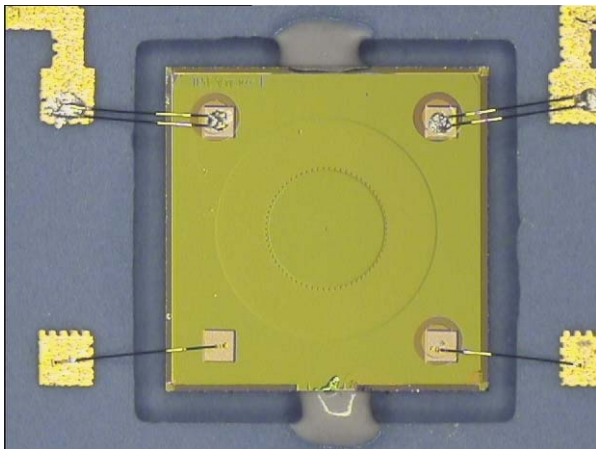

***Figure 2. FPI device on the LTCC substrate.***

The edge-emitting laser chip was soldered with an In50Pb50 preform to the Cr/Ni/Au-metallized AlN substrate using the flip-chip bonder. The laser facet was positioned flush with the substrate edge and the top contact was bonded with 25-µm Au wires to the substrate.

The main challenge in the module assembly is the alignment of the vertically standing FPI device with the horizontal laser chip as shown in Fig. 3. There are six degrees of freedom, that is, three translations and three rotations, from which the FPI-to-laser separation and the pitch and yaw are the most critical ones. For example, if the FPI is tilted, it is impossible to bring it sufficiently close to the laser. The module assembly was performed using precision-positioning equipment that contained two CCD cameras. After the alignment the FPI modules were fixed with UV-cured adhesive.

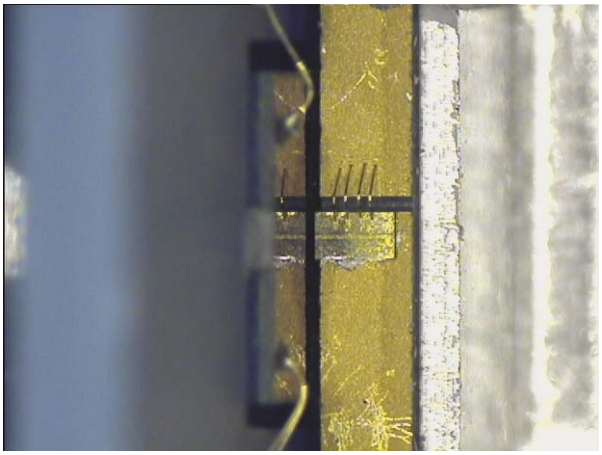

***Figure 3. FPI and laser assembly (top view).***

We measured the obtained FPI-to-laser-separations using a coordinate measurement system. The target value was 20 µm, whereas the measured separations varied between 20 µm and 88 µm. This rather large variation was caused by the residual angular errors and the movement of the aligned FPI module during the curing of the fixing adhesive. This clearly points out the difficulties encountered when aligning and attaching components that have different orientations and dimensions in the 3D space.

We verified the operation of the packaged FPIs by measuring their optical transmittance as shown in Fig. 4. The average bandwidth of 2.7 nm (FWHM) corresponds well with the values obtained from the chip measurements. This implies that LTCC structures have potential for optical MEMS packaging.

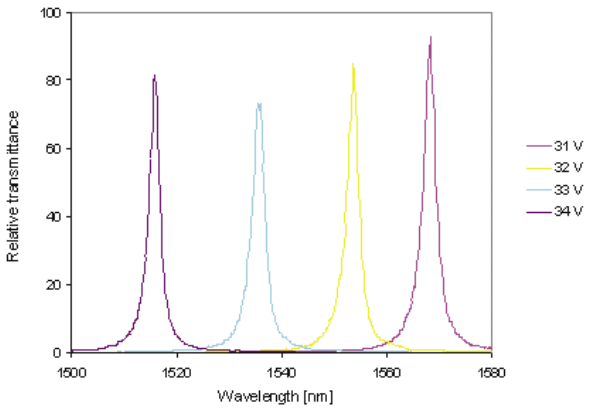


***Figure 4. Transmittance of the packaged FPI at driving voltages from 31 to 34 V.***

### *REFERENCES*

1. H. Kopola, J. Lenkkeri, K. Kautio, A. Torkkeli, O. Rusanen, and T. Jaakola, "MEMS sensor packaging using LTCC substrate technology," ***Proc. SPIE 4592***, pp. 148–158, 2001.
2. M. Blomberg, M. Orpana, and A. Lehto, "Electrically tunable Fabry–Perot interferometer produced by surface micromechanical techniques for use in optical material analysis," U.S. Patent 5 561 523, 1996.
3. Y. Sidorin, M. Blomberg, and P. Karioja, "Demonstration of a tunable hybrid laser diode using an electrostatically tunable silicon micromachined Fabry–Perot interferometer device**," *IEEE Photon. Technol. Lett.***, vol. 11, no. 1, pp. 18–20, 1999.

This paper was published in Proceedings of 2003 IEEE/LEOS International Conference on Optical MEMS, Waikoloa, Hawaii, USA.

Veli Heikkinen
***Veli.Heikkinen@vtt.fi***

Janne Aikio
***Janne.Aikio@vtt.fi***

Teemu Alajoki
***Teemu.Alajoki@vtt.fi***

Jussi Hiltunen
***Jussi.Hiltunen@vtt.fi***

Antti-Jussi Mattila
***Antti-Jussi.Mattila@vtt.fi***

Jyrki Ollila
***Jyrki.Ollila@vtt.fi***

Pentti Karioja
***Pentti.Karioja@vtt.fi***

# "Integrate-It-Yourself" Preamp and Multiplexer on LTCC Substrate, for PbS Array

### *INTRODUCTION*

Lead sulfide (PbS) array detectors offer an interesting possibility for NIR spectroscopy. They offer low cost, high linearity and low noise for wavelengths up to 3 µm. However packaging complexity limits typically pixel count to considerably less than 100, if the detector is packaged without multiplexing electronics. An application specific integrated circuit (ASIC) multiplexer circuitry solution for this application is typically too expensive if production volume is hundreds of units.

The purpose of this work is to integrate PbS array detector with the thermoelectric cooler element into a hermetically sealed package. A preamplifying multiplexing circuitry is also integrated into the package. PbS array needs to be temperature stabilised and PbS material is very sensitive for humidity and some gases. That is why PbS array has to be packaged hermetically. The integration of preamplifying multiplexing structure makes it possible to increase the number of detector elements with only slight increase in the pincount.

### *METHOD*

A preamplifying structure is implemented on to the LTCC substrate (Low Temperature Co-fired Ceramics) into a hermetically sealed package right next to the detector array, which minimises the coupling of the interferences into high ohmic leads. After the signal has been preamplified, it will be serialised by using multiplexers. The LTCC substrate makes it possible to integrate the preamplifier circuitry in a very efficient manner using discrete high quality passive components. LTCC has great electrical properties in wide frequency range. The design rules for typical LTCC process are presented in reference[1].

The number of layers can be easily made 20 with LTCC technology. This makes it possible to produce very high density and high quality substrates. By using either wire bonded ICs (Integrated Circuit) or CSP circuits (Chip Scale Packaged) with the smallest SMT (Surface Mounting Technology) passive components it is possible to make the integration density very high. This is very critical feature in integrating the electronics inside the hermetically sealed packages. It is also possible to integrate passive components into the substrate in LTCC technology. Figure 1 demonstrates some of the possibilities that the LTCC substrate offers. LTCC material is perfectly suited in hermetical environment because its material is ceramic that does not have any outgassing problems.

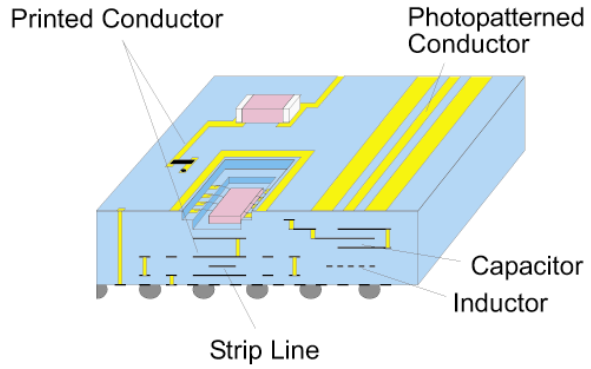


***Figure 1. The LTCC substrate and some possibilities that it offers for design.***

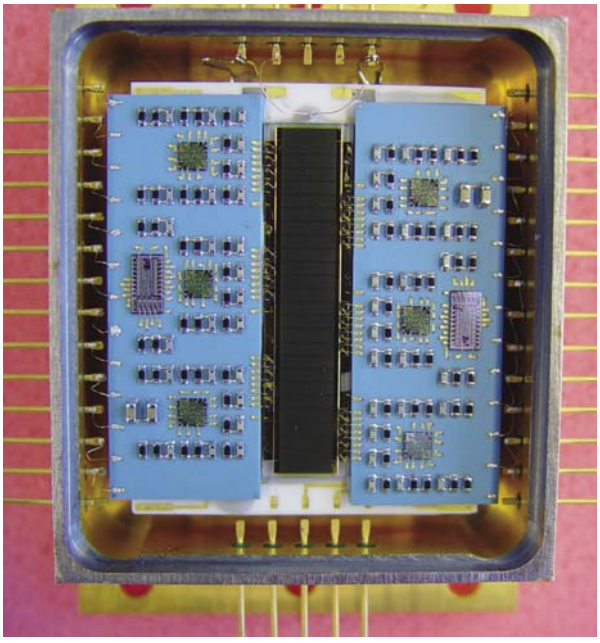

***Figure 2. PbS-array with the preamplifying and multiplexing modules.***

### *RESULTS*

A 24 element PbS array was integrated into the same package with the preamplifying and multiplexing modules. Figure 2 shows the structure before enclosing it to the package. The modules have 12 channels each and their dimensions are 32 mm * 12 mm. The inner dimensions of the package are 40 mm * 35 mm. The dimensions of PbS array are 28 mm * 7 mm.

During the layout design it was also demonstrated that one can reduce size of the 16 channel preamplifying and multiplexing module in 8 mm * 12 mm by using the smallest available passive components and bare chips on both sides of the substrate. This small size would allow

one to fit 128 element array with the 8 pieces of 16 channel preamplifying and multiplexing modules into the package shown in figure 2.

The measurements of the structure shown in figure 2 have revealed that by using good layout design procedures one can control the capacitive crosscoupling regardless of small dimensions. Also the detectivity remains high even if the detection procedure used was not typical phase sensitive detection (PSD).

### CONCLUSION

The LTCC substrate technology has many advantages that can be exploited in various kind of radiation detectors. It makes it possible to use standard assembly methods together with high integration grade. For example one can select substrate material on the basis of it's thermal coefficient of expansion so that direct attachment of detector elements to the substrate can be done with high reliability. LTCC has no vapour outgassing problems so it is perfectly suited in hermetical packaging. During this work it was demonstrated that LTCC substrate offers a great possibility to integrate electronics into the same package with the detector array.

Typically production volume for optical detection modules is quite low. LTCC's design and production starting costs are low compared to full ASIC solutions. LTCC is competitive in price in small series production and prototyping is fast. It's mechanical accuracy is high and it is reliable substrate material.

### REFERENCES

1. K. Kautio, Design Guidelines Low Temperature Co-Fired Ceramic Modules. (2000). VTT Electronics, Oulu, Finland URL: http://www.vtt.fi/ele/research/ope/pdf_files/lcdes.pdf

Ville Moilanen
***Ville.Moilanen@vtt.fi***

Antti Kemppainen
***Antti.Kemppainen@vtt.fi***

Jouko Malinen
***Jouko.Malinen@vtt.fi***

Markku Känsäkoski
***Markku.Kansakoski@vtt.fi***

Ralf Marbach
***Ralf.Marbach@vtt.fi***

# Roll-to-roll Fabrication of Organic Light-emitting Devices

### *INTRODUCTION*

A lot of interest has been generated in the use of organic materials for electroluminescent devices. Organic light-emitting device (OLED) meets many of the targets necessary for display and instrumentation applications, for example in the devices, which use small screens such as cell phones, personal digital assistants, wristwatches and cameras. OLEDs have attracted a lot of attention, mainly due to their simplicity of fabrication, low operating voltage and power consumption, high brightness, very thin structure, mechanical flexibility, light weight and full-color range in visible wavelengths [1].

There is an ever-increasing demand for smaller and lighter weight electronic and optoelectronic devices that consume less power, have greater functionality and can be fabricated using environmentally benign processes. Recent advances in OLEDs enforce the notion that organic- and hybrid-based materials, and devices, are indeed key enablers for novel electronic and optoelectronic devices. The ability of these molecular and/or polymeric organic materials to be processed and fabricated on plastic substrates will be a key factor in the development, for example, of roll-up-displays, disposable plastic electronics and decorative illuminations [2].

Currently, processing and fabrication of organic-based electronic, optical and optoelectronic materials and devices is carried using traditional techniques such as spin coating, dip coating and vacuum thermal deposition. However, these techniques are either limited to certain substrate geometry or costly and time consuming. A tremendous advantage can be gained by incorporating printing techniques in the processing and fabrication of organic materials and devices. Printing methods such as ink jet, screen and gravure printing can be useful in the fabrication of certain types of devices based on organic materials [3]. In this study, semiautomatic screen and gravure printing machines were used to fabricate thin organic and metal layers on flexible substrates like plastic and paper for the OLED applications.

### *ROLL-TO-ROLL FABRICATION PROCESS*

Single layer OLED structure consists of transparent and conductive anode substrate, light-emitting organic layer and a reflective metal cathode layer (Figure 1). An externally applied voltage drives electrons and holes from cathode and anode, respectively, into the recombination region where they form an excited state. The recombination of the electron-hole pair leads to a photon emission.

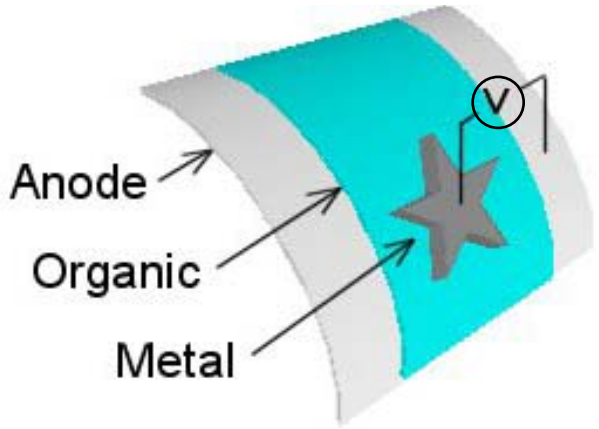


***Figure 1. Flexible OLED consists of anode substrate, organic and metal layers. Light is generated in organic layer when the electric field is applied between electrodes. The emission is observed through the polymer substrate.***

Common anode material nowadays is the sputtered indium-tin-oxide (ITO), but another choice is the printable PEDOT:PSS conductive polymer. The demands for anode film are high transparency at the visible region, small sheet resistance, high work function and low surface roughness.

Deposition of organic materials is done by semiautomatic screen or gravure printing techniques, where the organic solution is printed using the squeegee and the screen or the gravure roll, respectively. Printed organic layer is 100-300 nm thick depending on the process parameters (Figure 2).

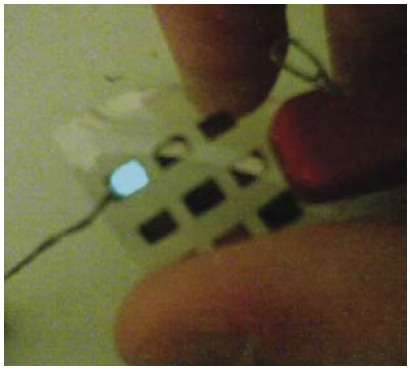

***Figure 2. Photograph of a flexible OLED with gravure printed emitting layer.***

After that, a metal paste is screen printed onto organic layer using patterned screen. Patterning is needed to define the active emission area in the device (Figure 3).

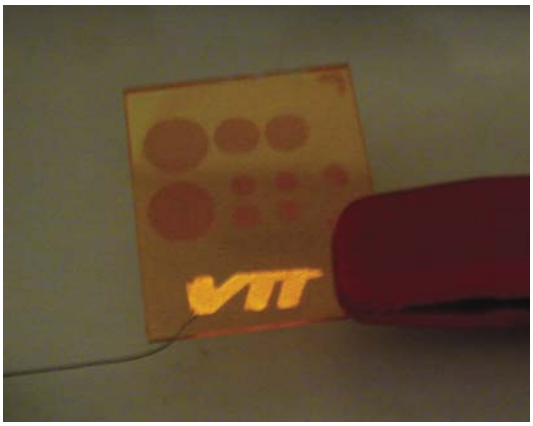


***Figure 3. Photograph of an OLED with screen printed metal cathode layer, which has unique logo patterning.***

Because the organic materials are very sensitive to oxygen and moisture, the fabricated device must be encapsulated. OLED structure is hermetically laminated between its anode substrate and plastic foil using roll-to-roll lamination equipment. In summary, the flexible organic light sources can be fabricated continuously in the same roll-to-roll process, which consists of printing and lamination units.

## CONCLUSIONS

Conventional roll-to-roll organic thin film coating processes, screen and gravure printing techniques, have been developed for the fabrication of OLED devices and other plastic optoelectronic components. The performance of the devices can be improved by optimizing the process conditions, such as proper solvent, solution viscosities, solvent evaporating temperature, printing parameters, etc.

## REFERENCES

1. J. Hiltunen, M. Tuomikoski, J. T. Rantala, Optics Days 2001. Finnish Society Conference, 2001, 20.
2. G. E. Jabbour, Y. Yoshioka, M. Tuomikoski, T. Kololuoma, H. Kopola, Northern Optics: The Joint Conference of the Optical Societies of Denmark, Finland, Norway and Sweden, 2003, 35.
3. G. E. Jabbour, R. Radspinner, N. Peyghambarian, IEEE Journal on selected topics in quantum electronics, vol. 7, no. 5, 2001, 769-773.

Markus Tuomikoski
***Markus.Tuomikoski@vtt.fi***

Dr. Ghassan E. Jabbour
***gej@optics.arizona.edu***
***University of Arizona, Optical Sciences Center, USA***

# BioOulu - Combining IT and Biotechnology to Create Tomorrow's Biosensors

***INTRODUCTION***

BioOulu is a multidisciplinary project developing new analysis methods and instruments combining biotechnology, information technology and electronics expertise. The BioOulu project studies and develops new methods for manufacturing cheap and disposable biosensors.

BioOulu, a spearhead project of Bioforum Oulu, combines top expertise in biotechnology and information technology into a new multidisciplinary research group. BioOulu links the expertise of research institutes into new innovative activity, transfers expertise, technologies and study results from research institutes to companies, and develops new technologies and products to companies.

BioOulu also aims at promoting networking between companies and creating new businesses. The goal is to develop solutions from ideas to final products and to create new spin-off companies.

***MULTIDISCIPLINARY PROJECT – CHALLENGE AND OPPORTUNITY***

One of the greatest challenges in developing biosensors is the multidisciplinary nature of the field. Improving current methods requires special expertise in measurement technology, biotechnology, molecular biology, chemistry, physics and optics. The new measuring instrument also has to be built economically and the operating costs have to be reasonable. (Figure 1.)

Combining biotechnical and electronics expertise creates significant synergy for developing new analysis methods and measuring instruments for medicine, welfare technologies, food industry, environment and industrial processes.

The operation BioOulu is characterised by biomolecular recognition methods and instruments, and their miniaturisation (laboratory-on-chip). (Figure 2.)

Disposable and cheap multipurpose sensors are developed for mass production with printing technology. (Figure 3.) The first sensor to be manufactured with the new printing technology helps diagnosing cardiac insufficiency

***FOUNDERS OF BIOOULU***

Oulu University has made significant research in electronics and biotechnology for decades. VTT Biotechnology is one of the leading research institutes in recombinant antibody technologies in Europe. VTT Electronics has internationally first-rate optical sensors research and development, for example.

BioOulu aims at strong networking with international research centres. New cooperation and research partners are welcome. BioOulu project is funded by The European Regional Development Fund, The Provincial State Office of Oulu and the city of Oulu.

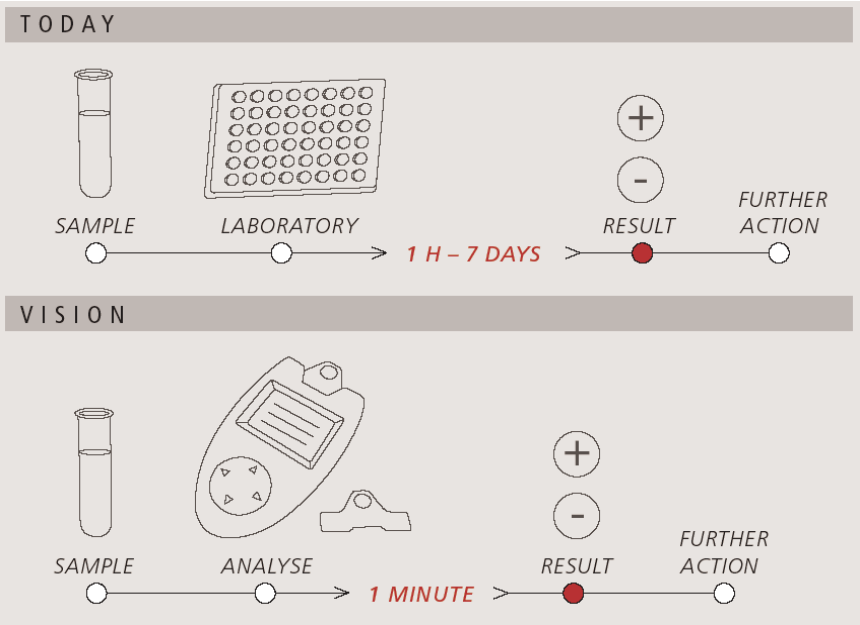


***Figure 1. New and cheap measurement sensors and instruments and quick analysis methods are required in clinical use and foremost in point-of-care diagnostics. The development of sensors is aimed at decreasing the cost of individual laboratory tests.***


***Figure 2. BioOulu develops biophotonic modules and disposable sensors for point-of-care diagnostics, environmental analysis, and food safety.***

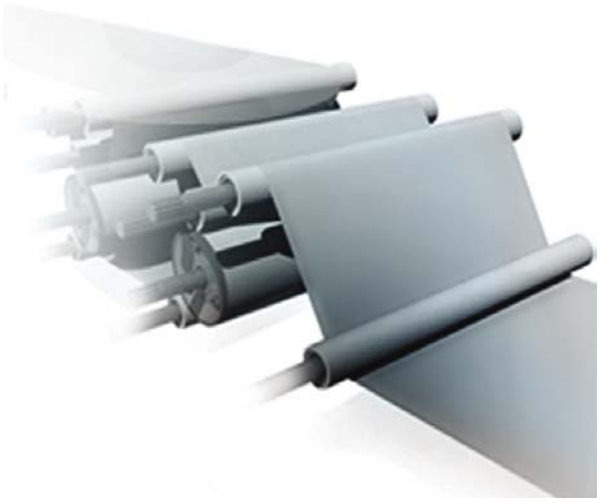

***Figure 3. Roll-to-roll production of cheap disposable bio-sensors.***

Matti Höyhtyä
***VTT Biotechnology***

Pirkko Suhonen
***Bioforum, Technopolis Oyj***

Minna Ala-Kopsala
Olli Vuolteenaho
Heikki Ruskoaho
***The University of Oulu, Medical Faculty***

Markku Känsäkoski
***Markku.Kansakoski@vtt.fi***

Liisa Kivimäki
***Liisa.Kivimaki@vtt.fi***

Harri Kopola
***Harri.Kopola@vtt.fi***

# Prototyping Process of Plastic Optics

***ABSTRACT***

The prototyping process of plastic optics is described. The sequence is divided into five main phases: specification, optics design, optomechanical design, manufacturing, and characterisation. The whole process can be applied to various optical prototyping tasks including both imaging and non-imaging optics.

## *1. INTRODUCTION*

One of the current trends in the field of optics is the move towards very high volume and low cost systems based on plastic components. Plastic optics can be found in Internet-cameras connected to home-PCs or in the built-in camera and display backlight modules of mobile phones. In order to be able to cope with the strict price and performance requirements of these complex multitechnological applications, the principles of concurrent engineering come into good use. One of the main ideas of concurrent engineering is to be able to make sensible trade-offs between different technological disciplines needed to produce a multitechnological module. For example, in the mobile phone environment several variables like the number of lenses, mechanical size, image sensor resolution, power consumption and cost need to be balanced in order to find the optimal camera module design. Naturally, there are also several trade-offs to be considered in the integration of this module into the mobile device itself. Many of these design variables need to be set already at the prototyping phase of product development. For this reason the knowledge of the prototyping processes involved in different sections of the development cycle are very important. By analysing the different processes it is possible to see what needs to be specified, which parts of the design have a co-dependence and therefore, how the design changes in one part affect the others.

## *2. PLASTIC OPTICS PROTOTYPING PROCESS*

Figure 1 shows the main iteration cycle of the plastic optics prototyping process. The sequence is divided into five main phases: specification, optical design, optomechanical design, manufacturing and characterisation. Although in principle the process can be seen as sequential the multitude of issues involved in each part of the cycle makes it practically impossible to divide the process into separate self-sufficient parts.

There are several contrasting issues to deal with between the different phases. One major trade-off is between the tolerances required by the optical design and tolerances achieved in manufacturing. If the nominal performance of the designed system is close to the optical specification, a set of very tight tolerances is required in order to keep the performance inside the specification after manufacturing errors. In manufacturing there are typically a set of tolerances that are impossible to achieve, a set which is possible but costly, and a

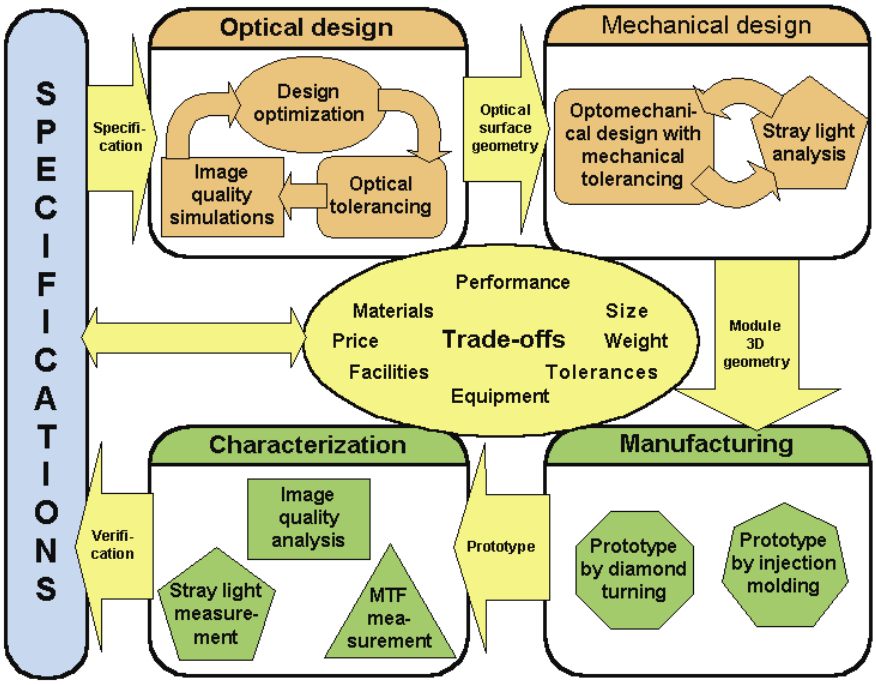


***Figure 1. The five main phases of plastic optics prototyping process.***

set of tolerances that is easy and less expensive. Generally, tighter tolerances cost more than loose and therefore the manufacturing method and its restrictions need to be considered even in the optical design phase. The same applies to the mechanical design. Characterisation facilities may limit the amount of properties that can be reasonably specified.

Inside the process efficient exchange of data is essential. Optical designs will have to be transferred to the mechanical design software and mechanical designs will have to be transferred to the formats used by the tools in manufacturing. By keeping the geometry in electronic format it is possible to shorten the project lead-time and avoid some of the possible human errors than can be introduced when the data is transferred manually from software to software.

### *2.1 Specification*

Specifications are used as a gateway to the rest of the device development process and therefore they are usually the channels through which the trade-offs between different modules of the whole device are routed. During specification, the optical and mechanical requirements of the optics module are defined. Also, the selection of manufacturing method will have to be made due to the fact that it has an effect on the available materials, achievable tolerances, feasible surface shapes, and cost.

Specification can be a difficult issue for a first prototype, because it is possible that there is only a small amount of prior knowledge available that is relevant to the application at hand. Usually, more than one prototype is built before the actual product is manufactured, and by verifying the successive prototypes it is possible to improve the specifications for the next round of the iteration process. For this reason it is also important to specify those things that can be measured in the characterisation phase. In order to be able to improve some feature its progress will have to be monitored in each cycle of the process. Figure 2 shows some of the contrasting issues to be considered when creating the optical specification.

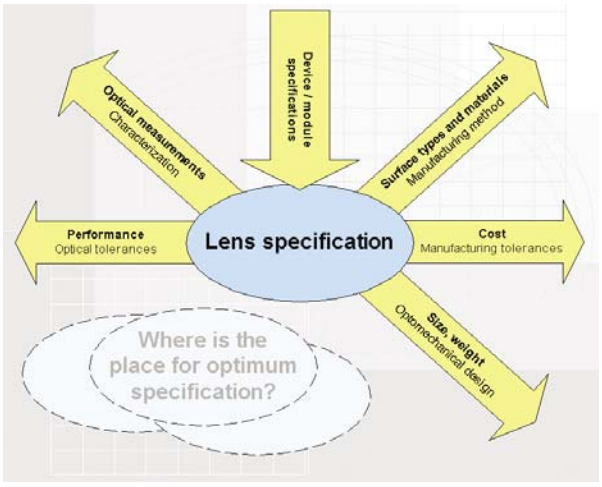


***Figure 2. Some of the issues to be considered while creating the optical specification.***

### *2.2 Optical design*

In the optical design phase, the system is optimised, and a tolerance analysis is carried out. Figure 3 shows some of the elements that have to be balanced in an optimum design.

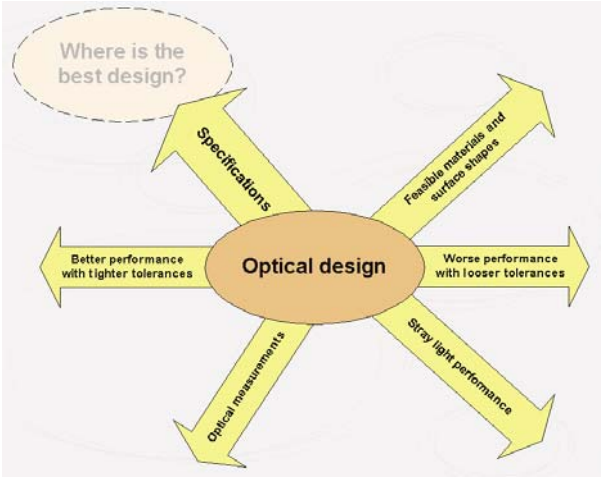


***Figure 3. Balancing the optical design.***

The best possible merit function design is not necessarily the best design to choose. There is always the possibility for a trade-off situation between optical performance and easily manufacturable tolerance values. The best design can be found by using iteration cycles between lens optimisation and tolerancing. In some cases this means a careful balancing between performance and cost.

### *2.3 Mechanical design*

Mechanical design is performed considering the geometrical specifications and optical tolerances of the system. In addition, stray light analysis is carried out to verify the optical performance of the optomechanics. Figure 4 shows some on the factors to be considered in optomechanical design

For an optical designer it is not a difficult task to scale down the design on a PC screen, but the reduction of size can be seen also in the optical design phase through the trade-offs that will have to be made between manufacturing tolerances and mechanical design. With strict size

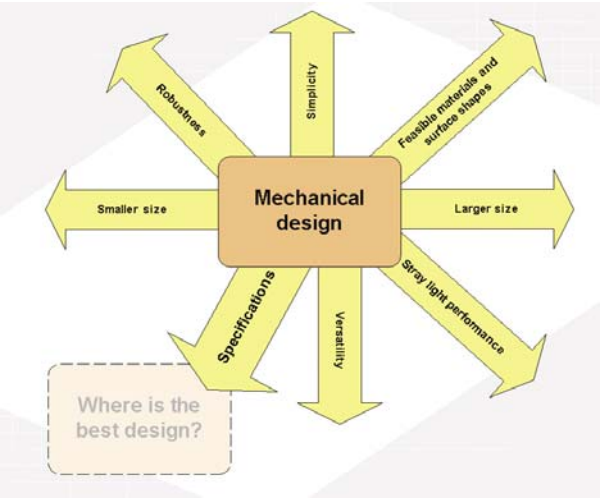


***Figure 4. Factors in mechanical design.***

requirements the mechanical designers will have to rely on simple and robust structures. Very small parts like spacers or aperture plates are hard to manufacture and handle during assembly. In plastic optics, however, one great advantage is the possibility to integrate mounting structures to the lens elements and this way to reduce the number of parts needed in the module. Unfortunately, this may have a negative effect on the stray light performance of the system. The integrated mountings provide additional paths for unwanted light through the module and therefore plastic optics can be particularly vulnerable to stray light. The size restrictions also limit the possibilities to position additional baffle structures inside the module.

### *2.4 Manufacturing*

The manufacturing method for a prototype is selected by considering the type of prototype and cost. For first round prototypes the most important thing is to show that the design actually can provide the optical performance that is expected from the simulations.

In the prototyping phase of product development the injection molding technique is somewhat problematic. Mold inserts for very small series are expensive to produce. For this reason separate machined and polished or diamond turned components are a compelling alternative for at least the first prototypes. With diamond turning it is possible to produce low-cost lenses with approximately the same complex surface shapes that can be expected from the injection molded components. Due to the fact that direct diamond turning or machining can be a more accurate method than injection molding, some consideration is needed in evaluation of the results. Figure 5 shows some of the differing elements of direct diamond turning and injection molding.

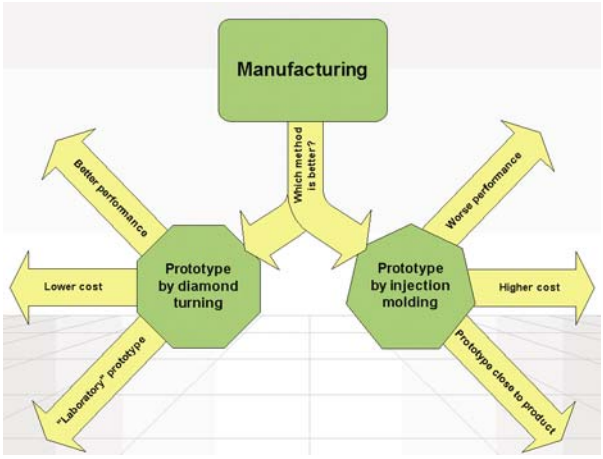


***Figure 5. Some of the differing elements of prototype manufacturing methods.***

If the manufacturing method chosen for the prototype system is injection molding, there will be some additional limitations and benefits for the optical and mechanical designs. Flat surfaces are very hard to achieve due to the shrinking of the part inside the mold during the curing phase of the injection molding cycle. If the mold has a flat face, the resulting lens will have a slightly concave surface. Curved surfaces are easier to control although they also will experience some changes in shape. The diamond turning machines can produce aspheric shapes as easily as spherical shapes and therefore this method will also give additional freedom for the optical design. One major limitation is the short list of plastic materials than can be used for refractive optics. Good colour correction is difficult to achieve with only a few lens materials. By using diffractive structures this problem can be somewhat relieved. Diffractive components performing other optical functions can also be easily integrated into the design.

### *2.5 Characterisation*

After the system is manufactured it is characterised, and the experimental results are compared to the original specifications and estimations obtained from the previous design verification simulations. Figure 6 shows the dynamics of the characterisation phase.

Several different measurements are necessary for thorough characterisation. When an imaging system is considered the most important characterisation method is probably the MTF measurement. This is especially true

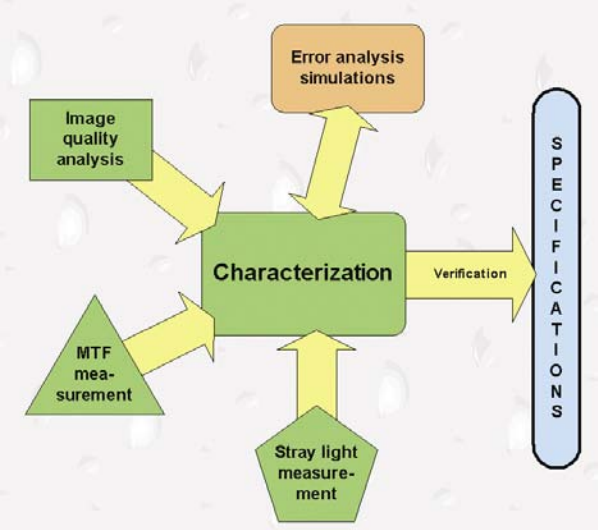


***Figure 6. Dynamics of the characterisation phase.***

if the specification of the lens states a value for the MTF. Some other characterisation possibilities include interferometric shape measurements of individual optical surfaces, roughness measurements with a profilometer and for example a stray light measurement of the whole system. Shape measurements are very important for injection molded optics since the shape of the optical surface is not identical to the shape of the mold. Injection molding process parameters have their own effects on the resulting surface shapes. Diamond turning of the lenses or molds gives a surface rms roughness in the range of 6 nm, which is good optical quality in the IR-region, but in the visible range some roughness induced light scattering will appear. If there are several optical components in the system the accumulation of scattered light may cause a stray light problem.

If the performance of the prototype is not sufficient, a new prototyping iteration cycle is needed. New error analysis simulations can also be performed in order to pinpoint faults in manufactured modules. Simulation software provides an ideal environment in which perfect systems can function without any disturbance from the outside world. By introducing a controlled perturbation to the virtual design it is possible to isolate the effect of one particular error to the system performance. In real life, all of the error sources act simultaneously and it can be difficult to see which issues have the greatest effect. By systematically going through these possible sources and comparing the simulation results to the actual measurements it is possible to extract some information that otherwise could not be obtained.

### *3. SUMMARY*

The prototyping process of plastic optics was described. The multitude of issues involved in each part of the development cycle makes it practically impossible to separate the process into self-sufficient and sequential parts. A concurrent engineering approach was taken by analysing the different considerations and trade-offs that will have to be made between the various phases inside the process.

Jukka-Tapani Mäkinen
***Jukka-Tapani.Makinen@vtt.fi***

Kimmo Keränen
***Kimmo.Keranen@vtt.fi***

Janne Aikio
***Janne.Aikio@vtt.fi***

Pentti Karioja
***Pentti.Karioja@vtt.fi***

# High-resolution Imaging Optics Needing No Assembly-phase Optical Adjustments

The use of modern computer numerical control (CNC) machining tools have opened new possibilities for the optical and optomechanical designs. The fusion of optics and optomechanics has been earlier demonstrated by the integration of mirror optics directly to the high-accuracy optomechanical parts of various non-imaging optical systems. The increased accuracy of the manufacturing of complex-shaped mechanical parts has also lead to the possibility of using the CNC machining in the reformation of the optomechanics for the imaging optical systems. The high-accuracy of the CNC machined optomechanical parts among with the fluent data transfer between the optical and mechanical design programs and the computer aided manufacture (CAM) gives a lot of freedom for the optical design.

We have designed and manufactured a 2.7 times de-magnifying imaging optical system (see Figure 1) capable of resolving features smaller than 5 µm in the image plane. The specification of the lens is shown in Table 1. The optical system is a double-telecentric catadioptric system consisting of the total of 13 optical elements: 9 lenses, 1 mirror, 2 polarising beam splitters and 1 quarter wave plate (Figure 2). The numerical aperture (NA) is 0.18 on the object side and 0.44 on the image side. The distortion of the lens is less than 0.01 %. The field size is 23 mm in diameter on the object side and 8.6 mm in the image side. The measured modulation transfer function (MTF) of the system is over 34 % at 200 linepairs/mm (see Figure 3).

***Table 1. Specification of the lens***

| | | |
|---|---|---|
| Magnification | 0.37 | 0.37 |
| Image size (diagonal) | 8.5 mm | 8.5 |
| Object NA | > 0.15 | 0.18 |
| Image NA | ≥ 0.41 | 0.44 |
| Distortion | < 0.03 % | < 0.01 % |
| MTF @ 200 lp/mm | 60 % | > 34 % |
| Wavelength | 405 ± 10 nm | 405 ± 10 nm |

The optomechanics are composed of 2 larger pieces and several smaller parts; all of the parts are made using the 5-axis CNC machining. One of the larger pieces provides a 90 degree angle in the optical path with less than 0.5' accuracy. The overall accuracy of the mechanics is 0.01 mm and the dimensions are 300 mm x 150 mm x 70 mm. The tolerances for the optical and mechanical components were determined via optical simulations. The performance predicted by the tolerance analysis is shown as a set of MTF curves in Figure 3. The measured MTF shown in Figure 3 is clearly below the predicted MTF values. The measurement was, however, done without a sheet of glass covering the object plane, and thus the measured MTF can be considered as a worst-case estimate. The influence of the missing cover glass was analysed with optical simulations and the estimated performance with the cover glass on is shown as the dashed line in Figure 3. The optomechanical design also included the stray light analysis (see Figure 4) resulting some minor modifications to the mechanical parts. The realised lens is shown in Figure 5.

Because of the use of the high-accuracy CNC machining of the optomechanics, the lens can be manufactured without any optical adjustments or testing in the assembly phase.

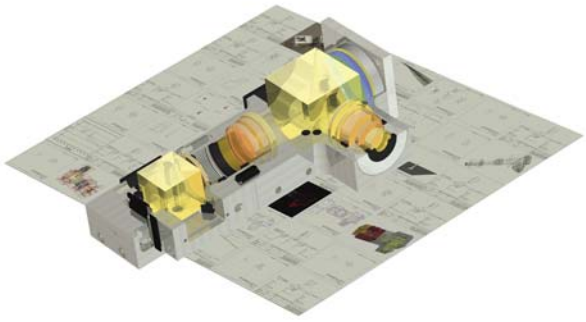

***Figure 1: Optical and mechanical 3-D modelling combined with CMC machining enables design and manufacturing of high resolution optics needing no optical adjustments.***

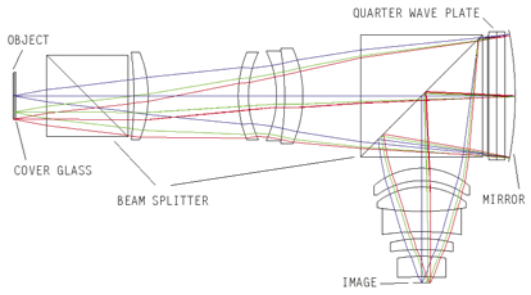


***Figure 2: The optical design of the imaging lens.***

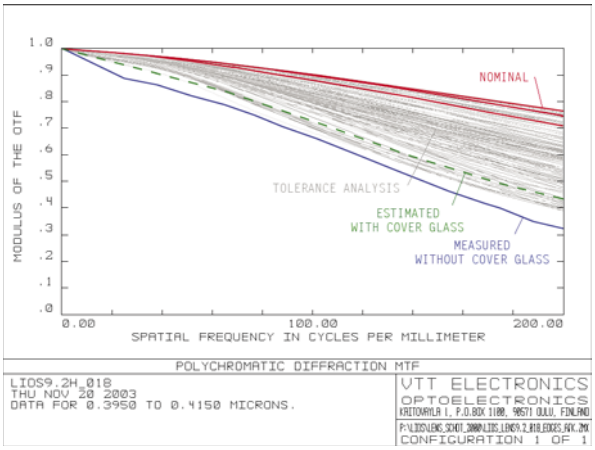


***Figure 3: Modulation transfer function of the designed optical system. The result of the tolerance analysis is based on 20 Monte Carlo runs. Due to mechanical limitations in MTF measurement system, the MTF curve was measured without the cover glass on top of the object plane. The optical simulation predicted, that this fault drops the MTF from the nominal design by 10 percentage units.***

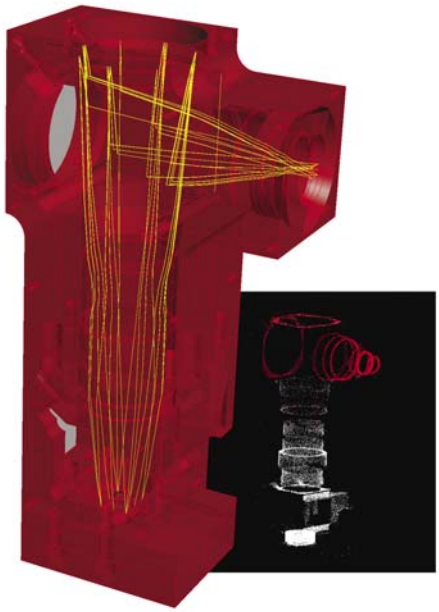

***Figure 4: The stray light analysis was used for fine-tuning the optomechanics. The optomechanical model is shown on the left side of the figure. A stray-light simulation result is shown on the right side. White dots illustrate the mechanical surfaces seen from the object plane (and thereby potentially illuminated with the stray light) whereas the red dots indicate the surfaces seen from the image plane. The stray light on the image plane is significantly decreased by eliminating the surfaces that can be seen from both the image and the object planes.***

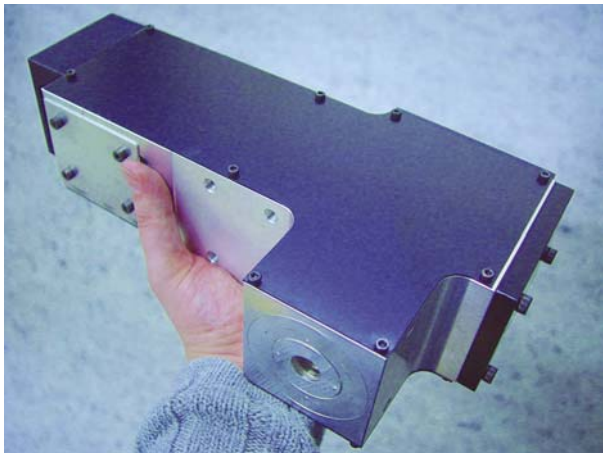

***Figure 5: A photograph of the realised lens.***

Janne Aikio
***Janne.Aikio@vtt.fi***

Pekka Suopajärvi
***Pekka.Suopajarvi@vtt.fi***

Tomi Seppänen
***Tomi.Seppanen@vtt.fi***

Mauri Aikio
***Mauri.Aikio@vtt.fi***

C. Edström
M. Tannemyr
***Beacon AB, Förrådsvägen 10, SE-901 32, Umeå, Sweden***

H. Vasama
***Suomen Optomekaniikka, Jokelantie 1 40270 Palokka, Finland***

# On-line Measurement of Wet Coating Thickness on a Coating Machine of Fiber Boards

### *INTRODUCTION*

Although the NIR method is an obvious choice for on-line measurement of coating thickness, no such instruments have been applied for wet varnish coatings on fiber boards. Measurement of coatings on a metal surface is often straightforward, as the NIR beam reflects totally from a smooth interface and experiences absorption in both passages through the varnish layer. However, the surface of a fiber board is usually rougher, its reflectivity in the NIR region is reduced and dependent on wavelength. Compensation for variations of surface properties was sought by measuring the difference between reflectances before and after the coating process. The current measurement method, which is based on the weight increase of test pieces in the process, was used as a reference method.

### *INSTRUMENTATION*

Construction of the prototype instrument was based on techniques developed earlier in our laboratory. The NIR detector has two parallel channels separated with narrowband interference filters, one situated within the varnish CH absorption band at 1.7 µm and another just outside this band (Fig. 1). An alternative CH band at 2.3 µm has stronger absorption and was used at the lower end of thickness values. All four channels were integrated into a 4-channel PbS detector package. A halogen lamp was used as an NIR source, radiation was chopped mechanically and standard PSD techniques were used in signal recovery. A special mirror optics developed in our laboratory was used in the probe heads, which were connected to the instrument with fiber-optic cables.

### *RESULTS*

Field tests were executed with a Barberan curtain coater (Fig. 2). Good correlation of NIR results with the reference weighing method was obtained for different types of coatings and fiber boards. The NIR method covers the usual thickness ranges from 50 to 500 g/m$^2$ and the obtained calibration error was typically 5-10 g/m$^2$ (an example is given in Fig. 3). In addition, the two-probe method enabled a separate measurement of each applied coating in multi-coating systems.

### *PARTNERS*

VARNISH-LINE-MEASURE was a 2-year CRAFT project funded by the European Commission under the 5th Framework Programme on Competitive and Sustainable Growth (Project no: 70223). The project partners were BARBERÁN (SME, Spain), SEITU (SME, Spain), TURRI (SME, Italy), MARQUES (SME, Portugal), IKERLAN (RTD, Spain), CIDEMCO (RTD, Spain) and VTT Electronics (RTD, Finland). The project was finalized by the end of the year 2002.

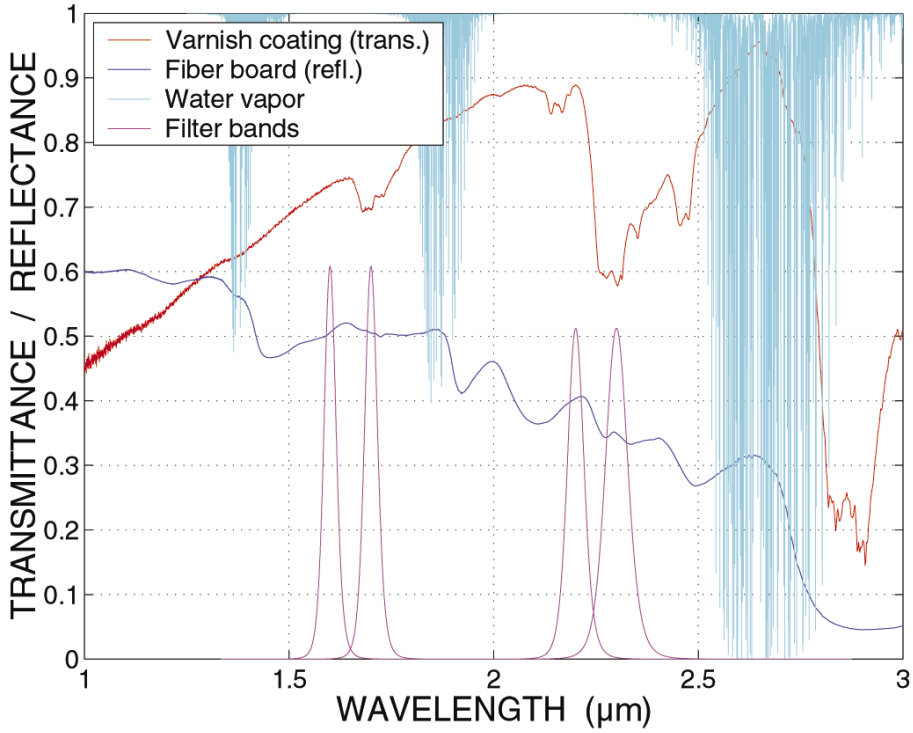


***Fig. 1. Typical spectra of varnish coating and fiber board. Filter bands are chosen outside water absorption regions.***

*Fig. 2. Developed on-line coating thickness meter on a Barberán curtain coater. Only one sensor head is shown in the picture.*

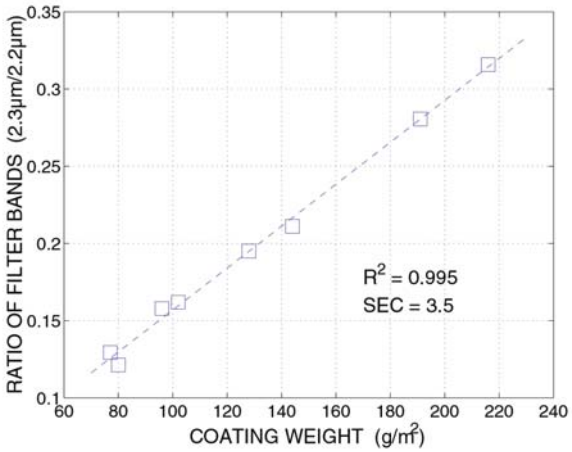


*Fig. 3. Calibration of polyester varnish on precoated cherry board. The values obtained without background subtraction were $R^2 = 0.87$ and SEC = 20 g/m².*

***REFERENCES***

1. Garmendia, I.; Niemelä, P.; Tornberg, J.; Hietala, E.; Nuevos desarrollos en maquinaria de aplicación de recubrimentos: Sistemas para medición del esposor húmedo en línea y control automático de la aplicación. Proceedings of Eurocoat, Barcelona, ES, 2002 . UATCM- Union of Technical Associations of Mediterranean Culture (2002), 811 - 821.

2. Manero, F.; Anduaga, J.; Mayora, K.; Garmendia, I.; Niemelä, P.; Hietala E.; Tornberg, J.; Development of an optoelectronic sensor for measuring varnish thickness on-line. 11th NIR Conference, Cordoba (Spain), 6 - 11 April 2003 and Proc. NIR-2003 (In press).

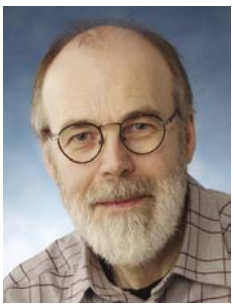

Pentti Niemelä
***Pentti.Niemela@vtt.fi***

Eero Hietala
***Eero.Hietala@vtt.fi***

Jouni Tornberg
***Jouni.Tornberg@vtt.fi***

# Remote Measurement of Vehicle Emissions

### *INTRODUCTION*

Energy-efficient and clean traffic is one of the key prerequisites for sustainable growth, and road vehicles account for the major share of all traffic-related emissions. Therefore, all new cars have been equipped with effective pollution control technology. New catalytic converters can turn most of the harmful exhaust components into non-polluting ones. However, emissions increase over the life of vehicles, as combustion residues accumulate on the catalyst and reduce the effectiveness of the conversion process. Furthermore, faults and malfunctions or even the deliberate tuning of the engine (e.g. tuning chips) in this rather complex system lead to less than optimum operation, higher fuel consumption and higher carbon dioxide emissions and other emissions. If not detected at an early stage, faulty vehicles can turn into "gross polluters", with high fuel consumption and emissions that account for a substantial part of total fleet emissions (Klein&Koskenoja 1996). Also, there is some evidence that car manufacturers intentionally optimize engine performance and emissions to pass the dynamometer driving cycles and outside these driving conditions emissions can be much higher (Kiencke 2000). Further, driving conditions strongly affect emissions but their effects are not well quantified. Bishop and Stedman (Bishop et. al. 1989, Bishop&Stedman 1996) have pioneered and developed an instrument to remotely measure vehicle emissions. In several studies it has been found that about 10% of the fleet generates more than 50% of total emissions of carbon monoxide (CO). Most cars are clean but a small number of malfunctioning or tampered with vehicles produce a major amount of regulated and un-regulated emissions. Idle tests are generally known to be a poor indicator of true emissions. In Finland the periodic inspection intervals have increased and therefore several years can pass without emission testing.

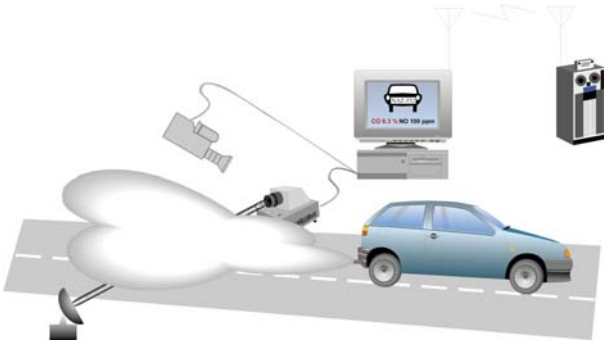

***Figure 1. Remote measurement principle.***

We present here a prototype analyzer for the remote measurement of vehicle exhausts from individual vehicles during normal driving conditions (Figure 1). Measured emissions include $CO_2$, CO, HC, $CH_4$, NMHC and NO. This prototype has been developed in co-operation with European research project REVEAL (1999-RD.10657). Partners in this project were: Bundesprüfanstalt für Kraftfahrzeuge, Centro Ricerche Euron settore AgipPetroli, Farside Technology plc, Golden River Traffic Ltd, National Centre for Scientific Research "Demokritos", Netherlands Organization for Applied Scientific Research (TNO), RWTÜV Fahrzeug GmbH, Sira Ltd, and the University of Hertfordshire.

### *MODELING*

Spectroscopic techniques have attracted much interest in recent years, because they provide very versatile tools for trace gas monitoring. Spectroscopic methods can be separated into two categories: laser-based and broadband light sources. Laser-based methods have especially profited from the development of tuneable lasers. Figure 2 illustrates various technological possibilities to implement absorption measurement (NOTE: this

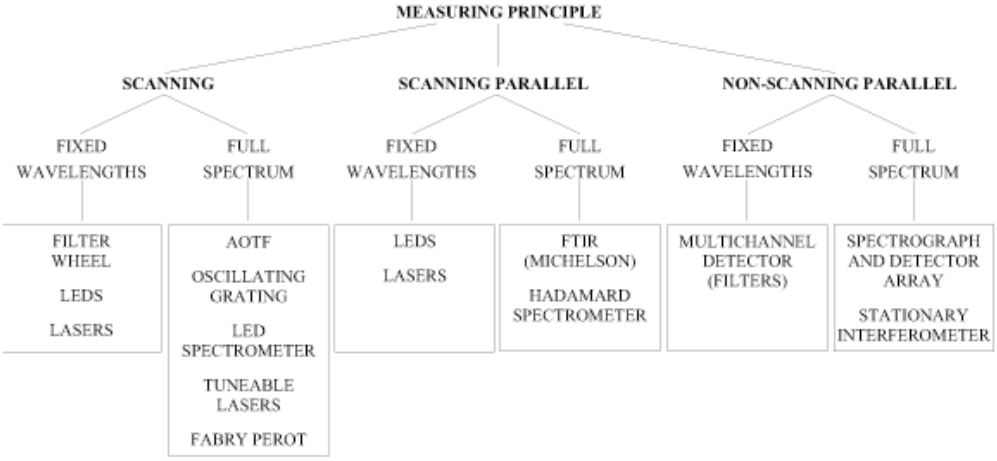


***Figure 2 Techniques for implementing absorption measurement.***

list is not comprehensive). The quantitative identification of exhaust constituents is limited by the spectral resolution and by the minimum detectable absorption, i.e., by the sensitivity and selectivity of the particular technique. A spectral resolution is of primary concern for the proper identification of species, i.e., for detection selectivity (cross interference reduction).

The USF HITRAN-PC (Rothman et. al. 1998) has been used to obtain the absorption coefficients of the various pollutants and other atmospheric gases and vapors. A spectral library Quantitative Infrared Database of Infrared Analysis Inc. (http://www.infrared-analysis.com/) was used as the spectral source of hydrocarbons, which have only limited availability in HITRAN96.

Transmitted IR intensity through atmosphere can be expressed using the following equation:

$$I_{\Delta\lambda} = \frac{A_o \Omega_o T_o}{\pi} \int_{\Delta\lambda} \varepsilon(\lambda) M(\lambda) e^{\sum_k^- \alpha_k(\lambda) \frac{P_{gk}}{P_{atm}} l_k} d\lambda \quad (1),$$

where $M$ is the spectral radiant excitance from the source
$\lambda$ is the wavelength
$T_0$ is the transmission of optics
$A_0$ is the area of the optics, which is limiting the throughput
$\Omega_0$ is the solid angle of the optics, which is limiting the throughput
$l$ is the path length
$\alpha$ is the absorption coefficient
$p_g/p_{atm}$ is the partial pressure of pollutant gas $g$ (=concentration)
$\varepsilon(\lambda)$ is the emissivity of the source
$k$ number of species.

For the purposes of remote sensing, only the absorption due to the vehicle plume should be considered, while the absorption of the background atmosphere should be subtracted.

This project has developed a new type of auxiliary filter (Fabry-Perot (FP) or gas-correlation filter (GCF)) for measurement of NO in vehicle exhaust (PCT Pat. appl. Känsäkoski and Niemelä). A major problem with NO IR absorption measurement is the high interference of water vapor. Spectral simulations have indicated cross-sensitivity values lower than 1/10 of those with the single filter. When equation 1 has been applied with the modeling results and are combined with application requirements, it shows that it is possible to measure CO, $CO_2$, HC and NO with required photometric accuracy. Table 1 presents the required signal-to-noise ratios for each species and the optical power reserve available (this reserve is required while the implementation is not optimal). For NO the values are given at 5 %-m water vapor background (appr. 10 m path length, 10°C and RH40%).

### *DESIGN*

Due to the fact that exhaust dilutes very rapidly it is extremely important to measure each gas almost simultaneously and through the same path. By combining these modeling results, knowledge of various technologies and application requirements the multiple detectors and beam splitting NDIR is currently the best choice for this application.

#### *Long path optics (LPO)*

Major design parameters for the long path optics were:

- efficiency (throughput)
- cost
- robustness (vibration, dirt, temperature,..)
- ease of alignment.

Cube corner design is well known to be not sensitive to angular misalignment. A modified cube corner design is applied to long path optics. This was realized so that outgoing and incoming beams are angularly separated as well. The optical system shown in Figure 3 was used in the tolerance analysis. The system sensitivity to the angular misalignment of the end mirror was studied. Toler-

***Table 1 Optical power at detector for each species and estimated SNR.***

| | Optical power @ detector | SNR (1) @ 10 ms (diluted) | RESERVE (2 ) |
|---|---|---|---|
| CO | 2.96E-6 W | 7.42E+4 | 22.6 |
| $CO_2$ | 3.08E-6 W | 7.71E+4 | 13.1 |
| HC | 6.44E-6 W | 1.61E+5 | 45.2 |
| NO ***(5 %-m BG)*** ***GCF 5mm (100% )*** | 3.14E-6 W | 4.43E+4 | 1.59 |
| REF | 3.44E-6 W | 8.62E+4 | |

ance analysis was done by using the Advanced System Analysis Program, ASAP, by Breault Research Organization, Inc. ASAP designs were converted into 3D models and the mechanical design was done with IronCAD. This design was again verified with TracePro, which is optical 3D simulation software. The majority of the optics are protected from dirt, only the large ellipsoid mirror and the large flat mirror are "outside" the instrument enclosure. These mirrors were left unprotected, because large IR windows are very expensive and fragile. The majority of mirrors have been made with a high accuracy 5-axis CNC machine, which allowed us to reduce the number of alignments during assembly. The mirrors and other mechanical components are very accurately positioned with dowels. The mechanics has a limited number of alignments, only detectors have alignment (due to the tolerance of detector packages) and one mirror requires alignment due to the manufacturing tolerances.

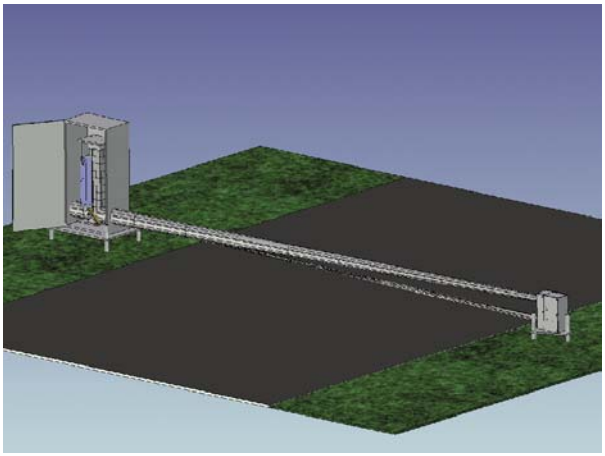

***Figure 3. Cube corner based long path optics.***

***Electronics***

All sensitive electronics and optoelectronics are stabilized; the temperature of the light source is measured and controlled, detector temperatures are measured and controlled; also, the chopper frequency and amplitude are measured and controlled, this should ensure a stable operation even in harsh conditions. Signal detection is based on matched digital signal filtering (Känsäkoski, et. al. 1998). The main advantages of this technique are:

- it is programmable;
- it is easy to design, test and implement;
- it does not suffer from drift, and so is extremely stable with respect to both time and temperature; and
- it is versatile in its ability to process signals in a variety of ways.

Also, digital filters can easily be modified without affecting the hardware. An analog filter can only be modified by redesigning the filter circuit. As a hardware platform we used VTT's ReMIX/104 I/O board, which is a general purpose I/O board for PC/104 bus.

***PERFORMANCE SUMMARY***

Performance of a filter-based infrared sensor system, has been evaluated as applied to the measurement of CO, $CO_2$ and NO concentrations of exhaust plume. All sensors have two channels: a measurement channel and a reference channel. The reference channel being common to CO, and $CO_2$. High selectivity was aimed for when specifying the filter for the measurement channel of each sensor, and selectivity of the NO sensor was further improved with auxiliary Gas Correlation Filters (GCF). Interference in all these sensors comes from the side of $H_2O$ (vapor); in CO and $CO_2$ sensors also from $N_2O$, and CO and $CO_2$ have some mutual interference in the measurement. An additional advantage of the two-channel sensor system is that it compensates for scattering caused by particles and small water droplets (fog) of the exhaust plume, and it might be possible to use the 4.0 µm reference channel, which is quite transparent for the gas and vapor components, even as a rough estimate for particle concentration (opacity).

High response gives high sensitivity for the sensor, but can also lead to non-linearity of the response, if the concentration-path length product is high, as is the case with CO and $CO_2$ sensors. The non-linearity error can be corrected with squared absorbance or non-linear calibration equation (3rd order polynomial fit give reasonably good results). More accurate results could be received with two different calibration equations - one for low concentrations and another for high concentrations. This would especially improve the zero point accuracy of the measurement.

***DISCUSSION***

Since the introduction of remote sensing of vehicle exhausts a new tool has been available for emission inventories. Remote measurement gives access to measurement data of thousands of cars / day in real life driving conditions. This data can be used for several purposes: to detect gross polluters (usually gross consumers as well), detection of specific vehicle models with poor emission performance, evaluating and improving the emission inventories, public information systems that display the emission status of cars as they drive by, measurements at toll booths to charge higher tolls for gross polluters, fleet

characterization, evaluation of inspection and maintenance programs or the impact or other emission reduction programs such as reformulated fuels, evaluation of the rates of deterioration and technological improvement of the emission control systems, environmental taxes based on emissions, and traffic management, just to name few possible applications. Future research should concentrate on applications development. Figure 4 is a picture of the developed remote sensor source optics and a 3D CAD model of part of the optics.

***Figure 4. A picture of REVEAL source optics and a 3D CAD model of the optics.***

***REFERENCES***

Bishop, G. A., Starkey, J. R., Ihlenfeldt, A., Williams, W. J. and Stedman, D. H. (1989) IR Long-Path Photometry: A Remote Sensing Tool for Automobile Emissions. ***Anal. Chem.*** 61, 671A-677A.

Bishop, G. A. and Stedman, D. H. (1996) Measuring the Emissions of Passing Cars. ***Acc. Chem. Res.*** 29, 489-495.

Bishop, G. A. and Stedman, D. H. (1993) Apparatus for remote measurement of vehicle emissions, US patent 5,210,702.

Kiencke, U. and Nielsen, L. Automotive Control Systems, Springer-Verlag, (SAE Order no. R-283),(2000), p. 412.

Klein, D. B. and Koskenoja, P. M. (1996) The Smog-Reduction Road Remote Sensing vs. The Clean Air Act Policy Analysis #249, Cato Institute.

Känsäkoski, M., Voutilainen, O. and Seppänen, T., (1998) The Performance of Near Infrared (NIR) Analyzers Can be Improved by Digital Filtering Techniques, Journal of Near Infrared Spectroscopy 6, 97–104.

PCT Pat. appl. WO02082059, Känsäkoski, M. ans Niemelä, P., A Method And A Measuring System For Determining And Monitoring Exhaust Gas Emissions From A Vehicle.

Rothman, L. S., et. al. (1998) The HITRAN Molecular Spectroscopic Database and HAWKS (HITRAN Atmospheric Workstation): 1996 Edition. JQSRT 60, 665-710.

Markku Känsäkoski
***Markku.Kansakoski@vtt.fi***

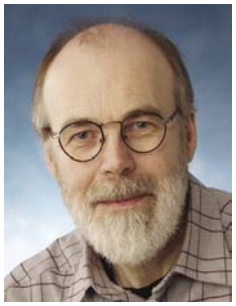

Pentti Niemelä
***Pentti.Niemela@vtt.fi***

Andrew Crookell
***Sira Ltd., South Hill, Chislehurst, Kent, BR7 5EH, UK***

# Paper Moisture Analyser (PIRMA) Using 4-Channel Near Infrared Spectroscopy

### *INTRODUCTION*

Moisture measurements play an important role when paper tensile properties are studied. It is generally known that the moisture content greatly affects the paper's tensile properties, which are particularly important with regard to paper machine runnability. VTT Processes has been studying the tensile properties of press dried and dry paper since 1995.

VTT Electronics has developed several on-line NIR-analysers for the paper machine environment. In this case, a laboratory paper moisture analyser, which is easy to move and use, was developed for the VTT Processes laboratory tensile studies.

### *INSTRUMENT*

The main goal in the design of the instrument was the fibre optic probe head, which should be easy to use, and the use of the instrument's case as a transport box so that during storage or transportation the probe head could be stored in a special probe holder inside the instrument case (fig. 1).

***Figure 1. Instrument case and probe head.***

The fibre optic probe head has been designed so that the same sensor rig can be used with different focusing mirrors. This means that if a different spot size or focal length is needed in future applications, only the part where focusing mirrors are needs to be redesigned and manufactured (green/gold part fig. 2). This also saves design costs for similar probe heads in the future.

For VTT Processes, the probe head was delivered with mirrors for two different spot sizes (circular diam. 10 mm and line 50x10 mm). The probe head also includes a reference sample (at the left in figure 3) that can be rotated to the front of the probe to compensate the instrument's drifts due to ambient temperature changes.

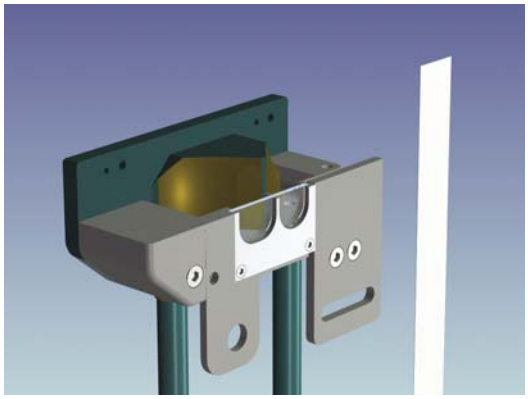

***Figure 2. Probe head and paper sample.***

The illumination and collection fibre bundles are low-OH quartz (diameter 3.0 mm).

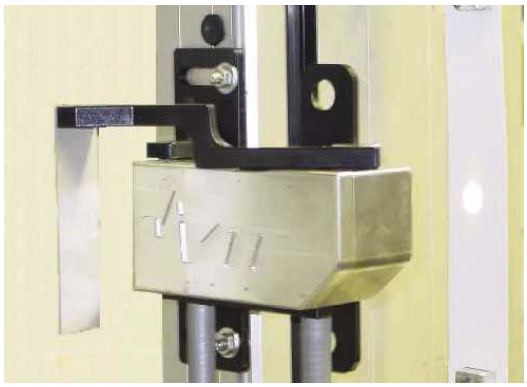

***Figure 3. PIRMA sensor rig and measuring spot on a paper sample.***

The detector technique is based on a four-channel detector component developed at VTT in Oulu. This component has four PbS-detectors covered with interference filters for measuring each wavelength, and the whole package is hermetically sealed in a single Peltier-cooled package. This structure provides true parallel measurement of all channels. The detectors are thermoelectrically cooled to achieve higher response and insensitivity to temperature variations. This same technique has been used successfully in many industrial on-line applications, such as paper machine analysers.

When selecting bandpass filters for the wavelength measurements, things that should be taken into consideration are : a) filtering of the wavelength's influence on the calibration b) filtering of the full-width influence on the signal c) ambient air moisture absorption, which can disturb the measurement, and d) the wavelength drift of the water absorption peak as a function of the temperature

(the wavelength should be selected near the water's isosbestic point).

The detection electronics are phase-synchronised amplification so the ambient lighting doesn't affect the measurement.

As usual, the user interface was realised with Labview, but in this case VTT Process implemented VTT Electronics measurement and calibration routines as part of their own Labview data collection software. This implementation was surprisingly straightforward and easy to do.

### *RESULTS*

The PIRMA moisture measurement range is fairly large, beginning as high as 50 % moisture content. The drying force of a paper sample in the PIRMA moisture measurement range is shown in Fig. 4.

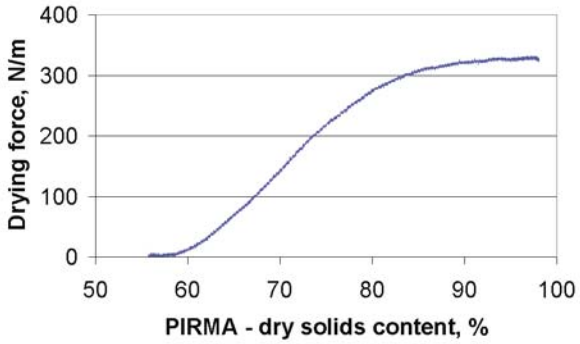


***Figure 4. Drying force of a paper sample as a function of the PIRMA dry solids content.***

The PIRMA measurement technique makes it possible to measure paper moisture accurately during a tensile test. Exact moisture data makes it possible to interpret changes in the tensile results related to the paper moisture content. The moisture content data is very important when the tensile properties of wet paper are being studied.

### *CONCLUSION*

VTT Electronics has built a tailored four-channel laboratory paper moisture analyser with a fibre optic probe head to meet VTT Processes' needs in paper tensile laboratory measurements. The same instrument can also be used for on-line measurements.

VTT Processes has utilised the PIRMA analyser in paper moisture measurements in laboratory-scale tensile tests for paper runnability research.

Juha Sumen
***Juha.Sumen@vtt.fi***

Jarmo Kouko
***VTT Processes***

# Monitoring the Internal Quality of Potatoes by NIR Transmission and Reflection Measurement

### *INTRODUCTION*

The internal quality of potatoes and other vegetables and fruits is an important quality factor for both consumers and the food industry. There are several diseases and defects which have no effect on the quality of potato skin. Therefore, internal defects remain invisible to the human eye and also to an ordinary camera. It is of the utmost importance to sort potatoes on-line in order to increase the quality of sorted potatoes intended for sowing, retail, and industrial processing. We will describe here a novel technique and instrumentation which enables us to non-destructively 'look inside' the potato and define the internal quality of the potato from a continuous flow of potatoes on a conveyor belt. This technique was originally developed at the Institute of Horticulture and Canned Foods.[1,2] This new instrument uses five different short wave near infrared (NIR) wavelengths for the measurement. The transmission and reflection of near infrared light from potatoes are measured from several different angles. The total number of measurement channels is sixteen. We will describe the optics and signal processing of this instrument and the first test results.

### *V-CAMERA INSTRUMENT*

The 'V' in 'V-camera' stands for "virtually-peeling". In this method and technology the potato, or other fruit or vegetable with a skin, is virtually peeled by measuring the NIR transmission of potatoes and simultaneously measuring the NIR reflection from the potato skin. This method has been explained in detail earlier in NIR news.[3]

Potatoes are measured when they drop from the end of the conveyer belt (the measurement can be performed on the conveyer belt, too).[4] When te potato falls and enters the measurement zone it attenuates the signal from a light source. This rapid attenuation is detected by a detector, which is just opposite the light source. Then the OBJECT PRESENT signal is created. This signal triggers the measurement cycle, which consists of "slices" of potatoes. The slice length is typically around 1 ms (equal to a 2-3 mm slice of potato). These slices are measured at three different wavelengths and 2Rx2T geometry (two reflectance 0º/45º geometry and two transmittance 0º/135º channels). In total, this is equal to 12 different measurement channels. Also, the "back" side of the potato is measured by reflectance geometry with two wavelengths. When the potato has passed the measurement zone the OBJECT PRESENT signal is reset. During the time between the falling of potatoes a standardization value is measured at two wavelengths with a detector, which is just opposite the light source. The total number of measurement channels then equals 16.

One measurement slice consists of a series of analogue to digital conversion (ADC) operations. Different measurement channels are measured sequentially (interval 1.6 µs). Within the time available for one slice this cycle is repeated n (n=slicetime/(16*1.6 µs)) times and the subsamples of each measurement channel are averaged.

### *ELECTRONICS: LIGHT SOURCE, DETECTORS AND DATA ACQUISITION*

The light source is a halogen lamp and the detectors are silicon (Si) photodiodes. Preamplifiers are transimpedance preamplifiers without bias. This kind of arrangement is especially suitable for low frequency photometric applications (as is the case with the V-camera). Data acquisition is based on the PC/104 standard I/O board developed at VTT Electronics (ReMix/104), which is connected to a PC/104 processor board. Some of the signal processing (e.g., subsample averaging and reflectance channels summing) is performed on ReMix/104. Classification is done on a PC/104 processor board. This kind of arrangement is very flexible and in future allows us to implement easily more complicated classification routines.

### *OPTICS AND MECHANICS*

The optical construction of the illumination unit is simple and robust. The only components are the light source, elliptical mirror, window, and target.

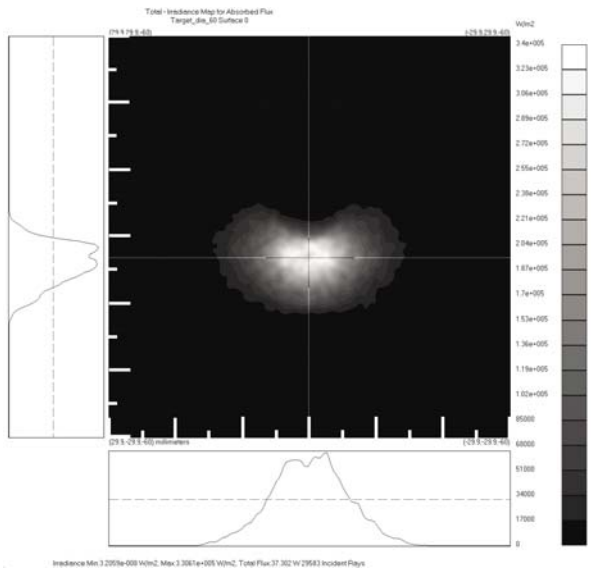

***Figure 1. Simulated spot diagram of the illumination on spherical surface (image area 60 mm x 60 mm)***

A 3-D model of the optics was built to optical design software and all simulations were carried out with the real construction of all optical and mechanical components. The simulations proved that the optics behave as designed, Figure 1. One of the main issues in the illumination unit was to ensure that as little stray light as possible is detected by the measurement channels. In that sense this construction is simulated to work well. The mechanical 3-D model of the illumination unit is presented in Figure 2.

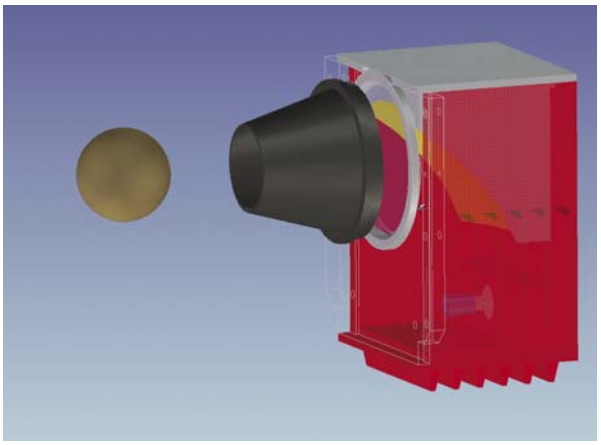

***Figure 2. Mechanical model of the illumination optics.***

To also minimize the chromatic aberration of the system the detection optics were designed using mirrors instead of lenses. This also gave free hands to place the components and to reduce the size of the construction.

The detection optics of the system is more complex, since each measurement geometry needs its own optics and each of these consists of three wavelength channels to be constructed. All wavelengths must be treated equally, so that changes in the measurement distance and intensity should not affect the intensity ratios of different wavelengths.

The detection optics consists of two main parts:

- Spatial filtering part – all components before the aperture including itself, and
- Chromatic filtering – all components after the aperture.

A 3-D model of the optics was built to optical design software and all simulations were carried out with the real construction with all optical and mechanical components (Figure 3). The simulations proved that the intensity instability of the system is less than 5 % when the size of the target sphere (potato) was changed from 35 mm to 60 mm and 80 mm. It also proved that all wavelength channels have an equal detection area and that the detector is large enough.

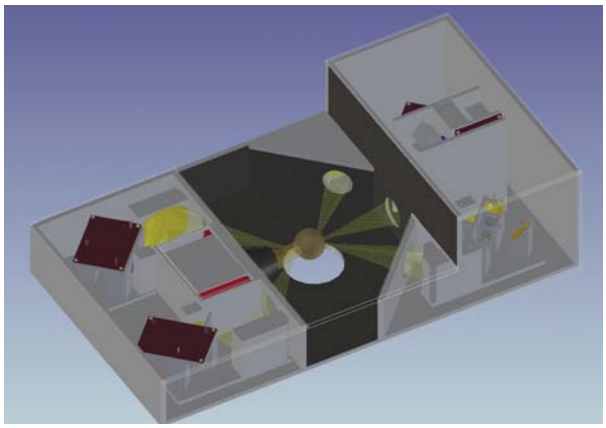

***Figure 3. Mechanical model of the V-Camera combined with ray paths from optical simulation***

### *MEASUREMENTS*

In Figure 4 are signals from an artificially defective potato measured by the developed V-camera. The potato had a 4 mm wide black tape around its center. For the purposes of clarity only transmittance and reflectance from one wavelength and one measurement angle are presented. Low reflection from the tape is clearly visible in the reflection signal and also the high absorbance of the tape is visible on the transmission channel.

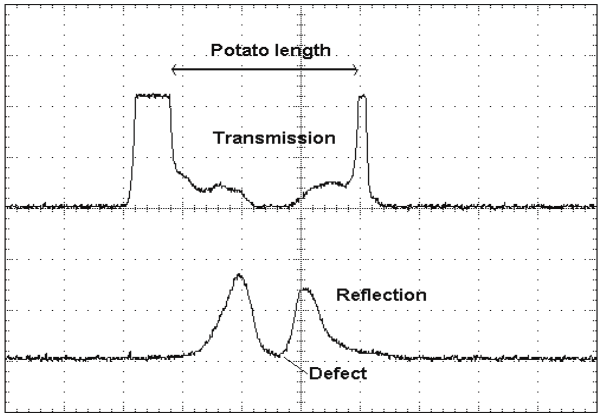


***Figure 4. Transmittance and reflectance signals at one wavelength from a defective potato, defect at the centre of potato.***

### *DISCUSSION*

The first measurements with the developed V-camera show that the system has a high signal to noise ratio. Also small defects are clearly visible. The system will be tested

extensively with a large range of potatoes and the capability to sort potatoes on-line will be demonstrated.

***ACKNOWLEDGEMENTS***

This project is funded under the Fifth Framework Programme of the European Commission, Thematic Programme ***Quality of Life and Management of Living Resources***, Key Action 1 ***Food Nutrition and Health*** (Project QLK1-2000-00455).

***REFERENCES***

1. G. Krivoshiev, Bulgarian patent BG No. 101 069 (In Bulgarian), (1996).
2. G. Krivoshiev, R. Chalucova, M. Moukarev, Lebensm.-Wiss. Technol. 33(5), 344 (2000).
3. G. Krivoshiev, R. Chalucova, M. Moukarev, NIR news 11(5), 7, (2000).
4. G. Krivoshiev, R. Chalucova, P. Bojilov, A. Lyongov, N. Katrandzhiev, M. Känsäkoski, Y. Gegov, V. Slavchev, and V. Fidanchev, Fifth European Symposium on Near InfraRed (NIR) Spectroscopy, 15-17 September 2003, Comwell, Kolding, Denmark, Report No. 03-09-02, ISSN 0906-8465, pp. 92-100.

R.P. Chalucova
G.P. Krivoshiev
P. Bojilov
***Institute for Horticulture and Canned Foods, 154 V. Aprilov Blvd., Plovdiv 4000, Bulgaria***

H. Vasama
***Suomen Optomekaniikka, Palokka, Finland***

Markku Känsäkoski
***Markku.Kansakoski@vtt.fi***

Veli Heikkinen
***Veli.Heikkinen@vtt.fi***

Pekka Suopajärvi
***Pekka.Suopajarvi@vtt.fi***

Risto Mitikka
***Risto.Mitikka@vtt.fi***

# Development of an Optical Detection System for Diseases in Field Crops

### *INTRODUCTION*

The most widely used practice in pest control is still spraying pesticides uniformly over the agricultural fields at different times during the cultivation cycle of arable crops. Most disease infestations are however not evenly distributed across the field but occur in patches with large areas of the field free of diseases or with a very low weed density in an early stage of infestation. Excessive use of pesticides raises the danger of toxic residue levels on agricultural products.

The main objective of the project was to develop a ground based real-time remote sensing system for detecting diseases in arable crops in an early stage of the development of the disease before the disease can visibly be detected. The methodology was based upon differences in reflectance variations between healthy and diseased plants. The early detection of diseases can be used to reduce pesticide use through spatially variable treatment.

### *THE MEASUREMENT*

The detection of the diseased plants is based on the changes of the plant's chlorophyll, which can be seen as a spectral change in the very near infrared range (800 - 1000 nm). These changes must be ratioed to the reflectivity at the green (550 nm) region of the plant's spectra. To evaluate the feasibility of the optical detection methods, a prototype was built on a 15 m spraying boom. The measurement area is covered by collecting 15 measurement points from the canopy with fiber optics. One additional fiber is used to measure ambient light spectrum used as a reference. The fibers are connected to Specim PGP (prism-grating-prism) spectrograph and CCD camera, which form a spectrum from each of the measurement points. The field of view of each fiber was limited to 30 cm diameter with a collimating lens in front of the fiber.

To be able to detect spatially more accurate information from the field, a high resolution Duncantech 3CCD CIR (Color Infrared) camera was used. The camera collects 1920 x 1080 pixel images centered at 550 nm (green), 660 nm (red) and 800 nm (NIR). The area imaged is only a small portion of the whole 15 m spraying width.

The measurement data is localized with a DGPS system integrated in the instrument giving submeter spatial accuracy.

As the result of the measurement, a disease map and further also a spraying map with a one meter grid can be generated. In the OPTIDIS project, also methods and equipment for precision spraying were developed.

### *INSTRUMENTATION*

VTT's role in OPTIDIS consortium was the instrumentation. The high demands for the application was set first by the harsh field conditions including high temperatures, highly varying ambient light level, dust, moisture and vibration. Secondly, as the instrument was used to collect experimental data with two cameras, the amount of collected data was very large. The system was required to measure at least one image per meter for both the CIR and spectrograph. This leads to requirement of data collection capacity more than 20 MB/s on typical spraying speeds.

The protype system consists of:

- multi-point fiber optic spectrograph
- 3CCD color infrared camera
- dGPS receiver
- PC with 20 MB/s input data rate

The instrument was packaged to sustain field conditions. The cooling air was filtered and fiber optics was air purged to avoid dusting problems (figure 1).

An easy-to-use and very flexible measurement software was designed for the instrument. The data collection was made based on either spatial triggering by dGPS signal or sequential fixed interval based measurement.

***Figure 1. The measurement prototype was made to withstand field conditions.***

### *THE FIELD TESTS*

The instrument was tested in wheat fields infected with yellow rust and septoria at Leuvain-la-Neuve in Belgium (figure 2). Variation was introduced also for the fertilization. The results were analyzed both, the CIR imaging and fiber optical spectral data. The diseases cause small lesions in the early stages. For this, the high resolution CIR imaging was successfully applied. Using simple algorithms like normalization and rationing the soil, leaves and lesions were recognized. A good correlation to visual inspection was achieved.

The multi-point spectrograph measurements showed too low sensitivity for the detection of the yellow rust and septoria. During the season, the disease came out late and severity was low even in the infected plots. Later during the season, the ears of the wheat interfere with the measurement. This does not typically harm the measurement since it is too late for spraying.

However, a good correlation to nitrogen stress (level of fertilization) was achieved.

***Figure 2. Field tests were performed at intentionally infected fields.***

### *CONCLUSION*

The CIR imaging based detection can be effectively used to detect early stages of wheat diseases like yellow rust and septoria. The diseases cause small lesions in the leaves that must be detected. Therefore, resolution of the instrumentation must be near the size of the typical lesions to effectively detect the diseases in their early phases. The sensitivity of the multi-point fiber optic spectrograph is not good enough for the disease detection, but it is very suitable for the properties that affect the whole plant like nitrogen stress. However, if the PGP could be used as a line imaging spectrograph effectively, then the width of the detection area would be limited.

Antti Kemppainen
***Antti.Kemppainen@vtt.fi***

Tapio Vaarala
***Tapio.Vaarala@vtt.fi***

Jari Miettinen
***Jari.Miettinen@vtt.fi***

Ralf Marbach
***Ralf.Marbach@vtt.fi***

Dimitrios Moshou, Cédric Bravo
***Katholieke Universiteit Leuven***

Roberto Oberti
***Università degli Studi di Milano***

# Micro-mechanical Shutter Array for Replacing Infrared Photodetector Arrays

## 1 INTRODUCTION

Infrared photodetector arrays offer performance advantages over other types of optical sensing architectures, but, especially when multiplexed, photodetector arrays come at a price:

- high unit cost (relative to single-element detectors)
- limited number of suppliers
- generally, arrays are often ”overkills” (only few pixels needed)
- high NRE is barrier to effective customization
- OEM customers have limited design control
- choice of array materials is more limited than for single-elements photodetectors

## 2 PROPOSED SOLUTION

A new type of low-cost MEMS shutter array, which was developed at CRF originally for displays in cars, has the potential to overcome the problems listed above and replace photodetector arrays in many infrared sensing applications. As shown in Fig. 1, the photodetector array is replaced with, a linear MEMS shutter array and a single-element photodetector.

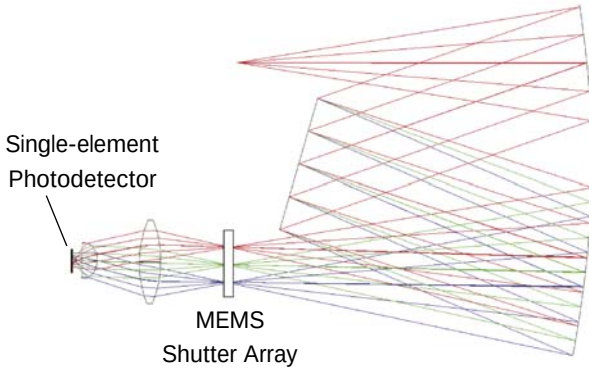


***Figure 1. Concept of proposed solution.***

## 3 DEVICE STRUCTURE

The structure of the device is shown in Fig.2. The device is based on an optically transparent substrate, e.g., glass or sapphire. The substrate is coated with two optically transparent layers, viz., first an electrically conductive layer and then an insulating layer.

The structure of the pixels is defined in the next layer, which is a metallic layer about 1 micrometer thick. The movable part of each pixel is realized by a flexible, rectangular, metallic petal, which is fastened to the substrate at one end but released from the underlying insulating layer over most of its length. Without any external forces applied, the pedal “curls up” away from the substrate due to internal stresses build into the metal. In this position, the pixel can transmit light. When a voltage is applied between the flexible metal and the conductive layer in the substrate, then the petal rolls down “flat” onto the substrate and the pixel is closed to light transmission. In this position, the petal reflects light. The overall structure of the device gives it a feeling of an optical device, rather than an electronic device.

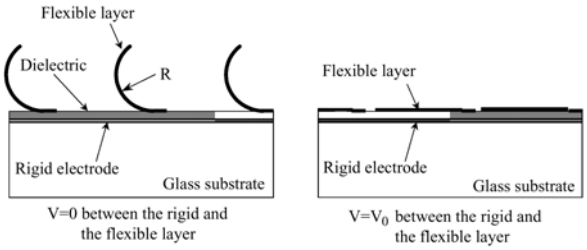


***Figure 2. Structure and working principle.***

## 4 DEVICE REALIZATION

A number of one-dimensional (linear) and two-dimensional shutter arrays were realized by CRF in Orbassano, Italy. SEM photographs of a 2D array are shown in Fig. 3, where all petals are shown in the curled-up position. With typ. 80 Volts applied, the petals roll down flat onto the substrate. Both the opening speed (curling up) and the closing speed (rolling down) are on the order of 2 – 3 m/s, or about 250 μs for 0.5 mm of active shutter length.

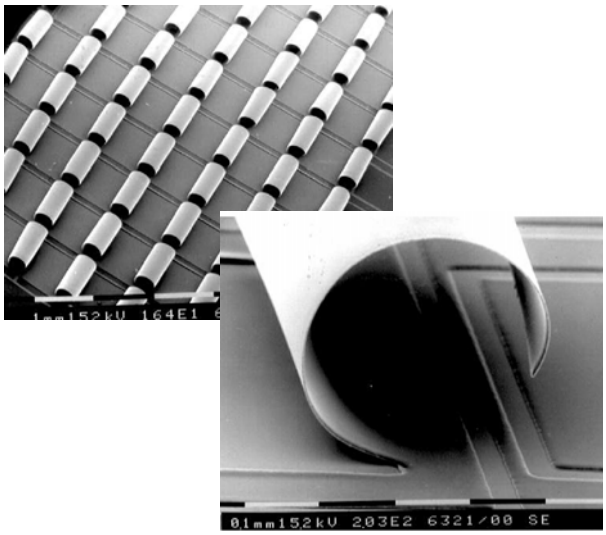


***Figure 3. SEM photographs of 2D shutter array.***

## 5 ADVANTAGES

The mfg’ing processes allows very low unit cost and is potentially multi-sourced. Both linear or 2D arrays are possible, with pixels being individually addressable in

both. Customization of pixel geometry is possible to system manufacturers at very low NRE. Pixels have a "digital" response that is freely programmable by the user, e.g., in a Hadamard sequence. A choice of substrate materials is available, including glass and sapphire, which in turn allows utilization over a wide wavelength range including the visible, near infrared, and mid infrared ranges. The device can be used in both transmittive and reflective optical architectures. Hermetic packaging is not required, instead, dust-proofing is sufficient.

### *6 STATUS AND OUTLOOK*

First devices based on this thin-film technology were made by CRF in 1996. A first display prototype was mounted into a car instrument cluster (dashboard) in 2000. Linear arrays of shutters have been fabricated at CRF for use in optical measurement systems; integration and test of first systems is ongoing at VTT. Lifetime of >3,000 hours of continous operation is already demonstrated. Current R&D efforts are directed at decreasing the operating voltage as well as at achieving an extremely low mfg'ing cost.

### *7 SUMMARY*

A new type of MEMS shutter array has become available that can be used as an alternative to photodetector arrays. The new MEMS array reduces part cost to a point where infrared sensing seems possible even in consumer-type applications. Companies interested in the commercialization of the technology are encouraged to inquire.

### *8 REFERENCES*

1 Marco Pizzi, Valerian Koniachkine, Elena Bassino, Sabino Sinesi, Pietro Perlo, "Electrostatic microshutters-micromirrors array for light modulation systems," ***SPIE Proc. 3878*** (Miniaturized Systems with Micro-optics and MEMS, Santa Clara, 1999), p. 164 - 171

2 V.Koniachkine, M.Pizzi, M.Nieri, S.Sinesi,P.Perlo, G. Innocenti, "MEMS based display for automotive applications," ***Proc. Vehicle Displays 2000***, Dearborn (USA), SID and IEEE

3 M. Pizzi, V. Koniachkine, O. De Martfis, R. Marbach, "New type of micro-mechanical shutter array for replacement of infrared photodetector arrays," ***Int'l Conference on Optical MEMS***, IEEE and LEOS, Waikoloa, Hawaii, USA 18-21 Aug. 2003, p. 173- 174

Financial support by the European Community under IST-2001-35150 is gratefully acknowledged.

Ralf Marbach
***Ralf.Marbach@vtt.fi***

Marco Pizzi
Valerian Koniachkine
Omar De Martiis
***Centro Ricerche Fiat. Strada Torino 50, 10043 Orbassano (TO), Italy.***

# Advanced Laser Triangulation

Industrial machine vision applications have increased strongly in recent years. For example, measurements monitoring and warning of errors in electronics assembly are already standard technique. Also solutions for inspecting the quality of different surfaces, e.g., color uniformity and surface smoothness are in an ever more important role in manufacturing high quality products.

The need for automated 3D measurements is evident when the volume or shape of different mass produced objects has to be estimated. We have a vision of an automated 3D measuring station which could gauge the 3D shape of any medium size product, between 10 - 100 mm in all dimensions, practically irrespective of its shape. The measuring principle is triangulation carried out with camera and line laser and the measured object could be moved either with a precise cartesian robot using embedded high-quality positioning or, alternatively, with any movers with accurate measurement of position. Camera image could also be used, e.g., for locating very small details and for inspection of surface quality.

Triangulation measurement is intended to carry out with a thin, 5 - 15 µm laser line. With line laser, hundreds of discrete 3D points on the object can be measured simultaneously. The measurement resolution is chosen according to tolerance needs. In very accurate measurements, the measured area on object is under 5 x 5 $mm^2$ which sets high requirements for positioning accuracy. A schematic drawing of the triangulation set-up and of an actual measuring system is depicted in figure 1.

As stated previously, triangulation with line laser can produce hundreds of 3D points from one profile measurement simultaneously. If a very small object, e.g., 100 x 100 µm, is measured with 5 - 10 scans, its volume can be estimated very accurately. Depending on the camera and the mechanics of the mover, anything from a few to hundreds of individual profile measurements can be made in one second.

Precise measurements can be carried out, e.g., with a commercially available low cost laser. One example of the laser has a wavelength of 670 nm, 30 mm working distance and 3.7 mm line length; the width of the line varies between 9 - 12 µm. An area of 3.7 x 1.0 $mm^2$ can be scanned accurately, with 20 µm intervals, in one second. In this arrangement, the image frequency would be 50 frames/s. An example of measurement possibilities is shown in figure 2, where the width and the depth of the groove are measured. The position of holes in the grooves can be tracked with camera image.

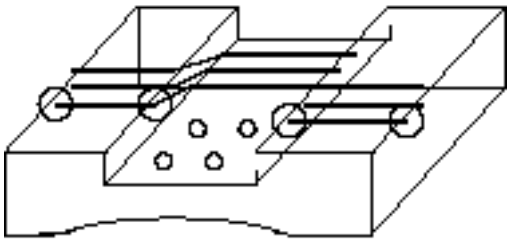

***Figure 2. A schematic diagram of a measured object.***

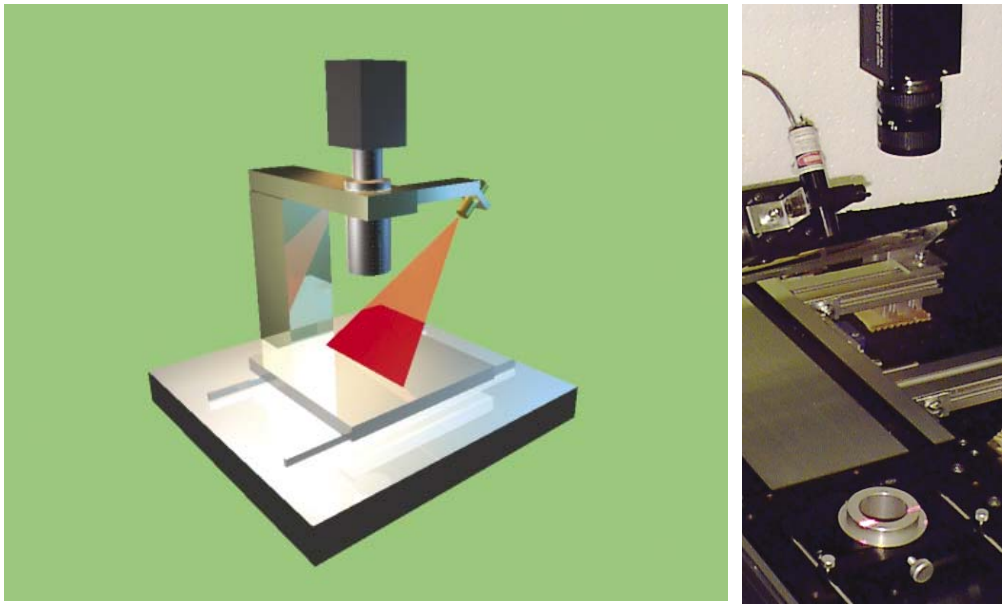

***Figure 1. Schematic drawing and actual measuring system of a triangulation system.***

The system can be used, e.g., for off-line measurements of a few control specimens of a specific batch. Monitoring of tolerance accuracy, surface quality or following up of the wear and tear of the machine tool could be carried out with the help of this precise measurement data.

### *EXPERIMENTAL SET-UP FOR TRIANGULATION*

In an experimental set-up, we examined one aspect of the 3D measurement station, namely the triangulation principle with a single axis mover. Our equipment consists of a single axis linear mover controlled by the PC, grabber card, microscope, 3CCD RGB camera and single line laser. The set-up was planned as follows: The resolution of one pixel corresponds to 6.4 µm on object. This enlargement can be, according to optionality of the resolution in our idea of the 3D measurement station, anything between 2.0 - 6.4 µm. Due to the large width of the laser line, appr. 60 µm, we decided to use one fixed resolution. The size of the object can be up to 4.9 mm wide and the length up to 400 mm, with the image size of 768 x 576 pixels. The scanning interval of the object is 60 µm. The scanning speed for one image is appr. 0.4 s. Due to the experimental nature, we didn't optimize for the speed of scanning.

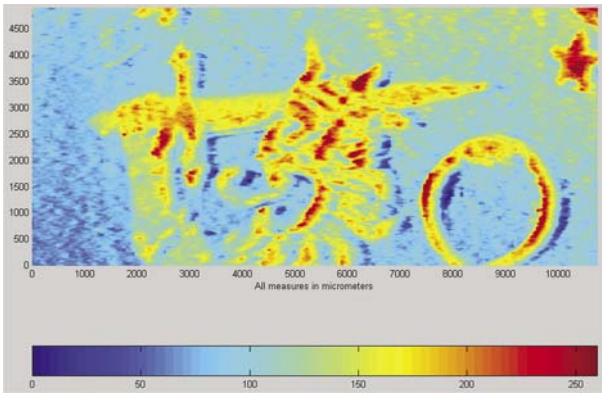


***Figure 3. The reverse side, the lion of the Finnish coat of arms, in the 5 cent coin.***

For image processing, we opted for Matlab programming because it gives more flexibility for experimentation in algorithm development. Thus, every separate red channel image was saved in the hard drive and the 3D image was composed immediately after the scanning. The laser line was extracted from the image with the center of gravity algorithm. First the noise, due to ambient light, was cut away and the center of the laser line was searched with two consecutive calculations, from coarse to fine. This method seemed to produce good results even though the laser line is in itself noisy because of the speckle. The location of the center line was then converted to height. The imaging geometry was set so that a height of 1 mm on object corresponded to 166 pixels in image. Thus, deviation of 1 pixel from the zero level in image meant appr. 6 µm in height. The combined height information of all images produces a 3D image. One example is shown in figure 3, where the reverse side of the Finnish 5 cent coin is depicted.

### *CONCLUSIONS*

There is a clear need for fast and simple, factory floor automated 3D measurements for off-line monitoring of the production quality in many fields of the industry. In this work, we demonstrated the viability of one aspect of the automated 3D measurement station. A lot more work needs to be done to develop a truly versatile tool for combined inspection and monitoring of surface quality and tolerances. This kind of tool can be made combining the many possibilities of camera-based machine vision.

Mikko Lindholm
***Mikko.Lindholm@vtt.fi***

# Preparation of Multifunctional Coating Materials and their Applications

VTT Electronics, Espoo. 62 p. + app. 33 p. VTT Publications : 499 ISBN 951-38-6227-5; 951-38-6228-3

Sol-gel technique has been utilized for the fabrication of multifunctional inorganic organic hybrid materials for specific applications. Synthesized methacrylic acid and benzoylacetone modified tin alkoxide precursors were used for the first time for the realization of directly UV-photopatternable antimony-doped tin dioxide coatings. These single-layered coatings have transmission values over 80 % at visible wavelengths and maximum electrical conductivity values around 15 S/cm. In comparison, multi-layered coatings without UV-photopatternability properties were fabricated. In this case, electrical conductivities are in the range of 102 S/cm. A novel material technique approach for laser protective eyewear was utilized for the synthesis and preparation of the mechanically tolerant and near-infrared absorbing filter coatings. Optical densities from 2 to 4 at laser threat wavelength, a ten fold increase in scratch resistance, and a hundred-fold increase in abrasion resistance, compared to uncoated polycarbonate substrates, were obtained by using absorbing dye-molecule doped sol-gel materials. Fabrication of a diffractive optical element, namely axicon, using hybrid-glass materials was demonstrated for the first time. Hybrid-glass material was tailored to fulfill the requirements of the functional axicon element.

Terho Kololuoma
***Terho.Kololuoma@vtt.fi***

# Reflective Thin-film Coatings of the Ultraviolet Region

University of Oulu, Department of Physical Sciences , Oulu. 87 p. Master Thesis

This thesis examines thin-film coatings, their design and manufacture. Special consideration is given to reflective thin-film coatings of the ultraviolet region, which are a certain application area of thin films. Many thin-film materials are absorbent at the ultraviolet light wavelength region, which causes special problems in the design and manufacture of coatings.

The first part of the work deals with calculating the properties of thin-film coatings. Starting with Maxwell's equation, the theory of electromagnetic waves will be dealt with and the results required for the handling of thin-film coatings are presented. Using the theory, the reflectivity and permeability of a simple two-medium interface are calculated. On the basis of the results, a matrix method is derived with which the discrete reflectivity, permeability and absorption ratio of the thin-film coating can be calculated. In addition, the light phase change caused by the coating and the effect on light polarization as well as the effect of the substrate on the coating properties will be examined.

The final part of the thesis deals with the design and manufacture of reflective thin-film coatings. First, different metal mirrors, protection of mirrors and the effect of a protective coating on the mirror properties as well as improvement of mirror reflectivity with dielectric thin-film coatings are examined. Then, reflective coatings formed only from dielectric materials and the use of absorbent coating materials are examined. In the section that deals with the manufacture of coatings, we become acquainted with the manufacturing process by presenting a typical vacuum vaporization apparatus, its various components and their operation. Additionally, a method for calculating the refractive index of coated materials is presented along with two coating materials.

The final section of the work deals with test coatings manufactured at the Finnish Defense Forces' optical depot. For the purpose of designing the coatings, the refractive indices of the coating materials are specified with the help of the test coatings. The coatings are designed using the specified refractive indices. Finally, the properties of the manufactured coatings are assessed. The test coatings show that manufacture of coatings is significantly more difficult than their design.

Antti-Jussi Mattila
***Antti-Jussi.Mattila@vtt.fi***

# Synthesis and Characterisation of Optical Sol-gel Waveguide Materials

University of Oulu, Department of Chemistry , Oulu. 81 p. + app. 3 p. Master Thesis

Plastics and glasses are materials traditionally used to transmit light in optical data transmission applications. Sol-gel technique takes advantage of the best parts from both materials. It is a technique, where solid organic/ inorganic hybrid glass materials can be derived from a liquid phase and can have a wide variety of properties.

Target for this thesis was to study sol-gel based passive optical waveguide materials for planar optical applications. Their usefulness in optics has been studied widely, but quite often these materials are not suitable due to high C-H and O-H contents. These bonds and especially O-H bonds cause strong absorption loss at telecommunication wavelength windows, which are around 1310 and 1550 nanometers. Therefore, materials were synthesised to contain these bonds as low amount as possible.

Several optical waveguide materials were synthesised within the framework of this thesis. Two of them were optically characterised (refractive indices, birefringences and optical losses) to study their applicability for planar optical applications. Raman technique was employed to study reaction kinetics in one system. In addition, a fluorinated silane precursor was synthesised and characterised by nuclear magnetic resonance (NMR). Fluorination (C-H to C-F) decreases optical losses in sol-gel waveguide materials. Other ways to decrease optical losses are deuteration (C-H to C-D) and chlorination (C-H to C-Cl).

Best results were achieved with chlorinated materials. Surface roughness of the planar waveguide structure (slab structure) was 3 nanometers. Optical losses of the waveguide were around 1 dB/cm at 1310 and 1550 nm wavelengths and around 0.4 dB/cm at 830 nm wavelengths. Film thickness for the same material was approximately 4 micrometers.

Mikko Keränen
***Mikko.Keranen@vtt.fi***

# Design and Implementation of Preamplifier for Lead Sulfide Array Detector

Department of Electrical and Information Engineering, University of Oulu, Oulu, Finland. Diploma Thesis, 70 p.

The purpose of this work is to integrate a lead sulfide array detector with the thermoelectric cooler element into a hermetically sealed package. The integration makes it possible to increase the number of detector elements without increasing the number of pins. As a detecting material lead sulfide's responsivity reaches to longer wavelengths than most of the photodiode's responsivities.

A preamplifier structure is implemented on to the LTCC-substrate into a hermetically sealed package right next to the array detector, which minimizes the coupling of the interferences into high ohmic leads. After the signal has been preamplified, it will be serialised by using multiplexers. This decreases the pincount through the walls of the package. The LTCC-substrate makes it possible to integrate the preamplifier circuitry in a very efficient manner using discrete high quality passive components.

The measurements of the implemented preamplifier structure have revealed that capacitive coupling of the signal between different channels is too high for proper performance. This can be solved with improved layout design. Due to multiplexing, the data logging and data handling are challenging and the amount of logged data is high.

Linearity and relatively high detectivity are the key benefits of lead sulfide detectors, when comparing these to other detector materials that reach to the same wavelength range. The measurements confirm this.

In the field of spectrometry there is a clear need for wide wavelength region array detectors, which are linear, competetive in price and which have high detectivity D*.

One possible solution for preamplifier implementation is the method used in this work.

Ville Moilanen
***Ville.Moilanen@vtt.fi***

# The Use of Raman Spectroscopy to Assess the Degree of Crystallinity of Lactose

University of Oulu, Department of Chemistry, Oulu. (2003), 84 p. Pro Gradu

The present study was carried out to evaluate the suitability of Raman spectroscopy to determine the crystallization rate of lactose. Raman spectroscopy offers the advantages of short measurement times, relatively low scatter between measuring points and the possibility of on-line measurements. No processing of the samples is required by the method.

A number of physical solution series were prepared by mechanically mixing lactose monohydrate with amorphous lactose in suitable proportions. Linear calibration lines were obtained for the physical solutions. A number of lactose samples made using the fog-drying method were also investigated. The results obtained for fog-dried lactose samples were compared with IMC determinations.

Raman spectroscopy is capable of reliably identifying the percentage of amorphous lactose, and the determination of the crystallization rate can be done much faster than with conventional methods (XRD, IMC, DSC) while the detection limit was equal or even superior to some of the reference methods (DSC, IMC). With the advancement of equipment design and methodology, Raman spectroscopy will probably become increasingly popular in pharmaceutical research and quality control.

Maarit Päällysaho

# List of Refereed Papers

Ailisto, Heikki; Lindholm, Mikko; Tikkanen, Pauli. A review of fingerprint image enhancement methods International journal of image and graphics. World scientific publishing, vol. 3 (2003) 3, s. 401 - 424.

Ge, J.; Turunen, M.P.K.; Kusevic, Maja; Kivilahti, J.K.. Effects of surface treatment on the adhesion of copper to a hybrid polymer material Journal of materials research., vol. 18 (2003) 11, s. 2697 – 2707.

Grenier, P; Bellon-Maurel, V; Wilson, R; Niemelä, Pentti. Using spectroscopic techniques to monitor food composition (chapter 15), Rapid and on-line instrumentation for food quality assurance.Tothill, Ibitsam E. (Ed.). Woodhead Publishing (2003)

Jääskeläinen, A.-S.; Nuopponen, M.; Axelsson, P.; Tenhunen, Mari; Löija, M.; Vuorinen, T.. Determination of lignin distribution in pulps by FTIR ATR spectroscopy Journal of Pulp and Paper Science., vol. 29 (2003) 10, s. 328 - 331.

Kololuoma, Terho. Preparation of multifunctional coating materials and their applications. Espoo, VTT Electronics, 2003. 62 p. + app. 33 p. VTT Publications; 499. ISBN 951-38-6227-5; 951-38-6228-3

Kololuoma, Terho; Kärkkäinen, Ari H. O.; Tolonen, Ari; Rantala, Juha T.. Lithographic patterning of benzoylacetone modified SnO2 and SnO2:Sb thin films, Thin Solid Films. Elsevier, vol. 440 (2003) 1 - 2, s. 184 - 189.

Kärkkäinen, Ari H. O., Rantala, Juha T., Tamkin John M.,and Descour, Michael R., “Photolithographic processing of hybrid glasses for micro-optics applications”, IEEE Journal of Lightwave Technology, Vol 21, No. 3, (2003).

Vyörykkä, J.; Paaso, Jouko; Tenhunen, Mari; Tenhunen, Jussi; Iitti, H.; Vuorinen, T.; Stenius, P.. Analysis of depth profiling data obtained by confocal Raman microspectroscopy, Applied Spectroscopy., vol. 57 (2003) 9, s. 1123 - 1128.

# International Conference Papers

Ailisto, Heikki; Haataja, Ville; Kyllönen, Vesa; Lindholm, Mikko. Wearable context aware terminal for maintenance personnel. 1st European Symposium on Ambient Intelligence (EUSAI 2003). Veldhoven, NL, 3 - 4 Nov. 2003. Ambient Intelligence. Lecture Notes in Computer Science Vol. 2875. Aarts, Emile et al. (Eds.). Springer-Verlag (2003), s. 149 - 159.

Anduaga, J.; Mayora, K.; Garmendia, I.; Munoz, M.; Niemelä, Pentti; Tornberg, Jouni; Hietala, Eero; Manero, F.. Development of a NIR device for measuring varnish thickness on-line. 11th International Conference on Near-Infrared Spectroscopy. Cordoba, Spain, 6 - 11 April 2003. NIR-2003 : stretching the NIR spectrum to the limit. NIR Publications (2003), s. P.8.16.

Gnyba, M; Keränen, Mikko; Suhonen, Janne; Niemelä, Pentti; Bogdanowicz, Robert; Jedrzejewska-Szczerska, Malgorzata. Raman scattering measurements in monitoring of polymer synthesis process. Lightmetry 2002: Metrology and Testing Techniques Using Light. Pluta, Maksymilian; Szyjer, Mariusz (Eds.) Proceedings of SPIE Vol. 5064. SPIE (2003), s. 103 - 108.

Gnyba, Marcin; Jedrzejewska-Szczerska, Malgorzata; Keränen, Mikko; Suhonen, Janne. Sol-gel materials investigation by means of Raman spectroscopy. XVII IMEKO World Congress: Metrology in the 3rd Millennium. Dubrovnik, Croatia, 22 - 27 June, 2003. Croatian Meterology Society (2003), s. 237-240.

Gnyba, Marcin; Keränen, Mikko. Optical investigation of molecular structure of sophisticated materials for photonics Photonics Applications in Astronomy, Communications, Industry, and High-Energy Physics Experiments. Romaniuk, Ryszard S.; Pozniak, Krzysztof T. (Eds.). Proceedings of SPIE Vol. 5125. SPIE (2003), s. 339 - 344.

Gnyba, Marcin; Keränen, Mikko. Raman diagnostics in manufacturing of polymer planar optical waveguides. Optical Fibers and Their Applications VIII. Dorosz, Jan; Romaniuk, Ryszard S. (Eds.) Proceedings of SPIE Vol. 5028. SPIE (2003), s. 219 - 224.

Heikkinen, Veli; Aikio, Janne; Alajoki, Teemu; Hiltunen, Jussi; Mattila Antti-Jussi; Ollila, Jyrki; Karioja, Pentti. Mems packaging using precision machined LTCC substrates International Conference on Optical MEMS (MOEMS 2003), 2003 IEEE/LEOS. Waikoloa, Hawaii, USA 18 - 21 Aug. 2003. IEEE (2003), s. 81 - 82.

Immonen M.; Karppinen Mikko; Kivilahti J.. Fabrication and characterization of optical polymer waveguides embedded on printed wiring boards. Proceedings of Polytronic 2003, 3rd International IEEE Conference on Polymers and Adhesives in Microelectronics and Photonics. Montreux, CH, 21 - 23 Oct. 2003. Tima (2003), s. 91 - 95.

Jaakola, Tuomo; Kautio, Kari; Petäjä, Jarno; Lenkkeri, Jaakko. Thermal management of power MMIC on LTCC substrate 14th European Microelectronics and Packaging Conference: EPMC 2003. Friedrichshafen, DE, 23 - 25 June 2003. IMAPS (2003), s. 86 - 91.

Jabbour, Ghassan E.; Yoshioka, Yuka; Tuomikoski, Markus; Kololuoma, Terho; Kopola, Harri. Prospects of printing techniques in low cost organic electronics and optoelectronics Northern Optics : The Joint Conference of the Optical Societies of Denmark, Finland, Norway and Sweden, 16 - 18 June 2003, Espoo, FI. Teknillinen korkeakoulu (2003), s. 35.

Kaitanen, Erja; Niemelä, Pentti; Päällysaho, Maarit; Harjunen, Päivi; Suhonen, Janne; Järvinen, Kristiina. Evaluation of the amorphous content of lactose by solution calorimetry and Raman spectroscopy. XVII Helsinki University Congress of Drug Research. Helsinki, Finland, 5 - 6 June 2003. European Journal of Pharmaceutical Sciences., vol. 19 (2003)Suppl. 1, s. S36.

Karppinen, Mikko; Mäkinen, Jukka-Tapani; Kataja, Kari; Tanskanen, Antti; Alajoki, Teemu; Tuominen, Jarkko; Hiltunen, Jussi; Keränen, Kimmo; Karioja, Pentti; Immonen, M.; Roos, R.; Kivilahti, J.. Optical interconnects on printed wiring board Northern Optics : The Joint Conference of the Optical Societies of Denmark, Finland, Norway and Sweden. Espoo, Finland, 16 - 18 June 2003. Eero Noponen (Ed.). Teknillinen korkeakoulu (2003), s. 93.

Kataja, Kari; Olkkonen, Juuso; Aikio, Janne; Howe, D.. Numerical simulations of super resolution structures Northern Optics : The Joint Conference of the Optical S cieties of Denmark, Finland, Norway and Sweden. Espoo, Finland, 16 - 18 June 2003. Eero Noponen (Ed.). Teknillinen korkeakoulu (2003), s. 40.

Kataja, Kari; Olkkonen, Juuso; Aikio, Janne; Howe, D.G.. 3D FDTD simulations of super resolution structures. ISOM 2003, International Symposium on Optical Memory. Nara, Japan, 4 - 7 Nov. 2003. Technical Digest ISOM03. (2003), s. 82 - 83.

Kataja,Kari; Olkkonen, Juuso; Aikio, Janne; Howe, Dennis. Super resolution modeling using FDTD method AIST/ LAOTECH Workshop on International Super-RENS and Plasmon Science & Technology Symposium ISPS. Tsukuba, JP, 20 - 21 Feb. 2003. (2003), s. 5 - 6.

Kolehmainen, Timo T.; Aikio, Janne; Karppinen, Mikko; Mattila, Antti-Jussi; Mäkinen, Jukka-Tapani; Kataja, Kari; Tukkiniemi, Kari; Karioja, Pentti. Simulation of imaging system's performance. Optical Science and Technology. San Diego, USA, 3 - 8 Aug. 2003 Optical modeling and performance predictions. Proceedings of SPIE, Vol. 5178, Mark A. Kahan (Ed.). SPIE (2003)

Kololuoma, Terho; Mäkelä, Tapio; Heilmann, Jali; Haring, Tomi; Kallioinen, Jani; Hagberg, Juha; Kettunen, Ilkka; Kopola, Harri. Printable electronics, optics and optoelectronics Northern Optics 2003, Finnish Optical Society Conference. Espoo, FI, 16 - 18 Jun. 2003. Helsinki University of Technology Publications in Engineering Physics (2003), s. 119.

Kondratyev, Vasili; Lahti, Markku; Jaakola, Tuomo. On the design of LTCC filter for millimeter-waves. IEEE MTT-S International Microwave Symposium - IMS 2003. Philadelphia, PA, USA, 8 - 13 June 2003. Microwave Symposium Digest, 2003 IEEE MTT-S International. Vol. 3. IEEE (2003), s. 1771 - 1773.

Krivoshiev, G.; Chalucova, R.; Bojilov, P.; Lyongov, A.; Katrandzhiev, N.; Känsäkoski, Markku; Gegov, Y.; Slavchev, V.; Fidanchev, V. Conveyor system for the precise determination of internal diseases and defects in potato tubers - NIQAT 5th European Symposium on Near Infrared (NIR) Spectroscopy. Kolding, DK, 15 - 17 Sept. 2003. Biotechnological Institute (2003), s. 92 - 100.

Kusevic, Maja; Maaninen, Arto; Tuominen, Jarkko; Hiltunen, Jussi; Hiltunen, Marianne; Caffola, T.. Fabrication and characterisation of novel sol-gel materials for waveguide applications Northern Optics : The Joint Conference of the Optical Societies of Denmark, Finland, Norway and Sweden. Espoo, Finland, 16 - 18 June 2003. Eero Noponen (Ed.). Teknillinen korkeakoulu (2003)

Kusevic, Maja; Wierzba, Pawel; Gnyba, Marcin; Karioja, Pentti. Low-cost differential refractometer using sol-gel integrated waveguides. Northern Optics : The Joint Conference of the Optical Societies of Denmark, Finland, Norway and Sweden. Espoo, Finland, 16 - 18 June 2003. Eero Noponen (Ed.). Teknillinen korkeakoulu (2003), s.72.

Känsäkoski, Markku; Kemppainen, Antti; Suhonen, Janne; Rantanen, Jukka; Yliruusi, Jouko; Luostarinen, Kari; Nauha, Pentti. Integrated multichannel detectors at process control. 11th International Conference on Near-Infrared Spectroscopy. Cordoba, Spain, 6 - 11 April 2003. NIR-2003 : stretching the NIR spectrum to the limit. NIR Publications (2003), s. P.2.7.

Känsäkoski, Markku; Suopajärvi, Pekka; Heikkinen, Veli; Mitikka, Risto; Chalucova, Raina; Krivoshiev, Georgi; Vasama, Hannu. Monitoring the internal quality of potatoes by simultaneous near infrared transmission and reflection measurement. 11th International Conference on Near-Infrared Spectroscopy. Cordoba, Spain, 6 - 11 April 2003 NIR-2003 : stretching the NIR spectrum to the limit. NIR Publications (2003), s. P.2.8.

Lahti, Markku; Jaakola, Tuomo; Kondratyev, Vasily. Integrated millimeter-wave band-pass filters in LTCC modules. IMAPS Nordic 2003. Espoo, FI, 21 - 24 Sept. 2003. (2003), s. 62 - 66.

Lautzenhiser, Franz; Reynolds, Quentin; Lahti, Markku; Kautio, Kari. High frequency performance characterisation of HeraLock HL2000 zero shrink low temperature cofire ceramic Proceedings of the 33rd European Microwave Conference (EuMC), 2003. Munich, DE, 6 - 10 Oct. 2003. Artech House (2003), s. 13 -16.

Lenkkeri, Jaakko; Jaakola, Tuomo. Advantages of multilayer ceramic technology for MEMS packaging Proceedings : workshop on MEMS sensor packaging. Lyngby, DK, 20 - 21 March 2003. DELTA (2003), s. 4 - 5.

Majamaa, Tero; Ollila, Jyrki; Salo, Timo. Research and development environment for micromodule technology at VTT electronics VTT Symposium 229. 34th R3-Nordic Contamination Control Symposium. Turku, Finland, 2 - 4 June 2003. Wirtanen, Gun & Salo, Satu (Eds).. VTT Biotechnology (2003), s. 311 - 320.

Malinen, Jouko; Kemppainen, Antti; Känsäkoski, Markku; Hietala, Eero. Application of NIR sensor modules for process measurements 5th European Symposium on Near Infrared (NIR) Spectroscopy. Kolding, DK, 15 - 17 Sept. 2003. Biotechnological Institute (2003), s. 85 - 91.

Malinen, Jouko; Lindström, Hannu, Marbach, Ralf. Performance evaluation of standard and extended ingas detector array spectrometers. 11th International Conference on Near-Infrared Spectroscopy. Cordoba, Spain, 6 - 11 April

2003 NIR-2003 : stretching the NIR spectrum to the limit. NIR Publications (2003), s. P.2.3.

Manero, F.; Anduaga, J.; Mayora, K.; Garmendia, I.; Niemelä, Pentti; Hietala, Eero; Tornberg, Jouni. Development of an optoelectronic sensor for measuring varnish thickness on-line. 11th International Conference on Near-Infrared Spectroscopy. Cordoba, Spain, 6 - 11 April 2003. NIR-2003 : stretching the NIR spectrum to the limit. NIR Publications (2003)

Marbach, Ralf. Regression vector as a direct function of the spectrum of interest and the interfering spectra. 11th International Conference on Near-Infrared Spectroscopy. Cordoba, Spain, 6 - 11 April 2003 NIR-2003 : stretching the NIR spectrum to the limit. NIR Publications (2003)

Marbach, Ralf; Suopajärvi, Pekka; Seppänen, Tomi. Zero-alignment rigid housing for offner-type imaging spectrograph by 5-axis CNC machining. 11th International Conference on Near-Infrared Spectroscopy. Cordoba, Spain, 6 - 11 April 2003 NIR-2003 : stretching the NIR spectrum to the limit. NIR Publications (2003), s. P.2.18.

Moilanen, Ville; Kemppainen, Antti; Känsäkoski, Markku; Malinen, Jouko; Marbach, Ralf. ”Integrate-it-yourself” preamp and multiplexer on LTCC substrate, for PbS array. 11th International Conference on Near-Infrared Spectroscopy. Cordoba, Spain, 6 - 11 April 2003. NIR-2003 : stretching the NIR spectrum to the limit. NIR Publications (2003), s. P.2.15.

Moilanen, Ville; Kemppainen, Antti; Känsäkoski, Markku; Malinen, Jouko; Marbach, Ralf. Integrated PbS-array sensor module for NIR analysers Northern Optics : The Joint Conference of the Optical Societies of Denmark, Finland, Norway and Sweden. Espoo, Finland, 16 - 18 June 2003. Eero Noponen (Ed.. Teknillinen korkeakoulu (2003)

Mäkinen, Jukka-Tapani; Aikio, Janne; Putila, Veli-Pekka; Keränen, Kimmo; Karioja, Pentti; Kolehmainen, Timo T.; Haavisto, Janne. Prototyping of miniature plastic imaging lens. Optical Science and Technology. San Diego, USA, 3 - 8 Aug. 2003 Optical modeling and performance predictions. Proceedings of SPIE, Vol. 5178, Mark A. Kahan (Ed.). SPIE (2003)

Niemelä, Pentti; Hietala, Eero; Tornberg, Jouni; Garmendia, I.; Munoz, M.; Anduaga, J.; Mayora, K.; Giménez, J.. On-line measurement of varnish thickness on a coating machine of fiber boards. Northern Optics : The Joint Conference of the Optical Societies of Denmark, Finland, Norway and Sweden. Espoo, Finland, 16 - 18 June 2003. Eero Noponen (Ed.). Teknillinen korkeakoulu (2003), s. 139.

Olkkonen, Juuso; Kataja, Kari; Aikio, Janne; Howe, Dennis G.. Finite difference frequency domain method: Maxwell equation solution for optical engineering applications. OSA 2003, Frontiers in Optics, The 87th OSA annual meeting, Tucson, Arizona, 5 - 9 Oct. 2003, 2003

Olkkonen, Juuso; Kataja, Kari; Aikio, Janne; Howe, Dennis G.. On the optimization of sub-wavelength aperture transmission. OSA 2003, Frontiers in Optics, The 87th OSA annual meeting, Tucson, Arizona, October 5-9, 2003, 2003

Olkkonen, Juuso; Kataja, Kari; Aikio, Janne; Howe, Dennis G.. Study of high throughput aperture for near field optical data storage. Technical digest, ODS 2003, Vancouver, Canada, 11 -14 May 2003, 2003

Pizzi, M; Koniachkine, V.; De Martfis, O.; Marbach, Ralf. New type of micro-mechanical shutter array for replacement of infrared photodetector arrays International Conference on Optical MEMS (MOEMS 2003), 2003 IEEE/LEOS. Waikoloa, Hawaii, USA 18 - 21 Aug. IEEE (2003), s. 173 - 174.

Pizzi, Marco; Koniachkine, Valerian; De Martiis, Omar; Marbach, Ralf. New type of micro-mechanical shutter array for replacement of photodetector arrays. 11th International Conference on Near-Infrared Spectroscopy. Cordoba, Spain, 6 - 11 April 2003 NIR-2003 : stretching the NIR spectrum to the limit. NIR Publications (2003), s. P.2.13.

Suhonen, Janne; Niemelä, Pentti; Päällysaho, Maarit. The use of CCD-Raman spectroscopy for the study of pharmaceuticals 5th Finland-Japan Joint Symposium on Optics in Engineering (OIE’03). Saariselkä, FI, 7 - 9 Aug. 2003. H.Kopola and T.Yatagai (Ed.). University of Oulu (2003)

Wierzba, Pawel; Karioja, Pentti. Coupled-field modelling of interferometric hydrophone with self-supported mandrel IX Conference on optical fibres and their applications, proceedings Vol 2, Krasnobrod, Poland, 9 - 11 Oct. 2003. Marii Curie-Sklodowskiej (2003), s. 840 - 846.

Wierzba, Pawel; Karioja, Pentti. Fibre Bragg Grating pressure transducer using a profiled membrane IX Conference on optical fibres and their applications, proceedings Vol 2, Krasnobrod, Poland, 9 - 11 Oct. 2003. Marii Curie-Sklodowskiej (2003), s. 847 - 854.

# Other Publications

Kivimäki, Liisa. Lead-free soldering. Espoo, KOTEL, 2003. 85 s.; 251. ISBN 951-8998-37-X

Kololuoma, Terho; Mäkelä, Tapio; Linna, Hannu; Haring, Tomi; Hagberg, Juha; Kallioinen, Jani; Kettunen, Ilkka; Kopola, Harri. Optiikkaa ja elektroniikkaa painokoneella. Prosessori., vol. 24 (2003) 11 (Elektroniikan suunnittelu), s. 75

Kondratyev, Vasily; Lahti, Markku; Jaakola Tuomo. On the LTCC band-pass filter design. URSI Conference proceedings. Oulu, Finland, 16 - 17 Oct. 2003. (2003), s. 43 - 45.

Harri Kopola, Terho Kololuoma, Tapio Mäkelä, Hannu Linna, Tomi Haring, Juha Hagberg, Jani Kallioinen, Ilkka Kettunen; Exploring materials and technologies for printable optics and electronics utilised in intelligent packaging, Smart and Intelligent Packaging 2003, 28-29 October, 2003, Barcelona, PIRA International, 21p.

Harri Kopola; Advanced materials and printing technologies for biomolecular recognition, Point-of-care testing - user needs and technological avenues, Diagnostics 2000 Technology Programme Annual Seminar May 20-21, 2003 Helsinki, TEKES, 15p.

Harri Kopola; PRINTO - Printattava optiikka ja elektroniikka, ELMO vuosiseminaari 12.3.2003, Helsinki, TEKES, 14p.

Optics in Engineering (OIE'2003), Technical Digest, Editors; H. Kopola, T. Yatagai, August 7-9, 2003, Saariselkä, Finland.

Harri Kopola; Oulun seudun teknologiapanostukset elektroniikkaan ja elektroniikan mekaniikkaan, CIM2005 - seminaari 'Elektroniikan mekaniikan tulevaisuuden näkymät', 26.8.2003, Oulu, POHTO, 27p

Lenkkeri, Jaakko; Kautio, Kari; Rautioaho, Risto; Nousiainen, Olli; Jääskeläinen, Jussi. LTCC-moduulien liitosten luotettavuus Elektroniikan valmistus 2003 : elektroniikan tuotanto- ja pakkaustekniikan konferenssi Porissa 22. - 23. 5. 2003. Julkaisusarja A, TTY, Porin yksikkö, A1/2003. Porin korkeakouluyksikkö (2003), s. 149 - 153.

Lenkkeri, Jaakko; Majamaa, Tero; Jaakola, Tuomo; Karppinen, Mikko; Kololuoma, Terho. Tulevaisuuden elektroniikan pakkaus- ja komponenttitekniikat. Espoo, VTT Elektroniikka, 2003. 78 s. + liitt. 4 s. VTT Tiedotteita - Research Notes; 2213. ISBN 951-38-6183-X

# Patents

Optoelectronic component and manufacturing method.Kopola, Harri; Rantala, Juha; Vähäkangas, Jouko; Karioja, Pentti Pat. US 6586268 B1, publication date 1 July 2003, application number 09/762635, application date 10 Aug. 1999, priority FI981731 (2003)

Laitinen, Jyrki. Puuaineksen mittausmenetelmä ja -järjestely. Pat. FI 110545 B, julkaisupäivä 14.2.2003, hakemusnumero FI 982341, hakemispäivä 28.10.1998. (2003)

Optinen mittapää ja optisen mittapään valmistusmenetelmä. Niemelä, Pentti; Suhonen, Janne; Sumen, Juha. Pat. FI 111191 B, julkaisupäivä 13.6.2003, hakemusnumero FI 20002250, hakemispäivä 12.10.2000 (2003) .

VTT TECHNICAL RESEARCH CENTRE OF FINLAND
VTT ELECTRONICS
P.O.Box 1100, (Kaitoväylä 1)
FI-90571 OULU, FINLAND
Tel. +358 8 551 2111
Fax +358 8 551 2320
e-mail: ele.info@vtt.fi
www.vtt.fi/ele